Field and Laboratory Tests of a Proposed Bridge Deck Panel Fabricated from Pultruded Fiber-Reinforced Polymer Components

by

Anthony B. Temeles

Thesis submitted to the Faculty of the
Virginia Polytechnic Institute and State University
in partial fulfillment of the requirements for the degree of

Master of Science
in
Civil Engineering

Thomas E. Cousins, Co-Chair
John J. Lesko, Co-Chair
Carin L. Roberts-Wollmann

May 14, 2001
Blacksburg, Virginia

Keywords: fiber-reinforced polymer (FRP), bridge decks, pultrusion, fiberglass

Field and Laboratory Tests of a Proposed Bridge Deck Panel Fabricated from Pultruded Fiber-Reinforced Polymer Components

Anthony B. Temeles

(Abstract)

Two 7” deep FRP deck panels were manufactured and tested in a controlled service environment. The deck panels were 15’ by 5’ in plan, and were composed of ten 15’ long, 6” by 6” by 3/8” standard pultruded FRP tubes. The tubes were sandwiched between two 3/8” thick standard pultruded FRP plates. The material constituents of the FRP were E-glass fibers in a polyester matrix. When subjected to two strength tests, the first deck panel exhibited a safety factor with respect to legal truck loads of greater than 10. The second deck was subjected to AASHTO design loads, and under a simulated HS-25 axle plus impact the deck exhibited a maximum deflection of L/470. Upon completion of the laboratory testing, the second deck was placed in the field for further study. The maximum strain recorded during field testing was approximately 600 microstrain, which is less than 15% of the ultimate tensile strain of the FRP in its weakest direction. After being subjected to approximately 4 million load cycles (assuming 100,000 5-axle truck crossings per month) over a period of 8 months, the deck exhibited no loss in stiffness. In two post-service strength tests, the second deck exhibited a safety factor with respect to legal truck loads of greater than 8 and greater than 13.

Acknowledgements

The author would like to thank the following people and organizations:

-**Dr. Thomas E. "Tommy" Cousins**, my committee co-chair and academic advisor. Dr. Cousins taught me a great deal about how to effectively deal with all kinds of personalities, and after having known him now for three years, I must say it's still the most valuable lesson I take with me as I leave Blacksburg. I must also thank Dr. Cousins for the tremendous patience he showed at a time when the completion of this thesis was in doubt. Dr. Cousins was always available to answer a question, to help me out at the lab, or to provide encouragement, and I can't thank him enough.

-**Dr. John J. "Jack" Lesko**, my committee co-chair, for the time, patience and knowledge he provided in helping me complete my research and particularly my thesis. Dr. Lesko is one of the most technically thorough persons I have ever met, and as such, he had a huge impact on the quality of my thesis as well as the quality of my technical writing in general.

-**Dr. Carin L. Roberts-Wollmann**, committee member, for her time and patience in reading my thesis and providing several good suggestions.

-**FHWA Innovative Bridge & Construction Program,** and **VTRC**, for their funding and support of the FRP deck research.

-**Dan Witcher** and **Glenn Barefoot** of Strongwell Corporation (Bristol, VA).

-**Jose Gomez** of VTRC.

-**Tony Slayden** and the **Salem Residency** bridge crew.

-**Brett Farmer** and **Dennis Huffman**, lab technicians in the Civil Engineering Structures and Materials Laboratory at Virginia Tech who helped erect my experimental laboratory setups.

-David Haeberle, Jolyn Senne, Ken Rux, Jason Coleman, and **Aixi Zhou**, graduate students at Virginia Tech who assisted me with my research.

-Bob Simonds and **George Lough**, lab technicians at Virginia Tech who assisted me with my research.

And finally, but most importantly, I'd like to thank my mother and father ("**Mom & Dad"**) for being such wonderful parents. Without them, none of this would have been possible.

Table of Contents

List of Tables

Chapter 1: Introduction and Literature Review

1.1 Introduction

Approximately 100,000—or 20 percent—of all bridges (circa 1998) in the U.S. are categorized as structurally deficient or structurally deficient and functionally obsolete (TRB, 1998). Approximately 35 percent of those bridges exhibit poor deck conditions. Rehabilitation of bridges in this category typically requires extensive repairs or, in extreme circumstances, replacement of the deck with a new reinforced concrete (RC) deck. Another rehabilitation option is to replace deteriorated bridge decks with decks that are built using a lighter high performance material. One class of materials that meets this criterion is fiber-reinforced plastic (FRP) composites. An immediate advantage of using an FRP composite bridge deck to replace a deteriorated RC deck is the reduction of the superstructure dead load—thus increasing the live load carrying capacity (and hence the structural rating) of the bridge. Another potential advantage is a decrease in construction time, which can reduce the amount of time a bridge would have to be closed for repair. New bridges could benefit from having an FRP bridge deck because a reduction in superstructure dead loads could lead to savings in the cost of the substructure. Other advantages of FRP decks that have been cited by various researchers are as follows: increased service life; lower life cycle costs; and superior fatigue damage resistance. While FRP composites *appear* to offer many advantages, more research needs to be conducted to determine whether these potential advantages can actually be realized.

Experience with composites in the bridge engineering community is limited. In particular, very little is known about the long-term durability of composite bridge deck systems; therefore the development of FRP bridge decks is still in the experimental phase. Several composite bridge deck systems have been proposed in recent years, and there is a growing need to understand the behavior of FRP bridge decks.

In an attempt to better understand this behavior, the author conducted laboratory tests on two bridge deck panels fabricated from pultruded fiber-reinforced polymer components. In addition, the author helped develop a testing facility to examine the field behavior of one of the deck panels. This paper describes the experimental program (both laboratory and field testing) and development of the testing facility. Finally, the results of the experimental program are presented.

1.2 Objectives

The objectives of this research endeavor were as follows:

• to develop a suitable test facility for conducting field tests of FRP deck panels

• to evaluate the viability of FRP deck panels made from pultruded, off-the-shelf components

• to evaluate the stiffness and strength of an FRP deck panel

• to evaluate the in-service behavior, durability, and post-service stiffness and strength of an FRP deck panel subjected to random and known truck loads

1.3 Literature Review

1.3.1 Design Live Loads and Tire Contact Area

The design live loads (not including pedestrian loads) specified in the 16th Edition (1996) of AASHTO's Standard Specifications for Highway Bridges are as follows: the H truck loads (*Figure 1.1*), the HS truck loads (*Figure 1.2*), the H and HS lane loads (*Figure 1.3*), and in special cases, the Alternate Military Loading (AASHTO, 1996, Section 3.7.4). When designing the superstructure members of a bridge, these loads are applied (one at a time) in critical locations to produce the maximum load effect. The load that produces the largest stress is considered to be the design load. Depending on stringer spacing and length of the bridge, any of the above four design loads above may govern.

In computing the load effects in a reinforced concrete bridge deck due to an AASHTO truck wheel, AASHTO (1996, Section 3.24) permits the designer to apply the design wheel load over a finite surface area of the deck. This area is defined as the "tire contact area" and the equation used to compute it is given by AASHTO (1996, Section 3.30). The AASHTO LRFD Specifications (1998, Section 3.6.1.2.5) utilizes a different equation (compared with the AASHTO Standard Specifications) to compute the tire contact area. Depending on which specification is used, and depending on what magnitude of wheel load is selected, the tire contact area can range from 8 inches (in the traffic direction) by 20 inches (for a 16 kip wheel using the equation in AASHTO's 16th Edition) to 14 inches (in the traffic direction) by 20 inches (for a 20 kip wheel using the equation in AASHTO's LRFD 2nd Edition [1998]). Although the specifications state that the above method of analysis is to be used for reinforced concrete bridge decks, most researchers have opted to apply HS20 truck loads to FRP decks (experimentally

and/or theoretically) using the tire contact area method since there are currently no provisions related to FRP decks in any of AASHTO's specifications.

Some researchers have used the equivalent of an HS25 design wheel when applying load to their deck. Although the reader won't find the term "HS25" in the AASHTO specifications, it is common for some state transportation departments to design their highway bridges using an HS25 design truck. An HS25 design truck is the same as an HS20 truck except that all loads have been increased by 25%.

1.3.2 Legal Truck Loads

The reader who is unfamiliar with the AASHTO design specifications should be aware that the AASHTO design trucks do not represent actual trucks. Rather, they are hypothetical vehicles that are used to analyze existing bridges and design new bridges. The inherent presumption is that the load effects caused by the governing AASHTO design truck should always be larger than the load effects caused by an actual vehicle that is at or below the legal weight limit (as discussed below).

The maximum allowable weight (without a permit) for a single truck axle is 20 kips. The maximum allowable weight (without a permit) for a tandem truck axle is 34 kips. Finally, the maximum allowable gross vehicle weight (without a permit) is 80 kips. These are federal weight restrictions (USDOT, 2000) and are applicable in most states, including Virginia (VDOT, 1996).

Although there are no weight restrictions for a single wheel, the author will refer to a "legal wheel weight" in Chapter 5. This legal wheel weight shall be assumed to be 10 kips (50% of a legal axle), and will be used as a reference against the applied loads in the laboratory tests. For example, if the failure load of the deck was 80 kips, it could be said that the factor of safety with respect to a legal wheel load is 8.

1.3.3 Live Load Deflections

AASHTO (1996) contains *recommended* limits on superstructure deflections. The word "recommended" is in italics to emphasize that these are not allowable deflections imposed by AASHTO but rather they serve as guidelines that designers may exceed at their discretion. The reason that the deflection limits in AASHTO are optional is that (at present) there are no simple,

definitive guidelines for the limits of tolerable static deflection or dynamic motion due to vehicular traffic (Taly, 1998, Chapter 5).

The deflection criterion most often cited in the FRP deck literature is L/800—herein referred to as a deflection index—where L is the center-to-center distance between supports. This deflection limit of L/800 applies to superstructure members (steel, reinforced concrete, or prestressed concrete) having simple or continuous spans that undergo deflections due to service live load *plus* impact. Many researchers have compared the deflection indices of their experimental (or theoretical) FRP bridge decks against the L/800 deflection index. In this context, L is the center-to-center distance between deck supports (*Figure 1.4*), and it is this definition of L that will be used throughout this thesis.

1.3.4 Discussion of Previously Conducted Research

The following literature review will cover research that deals strictly with all-FRP decks that have possible applications for bridges. To qualify as an all-FRP deck, the structure must satisfy certain requirements. The first requirement is that the deck's primary function is to transfer vehicular loads to the primary superstructure members such as stringers or floor beams. For example, an FRP deck panel that serves as the entire superstructure would not be considered relevant to this review. The second requirement is that the deck must be made solely of FRP (not including the wearing surface). For example, research dealing with FRP grating encased in concrete would not be relevant to this literature review, nor would an FRP deck filled with concrete.

The author's prime concern is with previous research that deals with the *structural behavior*—whether theoretical or experimental—of FRP decks subjected to applied loads. Other issues related to FRP decks, such as marketability and cost, while important in their own right, are not part of the author's scope and will not be discussed.

To the author's knowledge, the earliest documented literature on FRP decks is based on research conducted by John Henry in the early 1980's (Henry, 1985). Henry used the computer program SAP IV to analyze five single-span, E-glass/epoxy deck panels with various cross sectional configurations (*Figure 1.5*). The deck panels were 8 inches long (in the traffic direction) by 9 inches thick, and were supported such that their effective span was 7 feet. Henry studied the deflections of the panels by applying the equivalent of one HS20-44 wheel load (16

kips), distributed over an 8-inch (traffic direction) by 20-inch area. The results showed that the two sections with the X-shaped panels underwent the smallest deflections (*Table 1.1*), although these deflections exceeded the L/800 (.105 inches) deflection index.

Henry next focused his work on the X-shaped panels and explored the following issues: (1) the effects of panel width (*Figure 1.5*) on deflections (2) the effects of using truss elements—versus plate elements—on stresses and deflections (3) the influence of boundary conditions and (4) stresses and deflections in a 28-foot, four-span continuous FRP deck system.

Azar (1989) and Plecknik and Azar (1991) conducted fatigue tests on an 18-inch long (traffic direction), 7-foot wide, 9-inch thick FRP deck (*Figure 1.6*). This experimental work was an extension of the theoretical work done by Henry. The deck tested by Azar and Plecnik was made of filament wound diamond shaped and triangular shaped components (E-glass/vinylester) bonded together with an epoxy adhesive. After curing, the bonded components were "sandwiched" between layers of woven roving and chopped mats that were applied using hand lay-up techniques. For testing, the deck was simply supported (7-foot effective span) and loaded at midspan. The load was transferred to the deck by a 20-inch by 7-inch (traffic direction) plate that rested on a rubber pad. Loading was done in two phases. In the first phase, the deck was loaded monotonically to 8500 lbs (wheel load based on the Bridge Gross Weight Formula) and back to zero, then loaded for 2-million cycles at a range of 2125 lb to 8500 lbs. In the second phase, the deck was loaded monotonically to 12,500 lb and back to zero, then loaded for 2-million cycles at a range of 3125 lb to 12,500 lb. The initial deflection at 8500 lb (monotonic load cycle) was .150 inches, but after 2-million cycles, the deflection increased to .153 inches (2% more deflection). The initial deflection at 12500 lb (monotonic load cycle) was .225 inches, but increased to .237 inches (5.3% more deflection) upon reaching 2-million cycles of load. Azar attributed the loss in stiffness to debonding between the epoxy adhesive and the diamond-shaped and triangular-shaped components.

McGhee et al (1991) developed a software package to obtain optimum cross sections for four different FRP bridge deck panel designs (*Figure 1.7*). The software combined commercially available optimization algorithms with general-purpose finite element analysis capability. The objective function (in the optimization routine of the software) represented the total material volume in one-half of a full FRP deck panel model. The design variables were (1) top plate thickness (2) web thickness and (3) bottom plate thickness. The three constraints were

(1) ultimate strength (2) local buckling and (3) deflection. Orthotropic plane stress elements and 3-D beam elements were used to model the FRP deck panels. The full panel dimensions were 40 inches long (traffic direction) by 24 feet wide by 10 inches thick. The panels rested on four equally spaced stringers (8 feet spacing). The applied loads consisted of a 24 kip point load and a 0.640 kip/ft line load (both applied in the middle of the center span). Material properties were taken from a manufacturer's design manual for fiberglass composites (Morrison Molded Fiber Glass Company, 1989). Of the four panel types considered, the Type 2 cross-section outperformed (i.e. it was the lightest) the other three types. Types 1 and 4 were a close second, while Type 3 was clearly the least desirable of the four types.

Bakeri and Sunder (1990) developed idealized structural models for two deck systems (the relevant system being a pultruded truss shaped deck with parabolically varying depth). The simply supported deck had a 7-foot clear span and had a maximum thickness of 10.25 inches. It was composed of E-glass fibers and a polyester resin. Four variants of the deck system were considered (*Figure 1.8*). Bakeri and Sunder used the finite element program ADINA to compute stresses and deflections of the deck when subjected to HS20-44 truck loading. The material properties used in the analysis were averaged engineering constants of the deck laminates. The results of the analyses indicated that the maximum deflections for all cases (*Table 1.2*) exceeded the L/800 (.105 inches) deflection index, but that all stresses were within the allowable limits for glass-reinforced plastic.

Zureick (1997) conducted FE analyses (using ANSYS and GTSTRUDL) on FRP decks with box-shaped cells (*Figure 1.9, Deck 1*). The deck models considered were 8 feet long (traffic) by 11 inches thick. They were all simply supported (40-foot span) on two stringers and subjected to one "wheel line" (not an axle) of an AASHTO HS20-44 truck. The material properties used in the analyses corresponded to E-glass/vinylester with a fiber-volume fraction of 45-percent. Zureick considered four different cases, where fiber directions and orientation of cells were the variable parameters. He found that in all four cases, the stresses were less than 4 ksi. It was evident that the design of this type of FRP deck was always controlled by deflection. Deflections were much lower for the two cases where the cells were aligned perpendicular to traffic. Zureick found this to apply to other FRP deck cross-sectional configurations.

Zureick then used an optimization routine in ANSYS using four different cellular FRP deck models (*Figure 1.9*). Deck widths of 9 to 10 cells (72 to 80 inches, traffic direction) were

considered in the analyses. In all cases, the cells were aligned perpendicular to the traffic and rested on 3 stringers, each spaced 8-feet center-to-center. The objective function of the optimization was the minimum volume (by weight) FRP deck. The design variables of the program were as follows: (1) top plate thickness (2) bottom plate thickness (3) web thickness and (4) "theta" for two of the six plies in the laminate. Several constraints were imposed so that strength, stiffness, stability and serviceability were not compromised. These constraints were as follows: (1) L/800 (0.120 inches at L = 8 feet) max deflection, where L was the center-to-center distance between supports (2) relative deflection between adjacent webs less than or equal to 0.1 inch (3) max Tsai-Wu failure criterion = 0.6 (4) top plate thickness greater than or equal to 0.5 inches and (5) bottom plate and web thickness greater than or equal to 0.25 inches. The material properties used in the FRP deck models were E-glass/vinylester. The decks were loaded by one HS20-44 axle on each span, for a total of four wheel loads—each of which was applied to the deck over a 6-inch (traffic direction) by 20-inch area. Optimum decks were found for 6 different deck depths (from 7 inches to 12 inches at 1-inch increments). Zureick found the box-celled deck and the V-celled deck to be the most efficient sections. The trapezoidal-celled deck converged to the box-cell deck at the optimum design. At every deck depth, the X-cell deck was heavier than the V-cell deck. At smaller depths (7 to 10 inches) the V-cell deck was lighter than the box-cell deck, but at 11 and 12 inches of depth, the box-cell deck was lighter.

After concluding that the box-cell and V-cell deck were optimum, Zureick tested these designs at larger stringer spacing. At 10-foot and 12-foot stringer spacing, none of the decks were able to satisfy the L/800 (.150 inches for L=10 feet and 0.180 inches for L=12 feet) deflection index.

Brown and Zureick (1999) developed a fiberglass, modular deck panel to be used for the Landing Ship Quay/Causeway and Mobile Offshore Base programs funded by DARPA (Defense Advanced Research Projects Administration). The 9-inch thick deck panel (*Figure 1.10*) consisted of pultruded triangular elements that were sandwiched between hand layed-up face sheets. The triangular elements were made up of E-glass braided fabrics embedded in a vinylester resin while the face sheets were made up of E-glass knitted fabrics in a vinylester resin. A 9.84-foot by 9.84-foot deck panel was fabricated and tested under 3-point bending. The deck was loaded to 140 kips (without failure) and experienced a maximum deflection of 0.7 inches, a max tensile strain of approximately 2300 microstrain and a max compressive strain of

approximately 1600 microstrain. Upon completion of the test program, two 10 feet by 20 feet (3 meter by 6 meter) deck panels were placed in a test pit at the Troutville, Virginia weigh station on I-81 in order to investigate the durability of this deck panel concept.

Researchers at West Virginia University developed an FRP bridge deck panel that lead to the construction of two FRP composite bridge decks in West Virginia (GangaRao et al, 1999). The FRP deck panel was composed of hexagonal shaped cells and double-trapezoidal shaped cells that were adhesively bonded together to form 8-inch-thick FRP deck modules (*Figure 1.11*). The hexagonal and double-trapezoidal components were composed of E-glass fibers embedded in a vinylester resin. The fiber architecture was in the form of stitched fabrics, continuous roving, and chopped strand mats. Prior to field installation of the bridge decks, static and fatigue tests were conducted on smaller scale models. First, a 36-inch long (traffic direction) deck panel (9-foot simply supported span) was loaded at a rate of 3 cycles per second up to 2 million cycles. The load range was 2 to 35 kips. The load was applied to the deck over a 20-inch by 10-inch area. After every 500,000 cycles, a static load test was conducted to see if the deck panel had lost any stiffness. Next, two static load-to-failure tests were conducted. The first test was done on the previously fatigued deck while the second test was conducted on a deck panel that had no prior load history. No visual damage was observed after termination of the fatigue test, and less than 4% loss in stiffness of the deck was recorded. The previously fatigued deck panel failed at a load of 124.5 kips and exhibited a maximum deflection (at time of failure) of 1.54 inches. The second deck panel failed at a load of 126.7 kips and experienced a peak deflection of 1.57 inches.

Harik et al (1999) conducted static tests on three FRP deck panels manufactured by Creative Pultrusions. The deck panels were made of pultruded double-trapezoids and hexagons that were adhesively bonded to form deck panels (*Figure 1.11*). The three deck panels were 36 inches long (traffic direction) by 8 inches thick. Each specimen was loaded in 3-point bending. Load was transmitted through a rectangular plate (simulating AASHTO tire contact area) that measured 22 inches (traffic direction) by 9 inches by 2 inches thick. A ½-inch rubber pad was placed beneath the plate so as not to locally damage the deck during loading. The test procedure consisted of four steps. First the specimens were loaded from zero to 26 kips and back to zero. The 26 kip load represented the wheel load (plus impact) of an HS25-44 truck wheel. Second, the specimens were loaded from zero to 12 kips and back to zero. This was repeated five times. The 12 kip load

represents the service load for a HS25 truck (4 kips/foot width). Third, the deck panels were loaded from zero to 26 kips and back to zero. This was also repeated five times. Last, all specimens were loaded to failure. The results of the tests for the three deck panels are shown in *Table 1.3*.

As part of the Advanced Composites for Bridge Infrastructure Renewal Program, researchers developed a FRP composite demonstration bridge deck system that can be compositely connected to steel girders (Cassity et al, 2000). Prior to construction of the full-scale demonstration bridge, static and fatigue testing was done on smaller-scale deck panels. The panels (*Figure 1.12*) were composed of pultruded tubes (each having a "male" and "female" end) bonded together with polyurethane adhesive. The tubes were 7 5/8 inches thick and consist of E-glass fibers in an isophthalic polyester resin. For the static testing, a 3-feet 4-inch (traffic direction) by 8-feet panel (7-feet 4-inch effective span length) was tested in 3-point bending. Load was applied through a steel plate resting on a neoprene pad—collectively referred to as a tire patch. The panel was loaded up to 110 kips (without failure), which represented a safety factor greater than 5 when compared to in-service loads (HS20 wheel plus impact). For the fatigue test, a 12-feet long specimen consisting of 3 pultruded tubes was subjected to 10.5 million cycles of load. Local bending of the top face of the panel in the vicinity of the tire patch resulted in interlaminar shear cracking on the underside of the top face sheet at a ply drop-off detail and at mid-depth of the top face sheet. The cracks did not grow far beyond the tire patch region and were not thought to affect the overall stiffness of the specimen. Upon completion of the fatigue test, the panel was loaded to failure up to 116 kips. The overall response of the deck was linear up to failure.

1.3.5 Research at Virginia Tech

Since the spring of 1998, Virginia Tech has worked with Strongwell Corporation (Bristol, Virginia) to develop and test FRP composite deck panels made from pultruded, off-the-shelf components. Strongwell first developed the FRP deck concept in an effort to have the deck panels used as replacements for the existing decking in the Schuyler Heim vertical lift bridge in Long Beach, California (CALTRANS, 1997). Researchers at Virginia Tech were given the task of testing a prototypical FRP deck panel under various loadings (Hayes et al, 1998) to test the feasibility of this FRP bridge deck concept.

The deck panel (*Figure 1.13*) tested by Hayes et al was 4 feet long (traffic direction) by 14 feet wide by 4 ¾ inches thick, and consisted of pultruded tubes and plates. The tubes and plates were made of E-glass mats (continuous) and roving embedded in an isophthalic polyester resin. The tubes were joined together using an epoxy adhesive as well as fiberglass thru-rods (running through the sidewalls of the tubes) spaced at 12 inches. The plates were bonded to the tubes using the epoxy adhesive.

For all testing, the deck was supported on four W16X40 steel beams spaced at 4 feet each. Load was transferred to the deck through a 12-inch (traffic direction) by 20-inch plate that rested on a neoprene pad. Three different tests were performed on the deck: (1) stiffness test (2) as-received strength test and (3) fatigue test followed by a strength test. *Figure 1.14* shows the test setup and the layout of the load plates.

For the first test, the center span of the deck panel was loaded to 25 kips. The midspan deflection at 20.8 kips (16-kip wheel load plus 30% impact) was 0.150 inches, which corresponds to a deflection index of L/320. For the second test, the left span of the deck panel was loaded until it failed (by "punching shear") at 78 kips. The largest strain recorded during the test was a tensile strain of 4680 microstrain on the bottom surface of the deck, directly beneath the loaded area. The midspan deflection at 20.8 kips was 0.150 inches, which was the same deflection observed beneath the middle span (during the first test). For the third test, the right span of the deck panel was subjected to a fatigue load for 3-million cycles, and then loaded (monotonically) to failure. For the fatigue test, the load was cycled between 2.5 kips and 25 kips at a rate of 2 to 3 Hz. During fatigue testing of the deck, there was no apparent loss in stiffness and no visible sign of damage was observed. After the fatigue loading was completed, the span was loaded until it failed (by "punching shear") at 83 kips. The largest strain recorded during the test was a tensile strain of 4150 microstrain. The midspan deflection at 20.8 kips was 0.170 inches—slightly higher than the 0.150 inches of deflection observed in the first two tests (at 20.8 kips).

1.4 Summary

Based on the above literature review, the FRP deck concept has been studied using several methods: (1) computer analyses (2) static load tests conducted in a laboratory environment and (3) fatigue tests conducted in a laboratory environment. Though not cited in the literature review,

some researchers have also installed FRP decks on actual bridges and conducted tests on the short-term behavior of the deck. The importance of the results from all of these studies cannot be overstated. However, it is also important that the long-term behavior and durability—in a field application—of the FRP deck concept be studied. Other than the research being conducted by Brown and Zureick, the author was unable to find literature that documented the long-term behavior of an FRP deck. This illustrates the need to conduct field tests of FRP decks and the need to gather data on the long-term behavior and durability of FRP decks, and it provides the impetus for conducting the type of research that is the focal point of this thesis.

1.5 Tables and Figures

Table 1.1 Deflections of the five deck types analyzed by Henry

Deck Type	Maximum Deflection (in.)	Deflection Indices
1	0.144	L/583
2	0.144	L/583
3	0.199	L/422
4	0.204	L/412
5	0.214	L/393

Table 1.2 Deflections of the four deck types analyzed by Bakeri and Sunder

Deck Type	Maximum Deflection (in.)	Deflection Indices
1	0.224	L/402
2	0.206	L/437
3	0.195	L/462
4	0.183	L/492

Table 1.3 Deflections and Failure Loads for FRP Deck Panels tested by Harik et al

Specimen Identification	Effective Span (ft)	Centerline Deflection at 12 kips (in.)	Centerline Deflection at 26 kips (in.)	Load at Failure (kips)	Safety Factor[1]	Maximum Deflection at Failure (in.)	Mode of Failure
CPD1	8	0.090	0.208	148.2	5.70	1.540	Punching
CPD2	10	0.160	0.362	147.0	5.65	2.408	Punching
CPD3	12	0.239	0.573	145.4	5.59	3.882	Punching

[1]Safety Factor = Load at Failure/ 26 kips

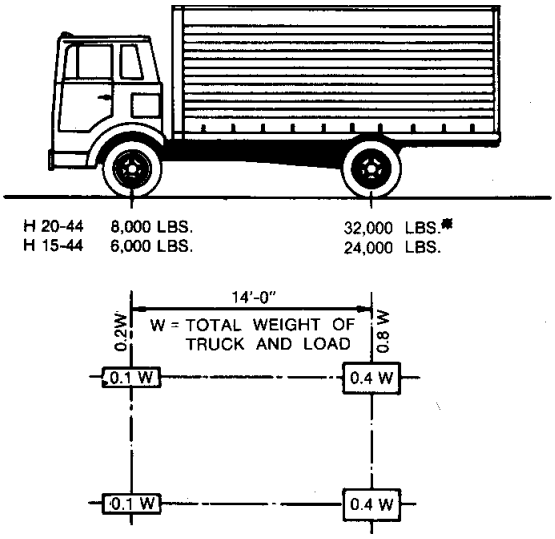

Figure 1.1 H-truck (AASHTO, 1996)

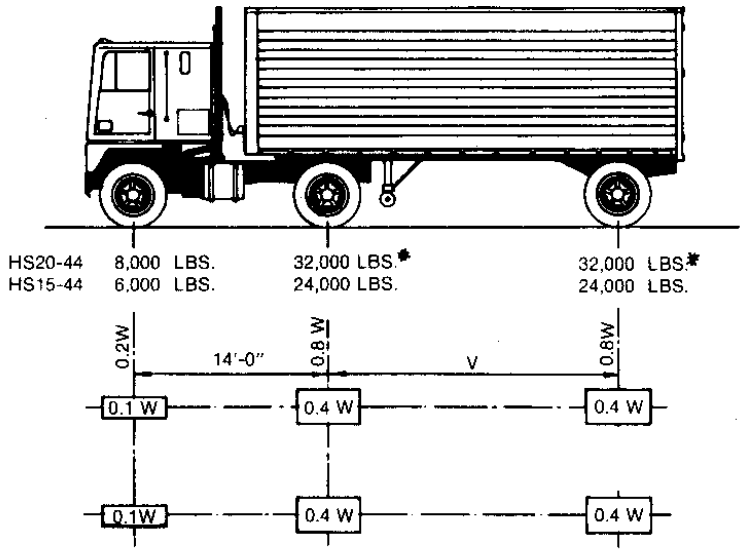

W = COMBINED WEIGHT ON THE FIRST TWO AXLES WHICH IS THE SAME AS FOR THE CORRESPONDING H TRUCK.
V = VARIABLE SPACING — 14 FEET TO 30 FEET INCLUSIVE. SPACING TO BE USED IS THAT WHICH PRODUCES MAXIMUM STRESSES.

Figure 1.2 HS-truck (AASHTO, 1996)

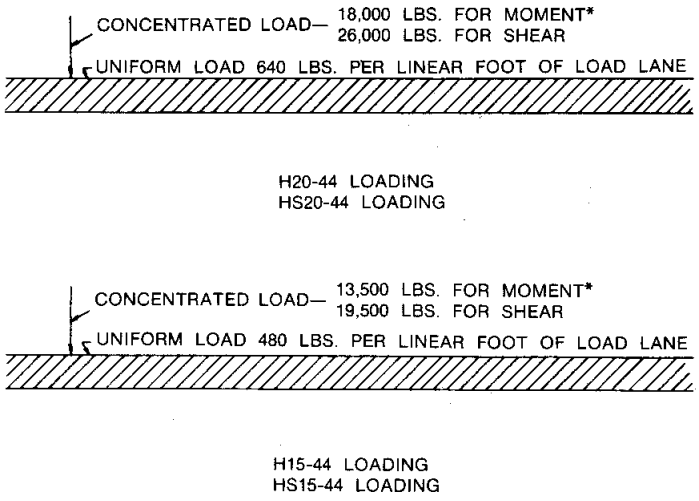

Figure 1.3 H and HS lane loads (AASHTO, 1996)

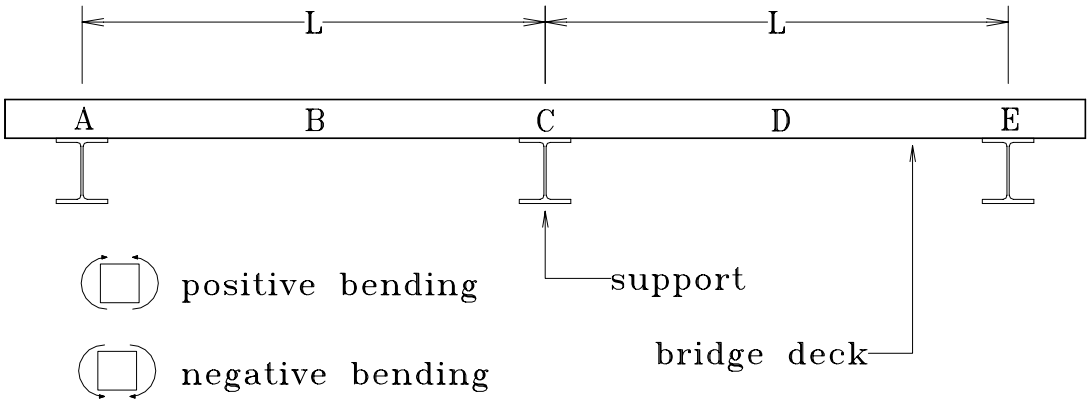

Figure 1.4 2-span bridge deck (traffic moves “into” paper)

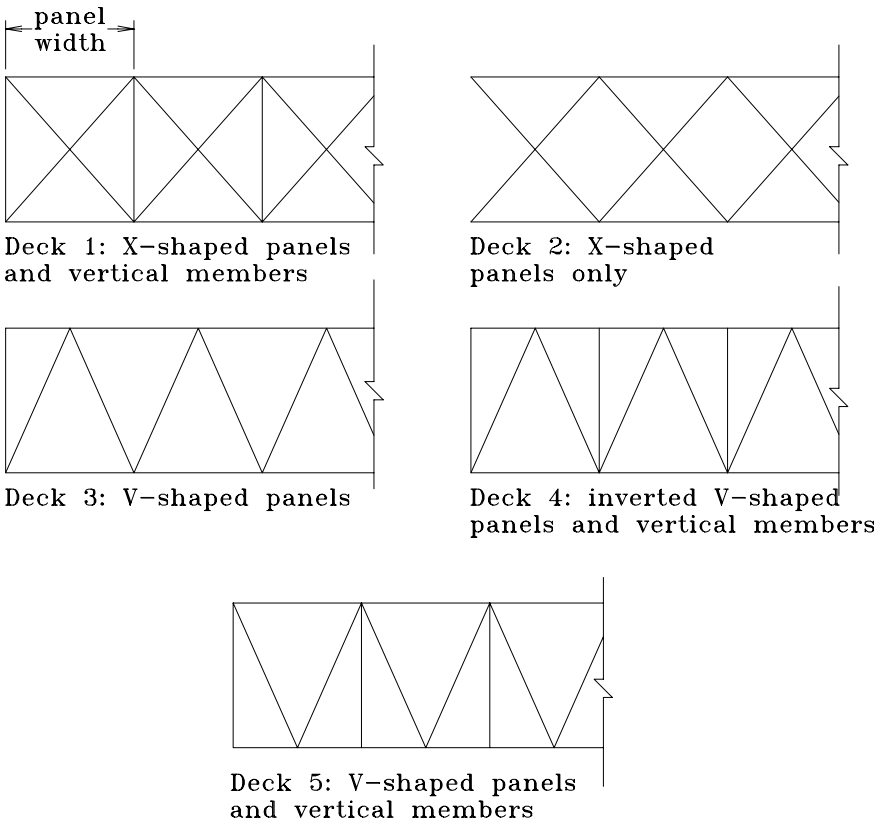

Figure 1.5 Partial sections of the four FRP deck panels analyzed by Henry

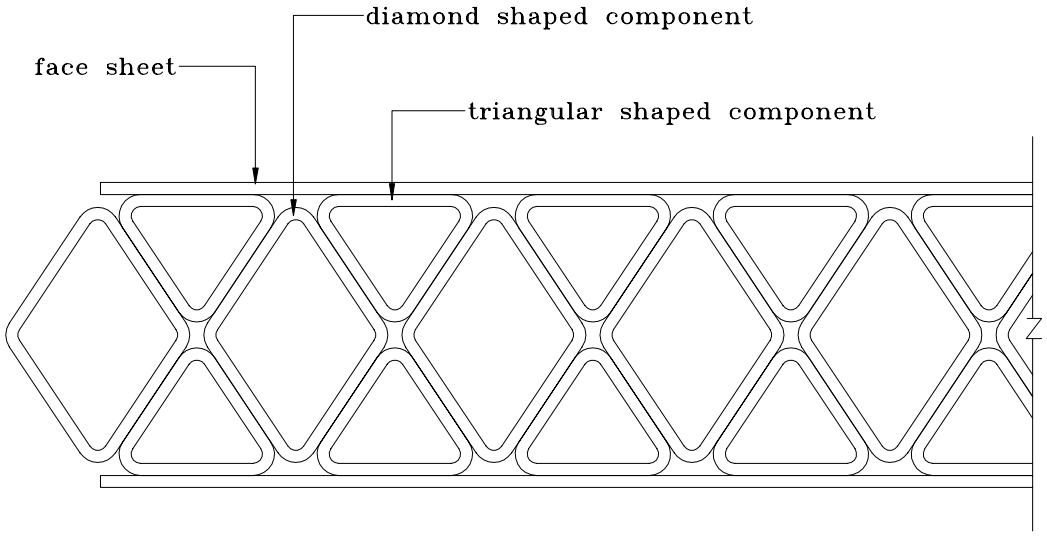

Figure 1.6 Partial section of FRP deck panel tested by Plecnik and Azar

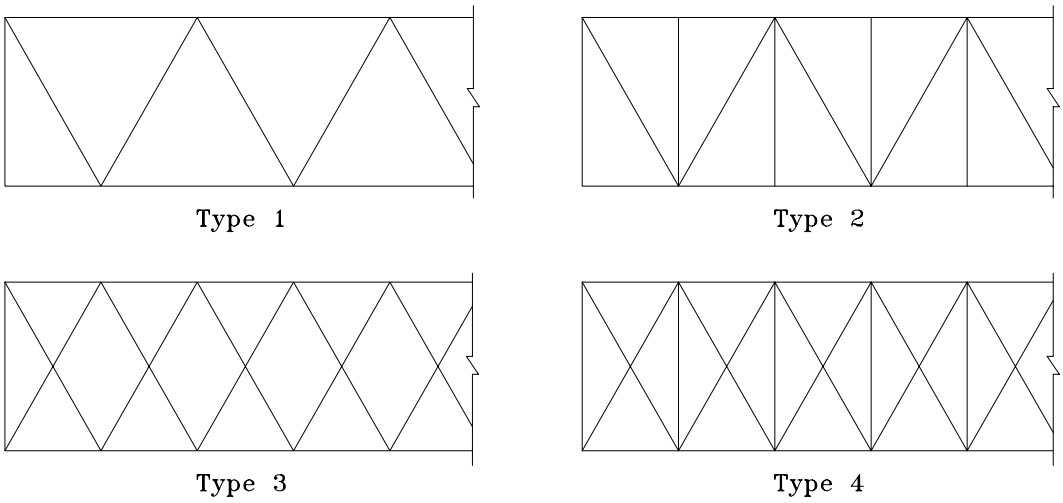

Figure 1.7 Partial sections of the four FRP deck panels analyzed by McGhee et al

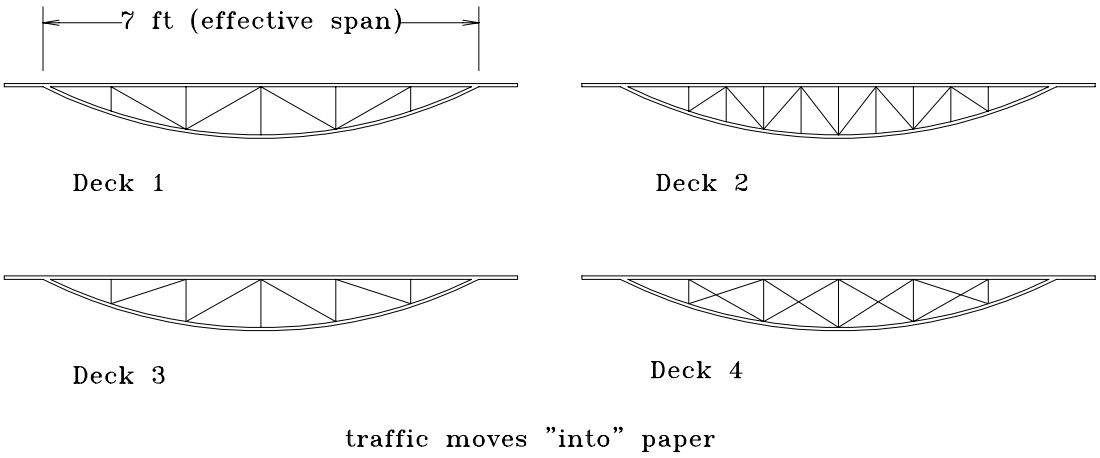

Figure 1.8 Cross-sections of the four FRP decks analyzed by Bakeri and Sunder

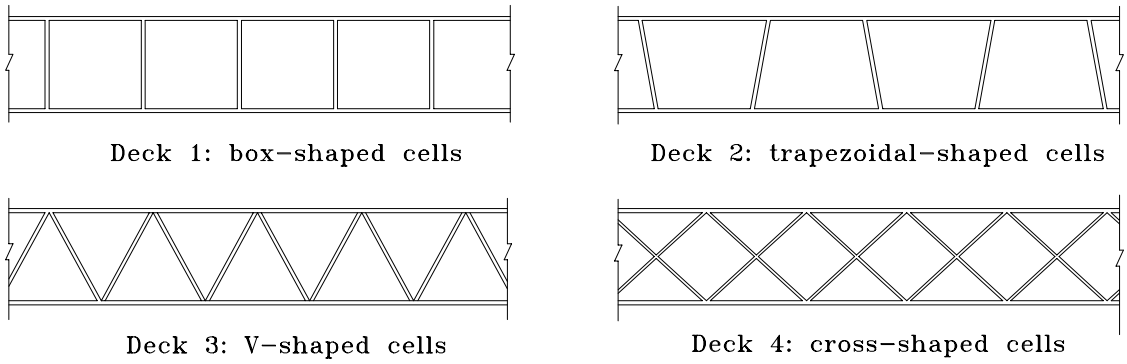

Figure 1.9 Partial sections of the four FRP deck panels analyzed by Zureick

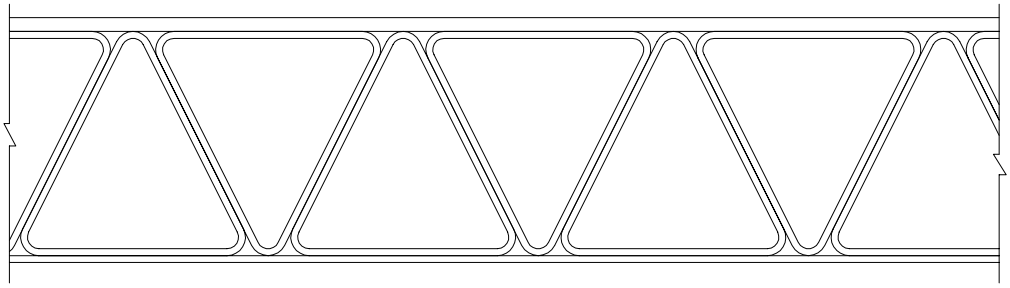

Figure 1.10 Partial section of FRP deck panel tested by Brown and Zureick

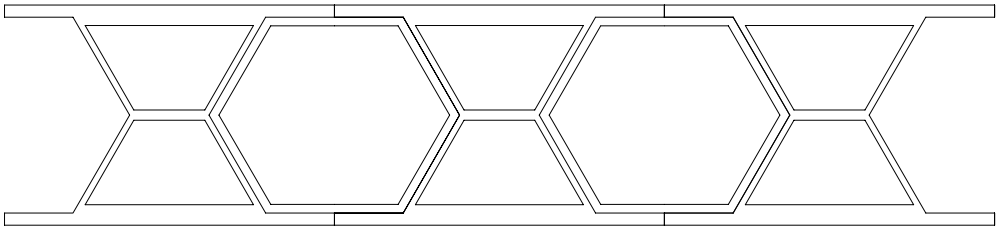

Figure 1.11 36-inch wide FRP deck panel tested by GangaRao et al and Harik et al

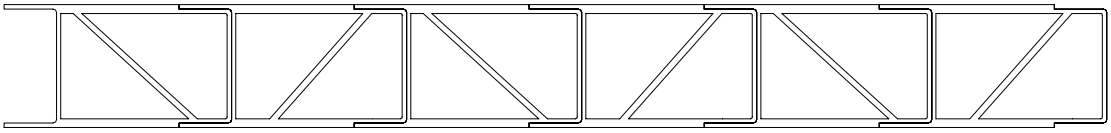

Figure 1.12 Partial section of FRP deck panel tested by Cassity et al

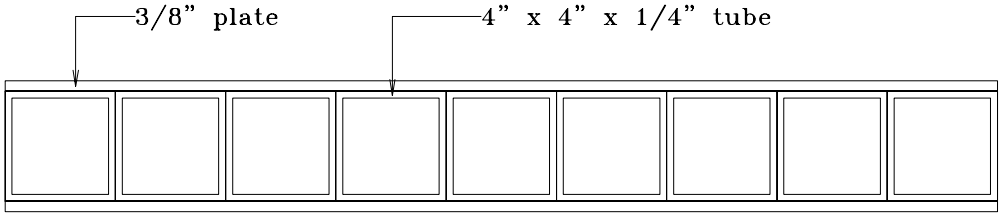

Figure 1.13 Partial section of FRP deck panel tested by Hayes et al

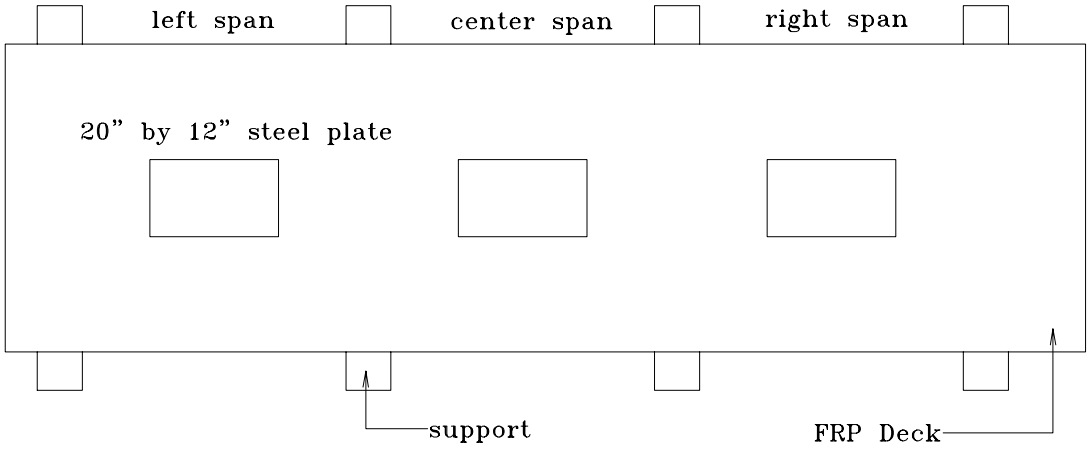

Figure 1.14 Test setup used by Hayes et al

Chapter 2: Materials and Fabrication

2.1 Introduction

In this chapter, the author describes the components of the two FRP deck panels as well as the material make-up of these components. The author also discusses the fabrication of the two decks, and finally, differences between the two decks are highlighted.

2.2 Components and Material Properties

The primary components of the FRP deck panel are 6-inch tubes (*Figure 2.1*) and 3/8-inch plates. The tubes and plates are pultruded fiberglass structural shapes (Strongwell, 1998) produced by Strongwell, Corporation. They contain E-glass reinforcement—in the form of continuous strand mats [CSM (*Figure 2.2*)] and roving (*Figure 2.3*)—embedded in an isophthalic polyester resin. The glass-fiber fraction of these particular shapes is typically 50-60% of the total volume of the shape while the mat and roving are present in approximately equal amounts. All the shapes had a surfacing veil of polyester non-woven fabric that encases the glass reinforcement and provides a layer of resin at the surface. The surface veil also eliminates "fiber blooming" (the presence of glass fibers on the surface) and thus provides a smooth finish to the structural shape.

The material properties of the tubes, plate and rods (discussed later) are listed in *Table 2.1 (tubes and plates) and Table 2.2 (rods)*. These properties were taken directly from Strongwell's design manual (Strongwell, 1998). The material properties are minimum values recorded from tests that are conducted in conformance with ASTM procedures. These procedures are cited in Strongwell's design manual.

2.3 Fabrication of FRP Deck Panels

A prototypical model of one of the FRP deck panels can be seen in *Figure 2.4*. Each deck panel (*Figure 2.5 and 2.6*) was 5 feet wide, 15.25 feet long, and 6 ¾ inches deep (not including the wearing surface). The two panels were made of ten 15.25-foot long FRP tubes "sandwiched" between two 3/8-inch FRP plates. Though similar in most respects, there were some significant differences between the two decks. Because of these differences, the panels have been given two distinct names. From this point on, the first FRP deck will be referred to as "Deck 1" while the

second deck will be referred to as the "Deck 2". The next two sections discuss the fabrication of the two FRP deck panels.

2.3.1 Deck 1

Deck 1 was fabricated in June of 1999 (at Strongwell Corporation in Bristol, VA) and took about one week to fabricate. Prior to assembling the tubes of the deck, holes were drilled in the sidewalls of the tubes. Next, the sidewalls of the tubes were sanded in order to remove the surface veil, thereby providing an improved bonding surface. The tubes were then bonded together with a high performance adhesive (Shell 828 Epoxy) and were mechanically fastened using pultruded, fiberglass reinforced vinyl ester rods (threaded at each end) and fiberglass hex-shaped nuts (Strongwell, 1998). The 1-inch diameter thru-rods were inserted through the holes that had been drilled in the sidewalls of the tubes *(Figure 2.7*). Material properties for the 1-inch diameter rod are shown in *Table 2.2*. The layout of the fiberglass thru-rods, which is typical of the thru-rod layout of both Deck 1 and Deck 2, is shown in *Figure 2.8*.

After allowing sufficient time to cure, the 10-tube panel was sanded on the top and bottom surfaces. This was done for two reasons: (1) to develop an adequate bonding surface and (2) to ensure that the top surfaces of all the tubes were "level" with one another. After adequate sanding, 3/8-inch FRP plate was adhesively bonded to the bottom surface of the tubes. To help develop the tube-to-plate bond, fifty-pound steel weights were placed (on a 2-foot grid) on top of the bottom plates (with the deck positioned upside down). The placing of the weights on the plates helped to keep uniform pressure on the plates while the epoxy cured.

The standard pultruded size of the 3/8-inch plate was 4-feet by 8-feet. Because the deck panel was 5-feet by 15-feet 3-inches, it was not possible to pultrude a single plate for the top and bottom of the deck panel. As a result, the top and bottom plates are not monolithic plates, but rather consist of several sections of plate that have been cut and sized to properly fit the top and bottom surfaces of the deck panel. *Figure 2.9* shows the layout of the plate sections on the top and bottom of the deck.

After bonding the bottom plates to the tubes, a wearing surface (approximately 1/4 inch thick) was applied to the top plates; the top surfaces of the plates were not sanded prior to application of the wear surface. The wear surface was composed of a bottom layer of gap graded angular quartz (sieve sizes 4 thru 16), while the top layer was made up of a finer angular quartz

(sieve sizes 16 thru 50). The resin used to bind the aggregate together (as well as bond it to the top plate) was Derakane 8084 Vinyl Ester (Rubber Toughened). Because it was intended that the deck be placed in the field and subjected to actual truck traffic, a wear surface was needed in order to provide a skid-resistant surface and to protect the top of the deck panel from abrasion.

Once the wearing surface had cured, the top plates were adhesively bonded to the top surface of the tubes. Then the fifty-pound steel weights were placed on top of the wear surface while the epoxy cured.

2.3.2 Deck 2

Deck 2 was assembled (at Strongwell Corporation) in October of 1999 and took one week to fabricate. Prior to assembling the tubes, holes were drilled in the sidewalls of the tubes. After sanding of the tube walls, the tubes were adhesively bonded together using Magnabond 56, Parts A and B and were mechanically fastened using 1-inch diameter AISI 1018 (ASM, 1978) cold drawn steel rods (threaded at the ends) with steel hex nuts.

After allowing the epoxy between the tubes to cure, the top and bottom surfaces of the tube were sanded. Next, 3/8-inch sections of plate were adhesively bonded to the top and bottom surfaces of the tubes (*Figure 2.9*). After all the plates were in place, the deck panel was put in a vacuum bag. The vacuum bag provided a uniform pressure of 10-14 psi (Ed Balaban e-mail, August 23, 2000) over both the top and bottom tube-to-plate interfaces, and thereby helped develop the tube-to-plate bond while the epoxy was curing.

Upon completion of the vacuum bagging of the deck, the top plate sections were sanded and the wearing surface was applied. The wearing surface thickness for the Phase II deck was approximately 3/8 inches, and it was composed of the same constituents as the wear surface on Deck 1.

2.3.3 Summary of Significant Differences between Deck 1 and Deck 2

During the initial testing phase of Deck 1, it became clear that changes needed to be made to the deck—hence the manufacturing of Deck 2. The end result is that there were some characteristic differences between Deck 1 and Deck 2. A summary of these differences is presented in *Table 2.3*. It may not be obvious what effects these changes had on the behavior of

the deck (or why the changes were made). Therefore, the author will discuss some of the changes in greater detail in Chapter 5.

2.4 Tables and Figures

Table 2.1 Material properties of fiberglass tube and plate (Strongwell, 1998)

Material Property (units in parentheses)	tube	3/8-inch plate
Ultimate Flexural Strength, LW (ksi)	30	30
Ultimate Flexural Strength, CW (ksi)	10	18
Flexural Modulus, LW (ksi)	1600	2000
Flexural Modulus, CW (ksi)	800	1400
Modulus of Elasticity (ksi)	2800	NA[1]
Ultimate Shear Strength (ksi)	4.5	6
Shear Modulus, LW (ksi)	425	NA[1]
Ultimate Tensile Strain[2], LW (με)	12000	11100
Ultimate Tensile Strain[2], CW (με)	8750	7100
Ultimate Compressive Strain[2], LW (με)	12000	13300
Ultimate Compressive Strain[2], CW (με)	15000	20000
LW = Lengthwise CW = Crosswise		
[1] not available [2] approximate values obtained by dividing ultimate stresses by elastic moduli		

Table 2.2 Material properties of fiberglass thru-rods (Strongwell, 1998)

Material Property	1-inch-diameter rod
Ultimate Shear Strength, Single Shear (kips)	15
Ultimate Flexural Strength (ksi)	50
Flexural Modulus (ksi)	2750

Table 2.3 Summary comparison of fabrication and material selection for Deck 1 and Deck 2

Description	Deck 1	Deck 2
Pultrusion of tubes	Non-uniformity of tube-wall thicknesses due to variability of mandrel position inside the die	Higher quality control in the pultrusion process: tube-wall thicknesses much more uniform
Adhesive used to bond FRP components	Shell 828 (epoxy)	Magnabond 56, Parts A & B (epoxy)
Thru-rod-and-nut connection	Pultruded fiberglass	AISI 1018 cold drawn steel
Plate-to-tube bonding	50-pound weights (2-foot grid) placed on top of plates; one side of deck panel at a time	Pates bonded to top and bottom surfaces of tubes; deck panel then vacuum bagged
Top-plate surface preparation for wear surface	None	Top surface of top plate sanded prior to application of wear surface
Chronology of wear surface application	Wear surface applied onto plates prior to plates being bonded to tubes	Wear surface applied after entire panel was vacuum bagged

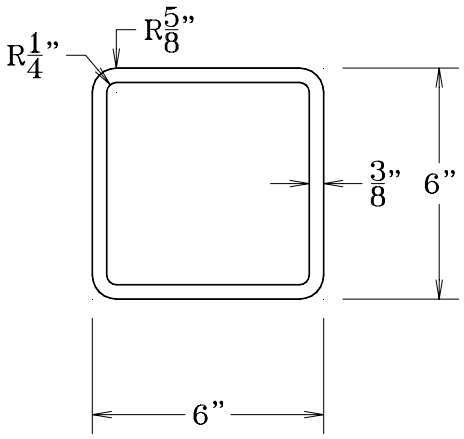

Area = 8.16 in^2
Weight/Length = 6.46 lb/ft
Moment of Inertia = 38.44 in^4
Section Modulus = 12.81 in^3

Figure 2.1 Section properties of a single FRP tube

Figure 2.2 Sample cutout of continuous strand mat

Figure 2.3 Sample of glass roving

Figure 2.4 End view of FRP deck panel

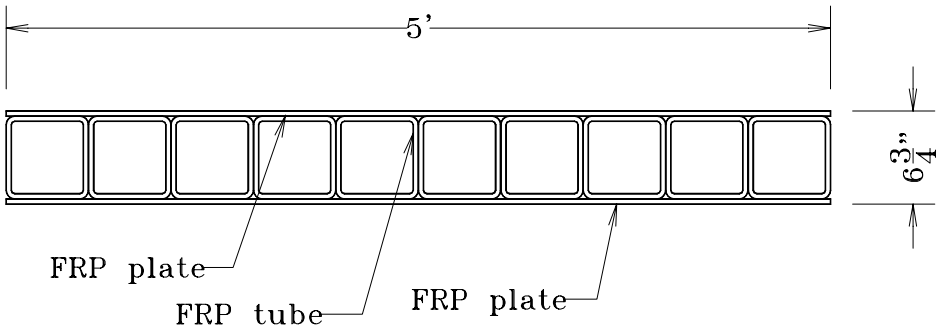

Notes:
1. Wearing surface not shown
2. Thru−bolts not shown

Figure 2.5 Cross-section of FRP deck panel

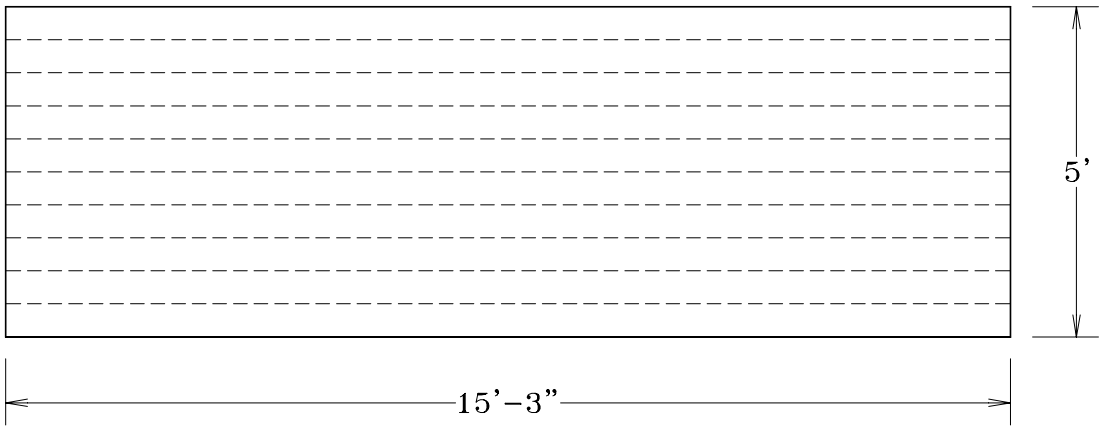

Figure 2.6 Plan view of FRP deck panel (thru-rods not shown)

Figure 2.7 End view of thru-rod assembly

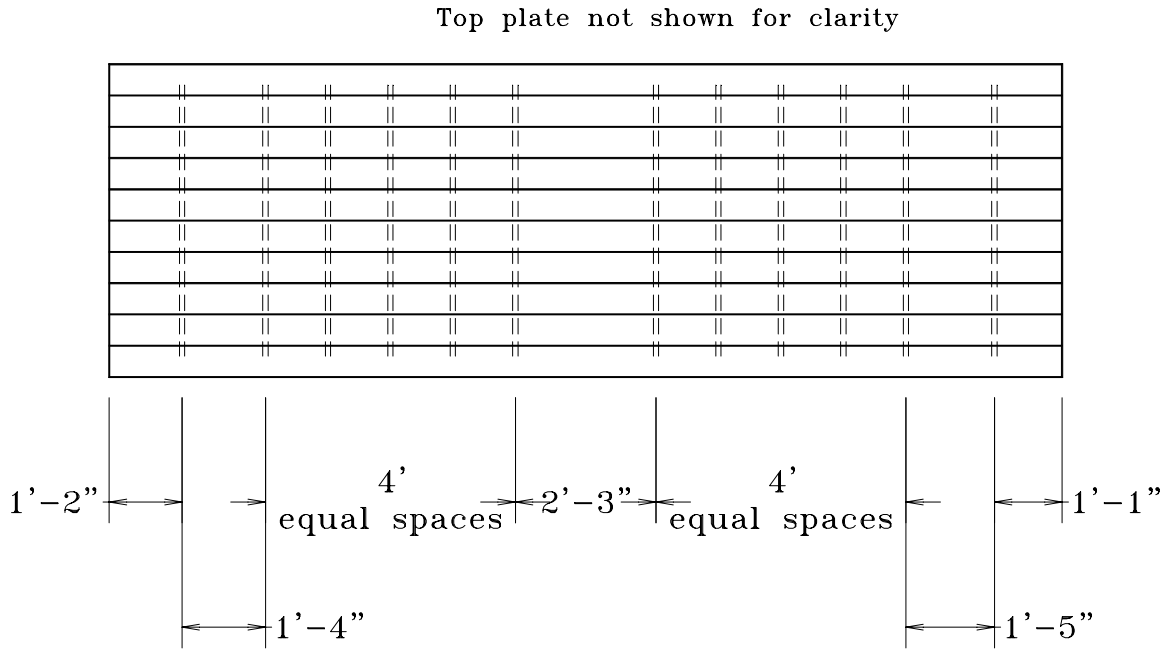

Figure 2.8 Plan view of thru-rod layout (Typical of Deck 1 and Deck 2)

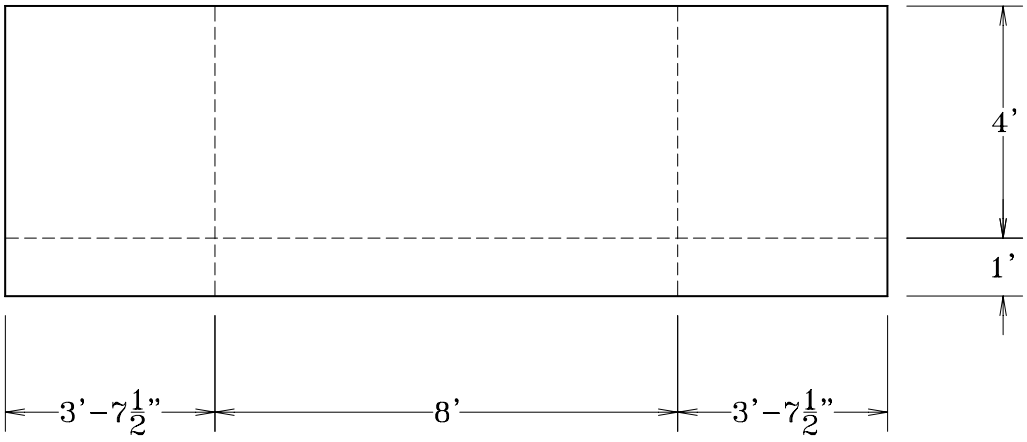

Top Plate

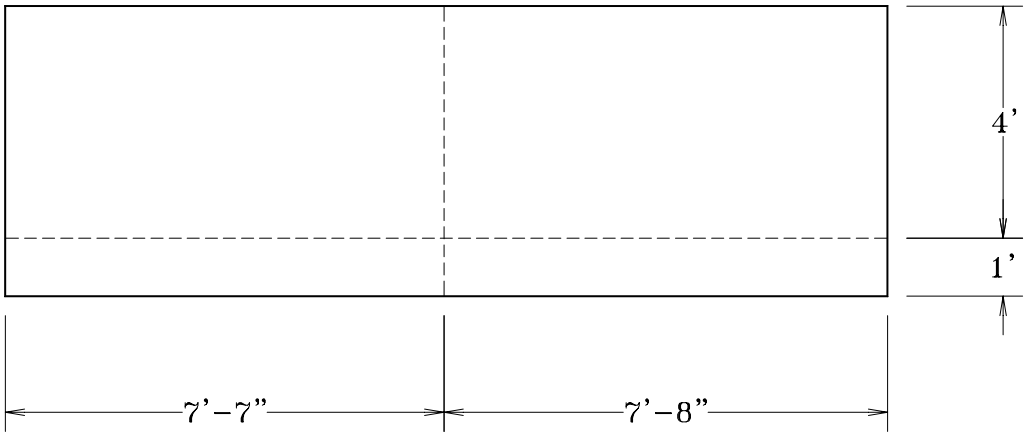

Bottom Plate

------- butt joint

Figure 2.9 Layout of top and bottom plate sections (tube-to-tube joints not shown)

Chapter 3: Weigh Station Testing Facility

3.1 Introduction

In this chapter, the author discusses the facility that was developed to test an FRP deck panel. The three topics of discussion are as follows: (1) the purpose of the facility; (2) the design of the facility; and (3) the construction of the facility.

3.2 Purpose and Motivation

With the exception of field and laboratory tests conducted by Fred McCormick in the late-seventies (McCormick, 1978) and into the eighties, most of the experimental research with composites for bridge applications has been conducted in the mid- to late-nineties. As a result, experience with composites for bridge applications (circa 2000) is limited and very little long-term durability data is available. It is against this backdrop that researchers at Virginia Tech worked to develop a facility that could serve as a testing ground for composite bridge decks—hence the design and construction of a testing facility at the Troutville, Virginia weigh station.

The Troutville weigh station is located on Interstate-81 (mile 148). One reason for implementing the test facility at a weigh station is that it was considered to be a low-risk setting in the case of an unexpected failure of an FRP deck panel. In addition, over 200,000 trucks (over 100,000 on each side) pass through the Troutville weigh station each month (personal communication with weigh station personnel, May 30, 2000). Because of this high volume of traffic, any bridge deck panel that would be installed at the weigh station would be subjected to a significant number of cycles of a fatigue-type loading. Furthermore, it would be possible to close the weigh station and run controlled tests (see Chapter 4). Because the deck panel would be "outdoors", it would be exposed to realistic environmental conditions. And if desired, the deck panel could remain in the test facility for months at a time, thereby allowing researchers to study the long-term durability of the bridge deck panel.

3.3 Final Design

Schematics of the test facility can be seen in *Figure 3.1* and *Figure 3.2*. The facility was located on the entrance ramp of the northbound weigh station. It consisted of a reinforced (portland cement) concrete slab-on-grade with a retaining curb (made from high early strength

grout) that spanned the entire perimeter of the test pit. The purpose of the curb was to retain the open graded material beneath the existing reinforced concrete (RC) panels (*Figure 3.1*). Another feature of the test pit was a PVC pipe (*Figure 3.1*) that drained excess water from the test pit.

Three W10X45 support beams (AISC, 1994a) rested on the RC slab (*Figure 3.3*) and were held in place with ¾-inch-diameter hooked anchor-rods (AISC, 1994b) that were embedded in the concrete (*Figure 3.4*). The support beams were coped at each end so they would fit in between the retaining curb (*Fig 3.5*). Additional anchor rods (*Figure 3.3*) were embedded in the concrete slab and were used to assist in mounting deflection instrumentation (discussed further in Chapter 4).

The support beams supported the FRP deck as well as two 15-feet 3-inch long steel access panels (constructed from I-beams and plates [*Figure 3.6*]) that were positioned on each side of the deck (*Figure 3.7*). The steel panels allowed access into the test pit for visual inspection of the deck and permitted installation of deflection instrumentation beneath the deck. The FRP deck was fastened at two locations on each support (*Figure 3.8*) using A325 ¾-inch bolts with A563 nuts (AISC, 1994b). *Figure 3.9* shows this connection detail. The steel access panels were bolted to the top flanges of the supports at nine locations (*Figure 3.10*). The connection detail for the access panels is very similar to the connection detail of the FRP deck. The nuts for the access-panel connection had to be welded to the underside of the upper flanges (*Figure 3.5*) prior to connecting the panels to the supports. This was the only feasible way to fasten the bolts because there was no access—the FRP deck and steel access panels were positioned side by side—to allow for the turning of a nut beneath the steel panel.

The design of the weigh station test facility was done at Virginia Tech. *Table 3.1* contains a list of the limit states that were considered in the design.

3.4 Construction

Construction of the facility began November 1, 1999. First, the existing concrete was sawed and excavated and the drainage pipe was installed. Next, re-bar was laid down and the concrete slab was poured. Before the concrete had hardened, the anchor rods were inserted and drainage trenches were formed into the concrete using a masonry trowel. Twenty-four hours later, the retaining curb was poured and the ends of the support beams were coped. While the curb was being poured, instrumentation trenches were dug and instrumentation conduit was laid down.

After laying down the instrumentation conduit, the instrumentation boxes (made of polymer concrete) were installed and the conduit was fitted to the ends of the boxes.

After the curb formwork was removed, the support beams were lowered into the pit and fastened to the anchor rods. Next, holes were drilled into the top and bottom flanges of the steel panels. The purpose of drilling holes in the tops of the panels was to allow access for inserting bolts into the bottom-flange holes.

Once all the holes had been drilled in the access panels, the FRP deck and access panels were lowered onto the support beams. The steel panels were then used as templates to mark the hole locations for the access-panel connections on the support beams. Once these holes had been marked, the steel panels were removed while the FRP deck remained on the support beams. The holes for the FRP deck connections were then marked on the support beams and the FRP deck lifted from the test pit.

All holes were then drilled in the support beams and the nuts for the access-panel connections were welded to the underside of the support-beam flanges. Next, the FRP deck and steel panels were fastened to the support beams (with the FRP deck being connected first). Finally, a skid-resistant wearing surface was applied to the steel panels.

The weigh station was closed for the duration of construction, and was re-opened on Thursday, November 11. A summary of the construction schedule can be seen in *Table 3.2*.

3.5 Tables and Figures

Table 3.1 Summary of limit states considered in design of weigh station test facility

Component and/or connection	Limit state(s)
reinforced concrete slab	•flexure •shear •bearing (from steel supports)
RC slab-to-beam connection	•pull-out of anchor rods •tensile rupture of anchor rods
support beams	•compression yielding of web •web crippling
support-to-deck connections	•tensile rupture of fasteners
support-to-steel panel connections	•tensile rupture of fasteners
steel access panels	•flexure •shear •local buckling of web •weld rupture (top-plate-to-flange connection)

Table 3.2 Summary of construction schedule for the weigh station testing facility

Date	Construction Tasks
Nov 1	•demolition and excavation of test pit •installation of drain pipe
Nov 3	•laid down re-bar •poured concrete slab •inserted anchor rods •formed drainage trenches
Nov 4	•poured concrete curb •coped ends of support beams •drilled holes in bottom flanges of supports and fastened supports to anchor rods •dug trenches and laid down instrumentation conduits •installed polymer-concrete instrumentation box
Nov 5	•drilled holes in top and bottom of steel panels •drill holes in top flanges of supports •weld nuts to underside of support flanges
Nov 8	•fastened FRP deck to supports •fastened steel panels to supports
Nov 11	•applied wearing surface to steel panels •re-opened weigh station

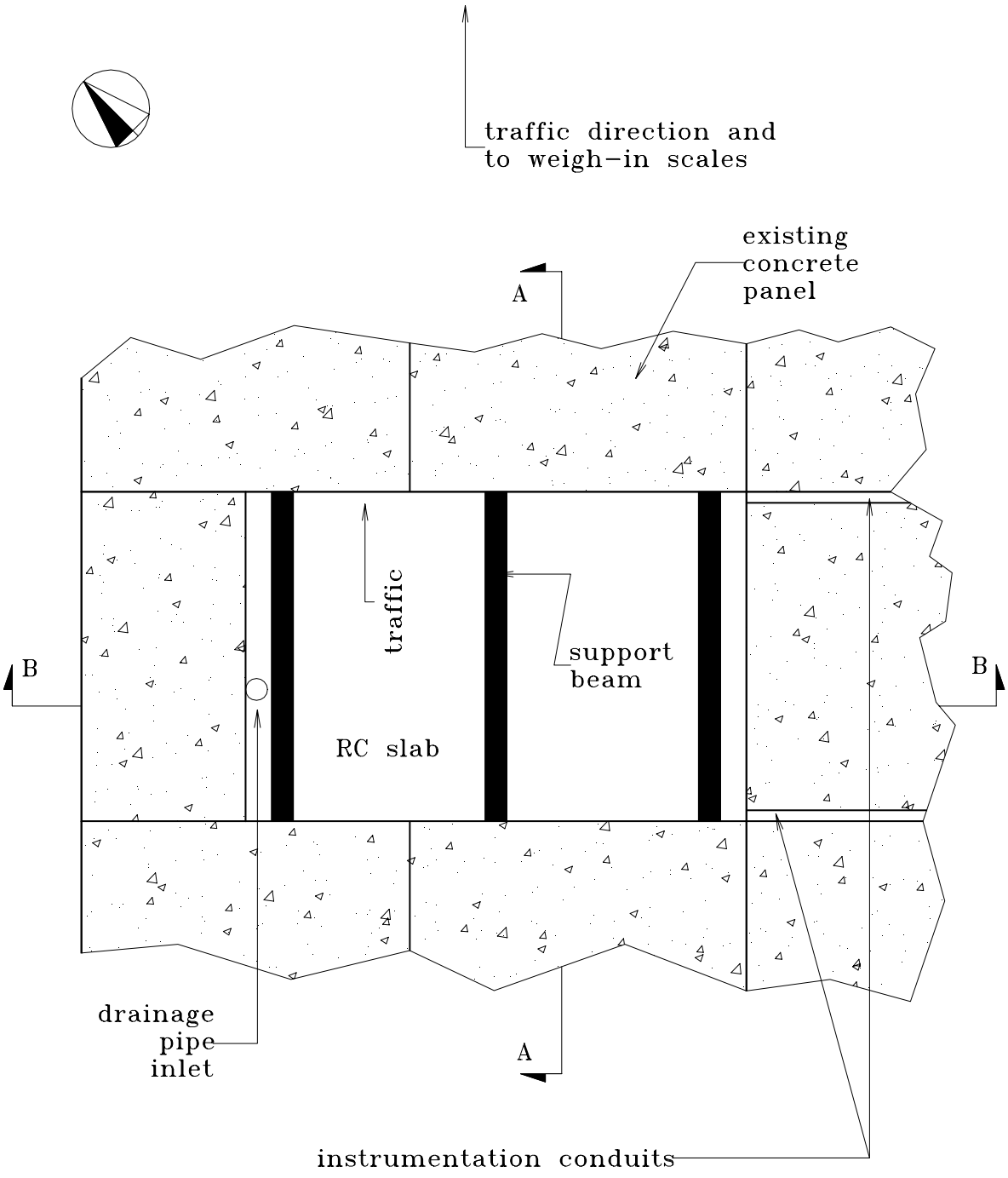

Figure 3.1 Plan view of the weigh station testing facility (FRP deck and steel access panels not shown)

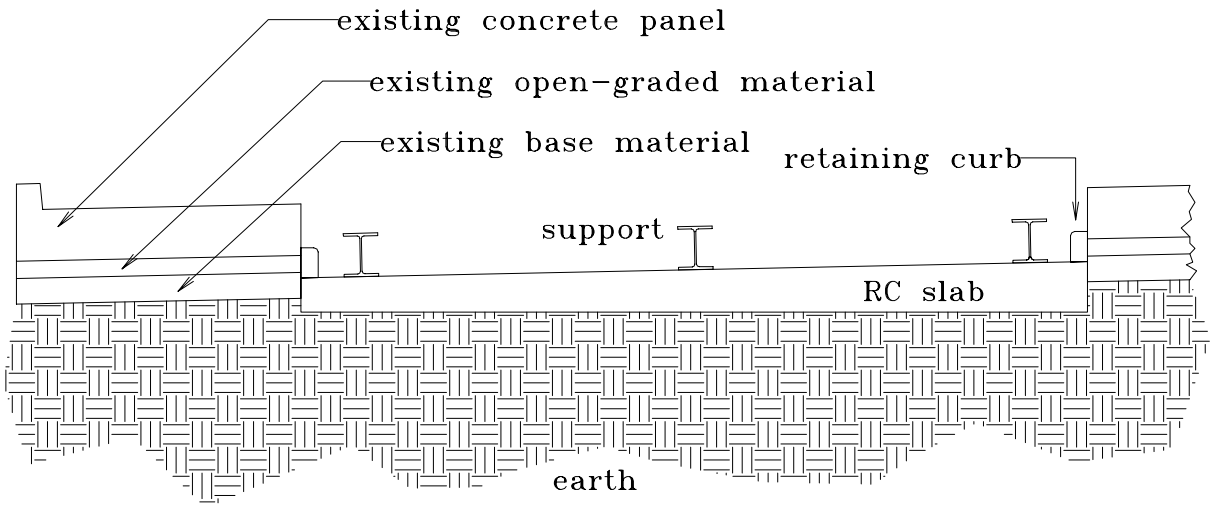

Notes:
1. drainage pipe not shown
2. drainage trenches not shown
3. anchor rods not shown
4. traffic moving "into paper"

Figure 3.2 Section B-B (from Figure 3.1) of the weigh station testing facility

Figure 3.3 Weigh station test pit, showing supports and anchor rods

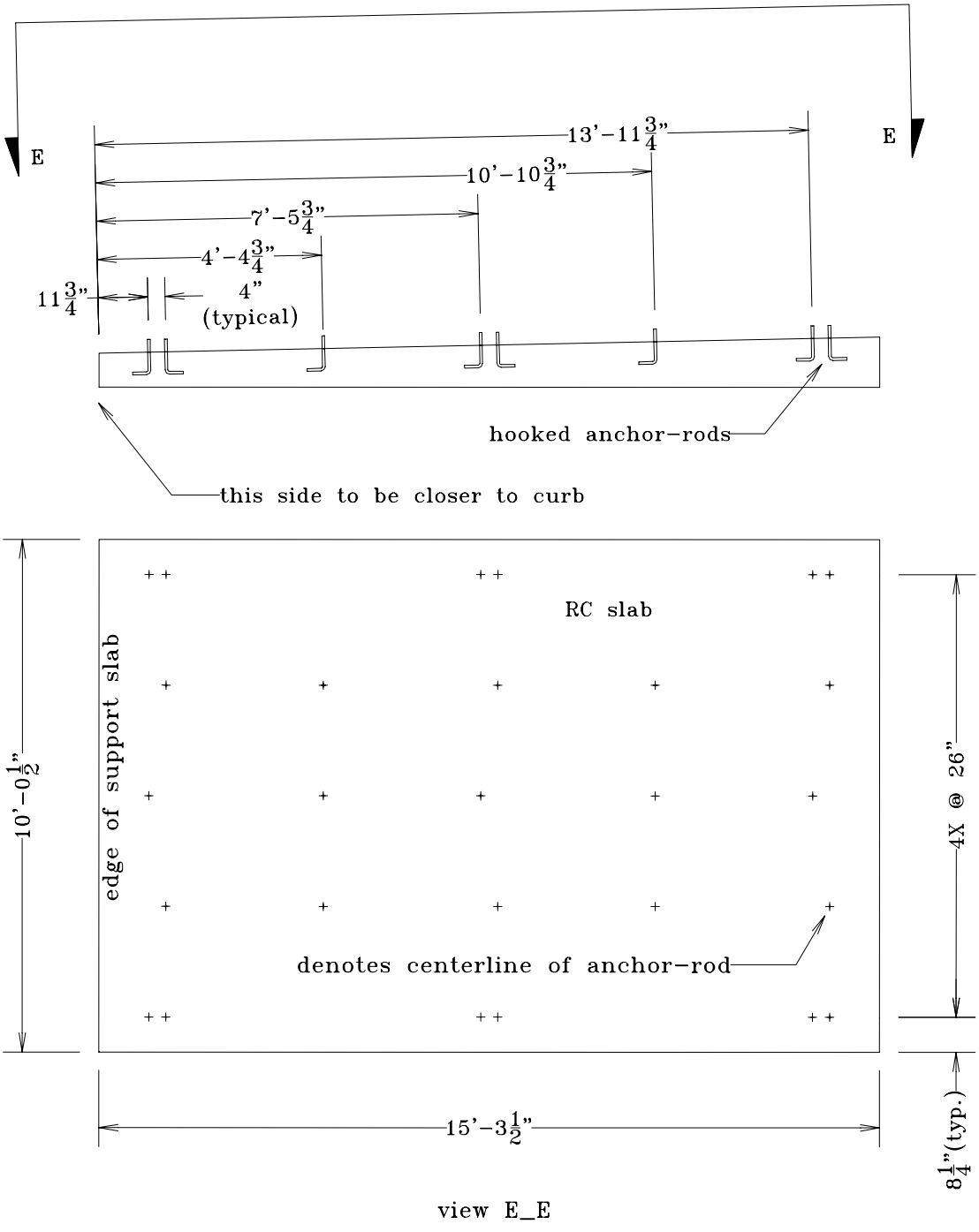

Figure 3.4 Location of anchor rods

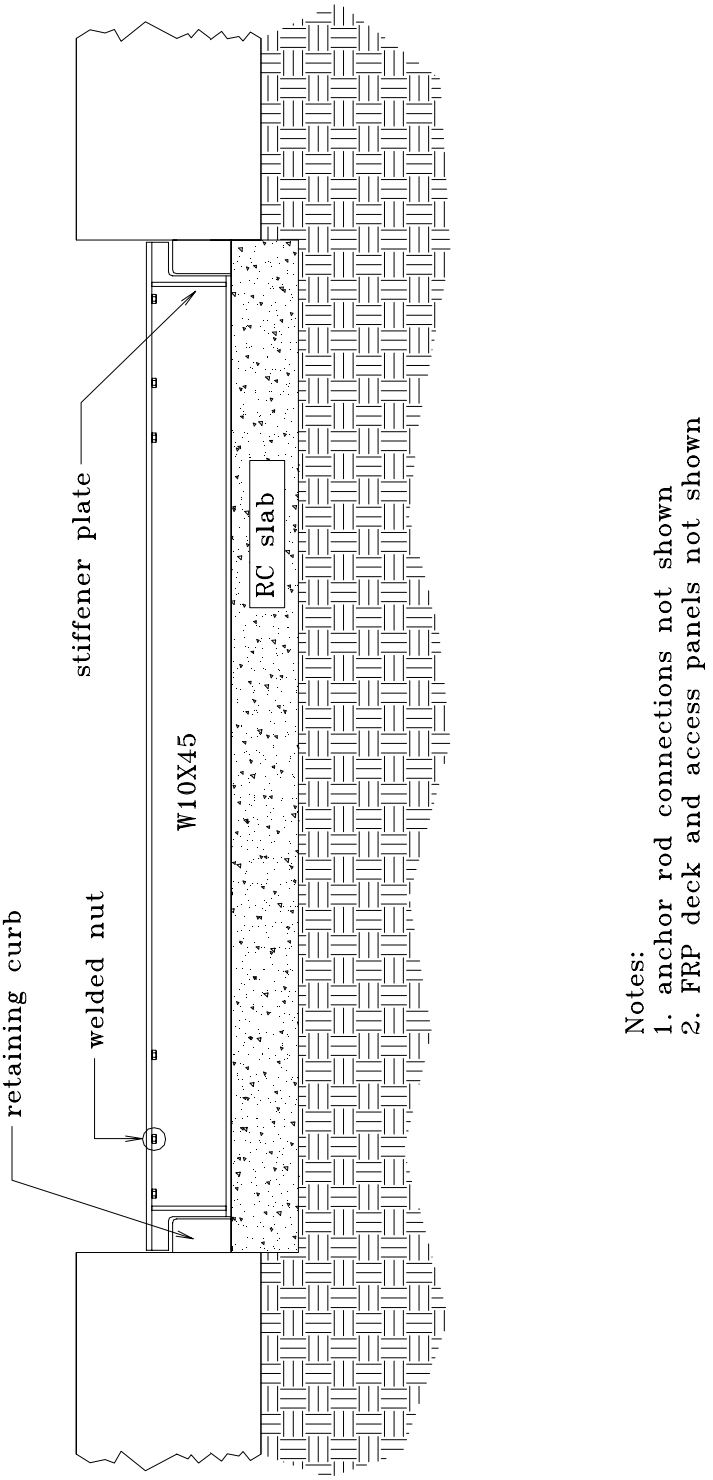

Figure 3.5 Section A-A (from Figure 3.1) of the weigh station testing facility

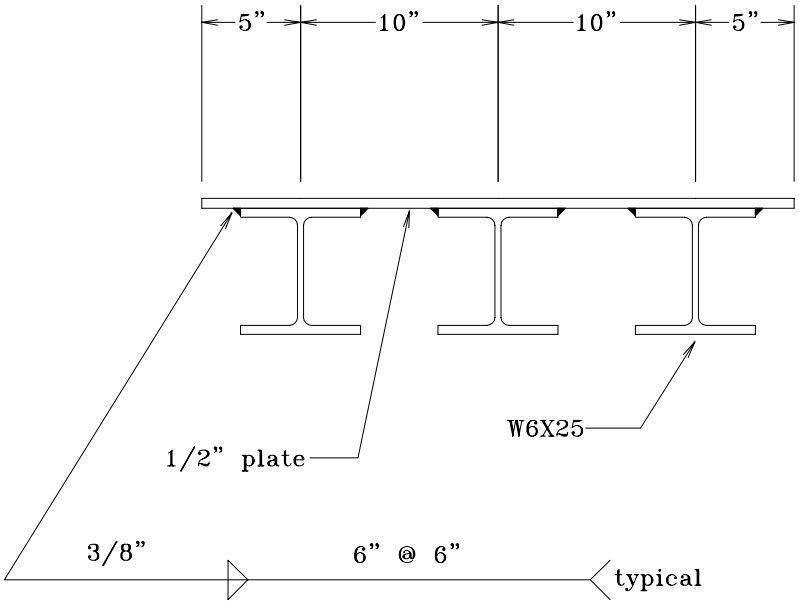

Figure 3.6 End view of a steel access panel

Figure 3.7 FRP Deck and steel access panels (weigh station test facility)

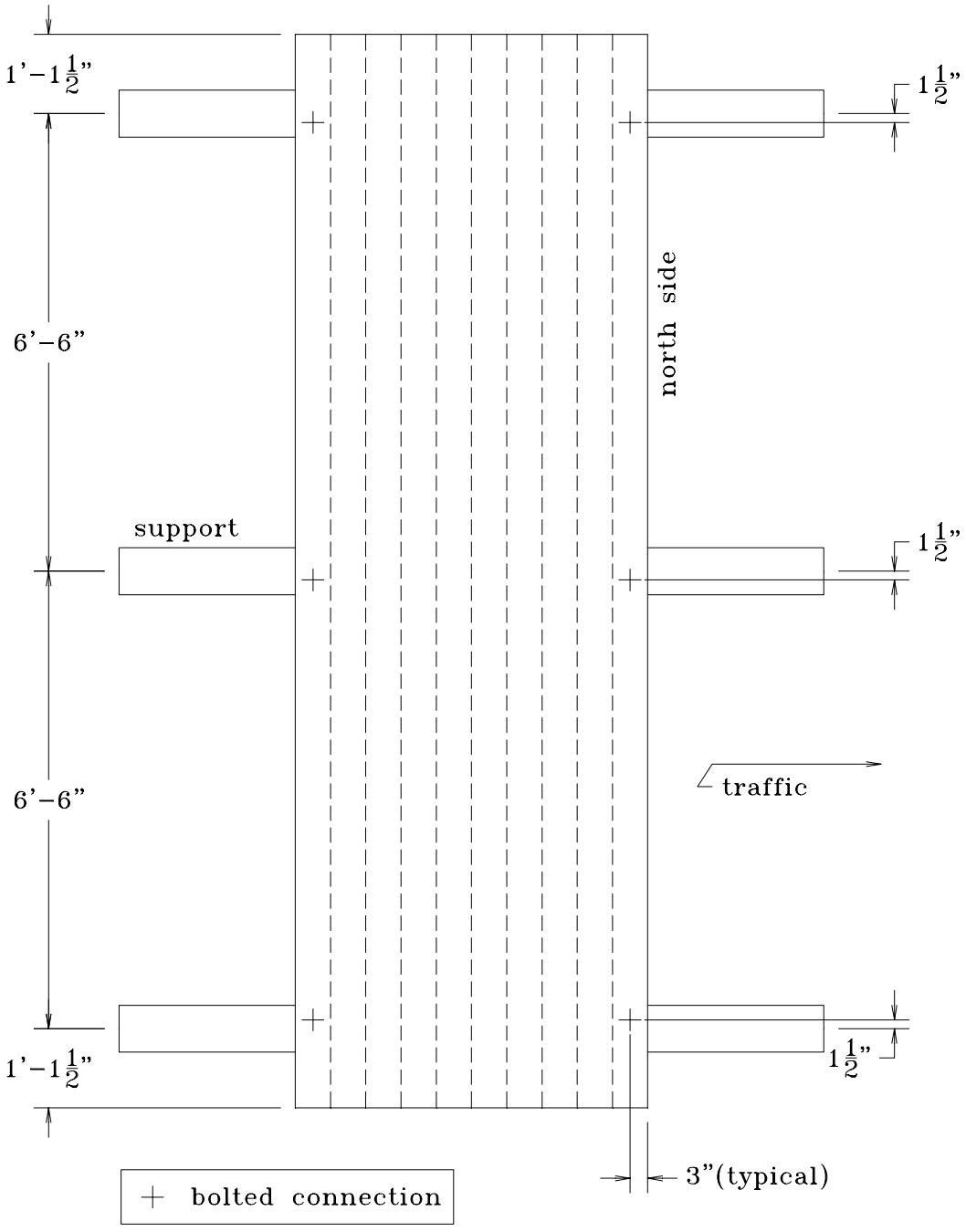

Notes:
(1) supports not shown beneath FRP deck for clarity
(2) steel access panels not shown
(3) outline of test pit not shown

Figure 3.8 Layout of FRP-deck-to-supports connections

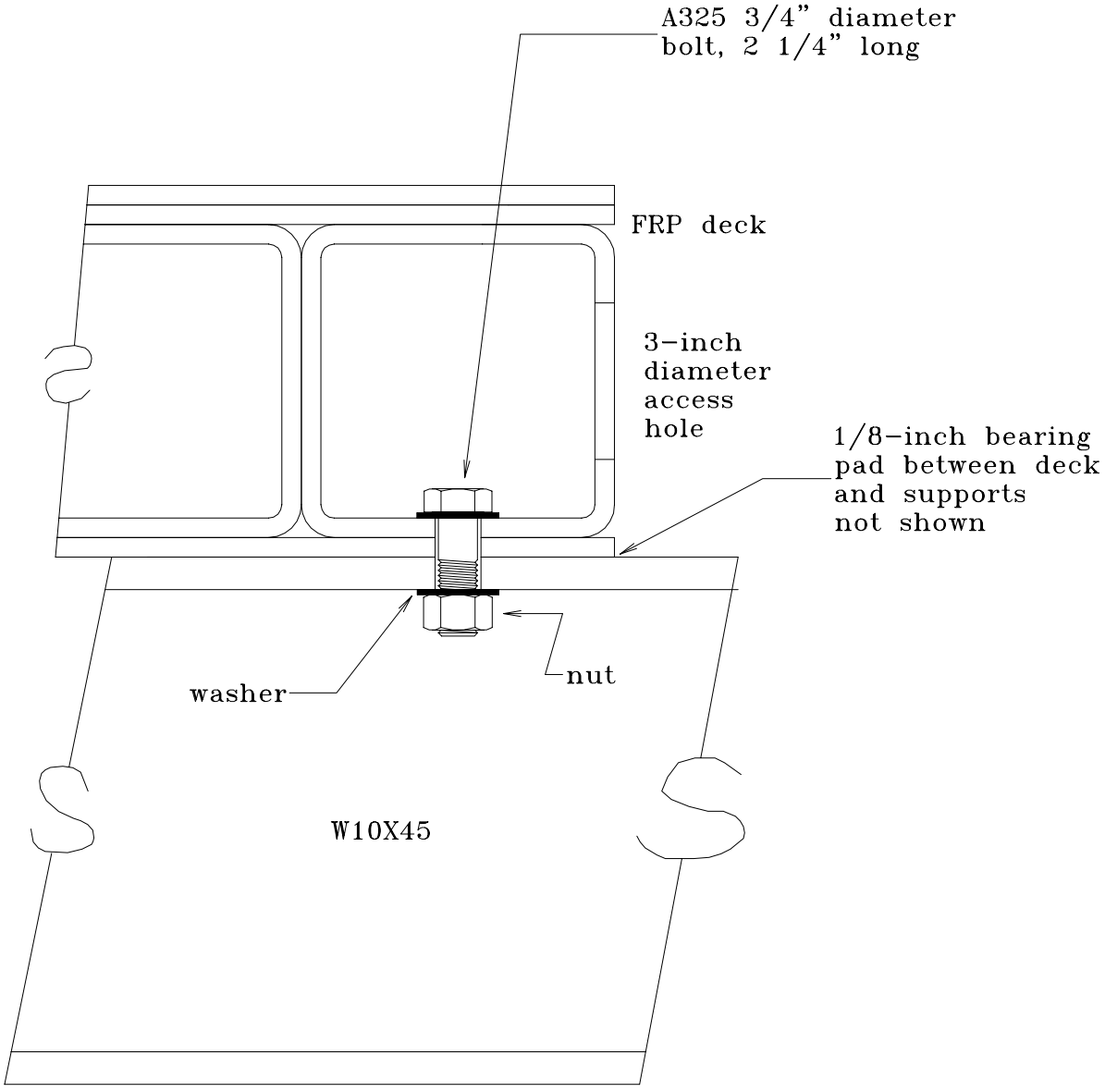

Figure 3.9 FRP-deck-to-support connection detail

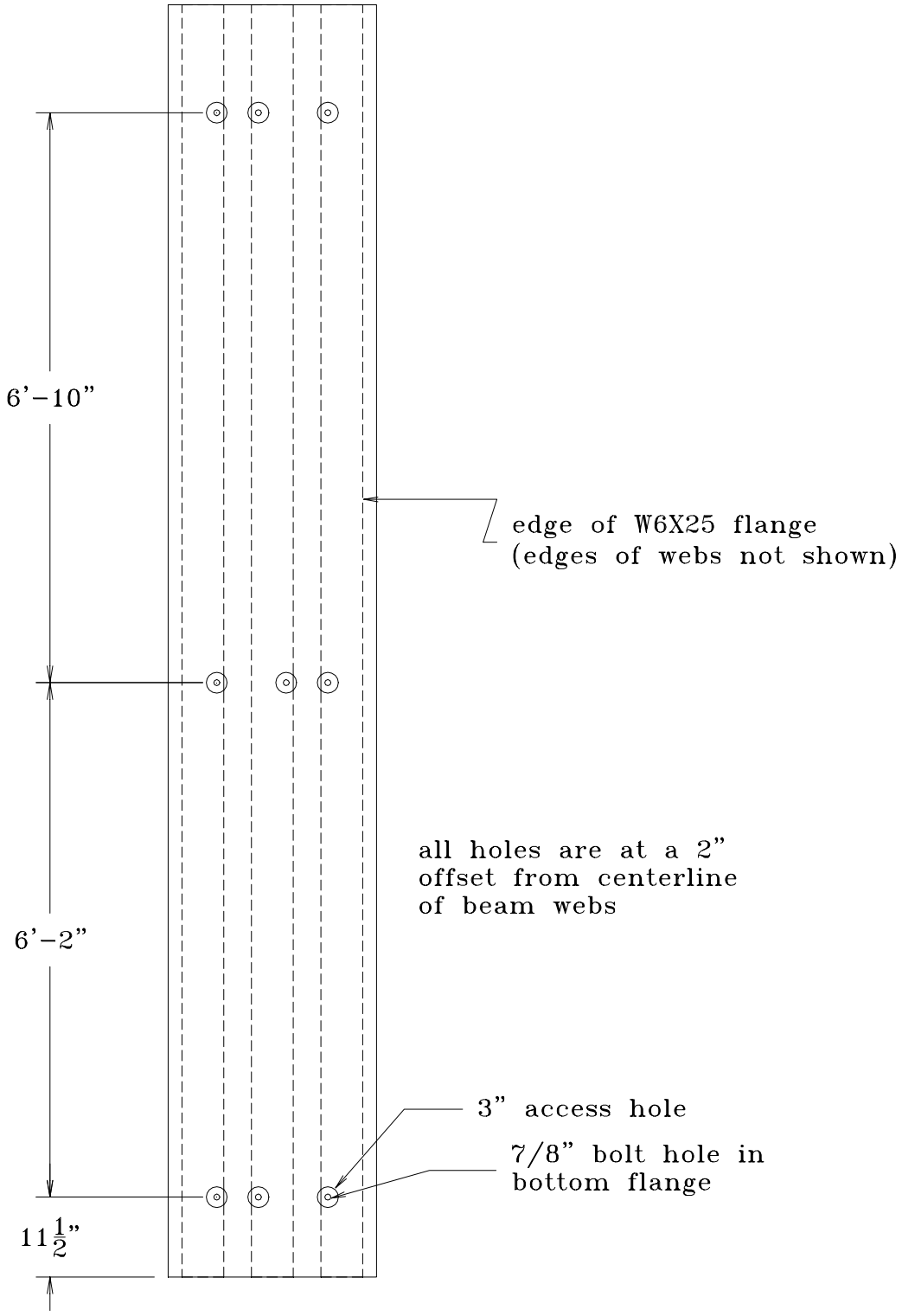

Figure 3.10 Plan view of steel access panel

Chapter 4: Experimental Testing Program

4.1 Introduction

Two FRP decks were tested—Deck 1 and Deck 2. For Deck 1, four sets of stiffness tests were run, followed by two strength tests (one on each span of the deck). The stiffness tests consisted of loading the deck to a predetermined load, whereas the strength tests consisted of loading the deck to failure.

For Deck 2, four different sets of "pre-field" stiffness tests were run, followed by the installation of the deck in the weigh station test facility. While at the weigh station, two sets of field tests were conducted (on two separate occasions) as well as periodic inspections. After removing Deck 2 from the weigh station, four sets of "post-field" stiffness tests were conducted; the pattern of loading for the four tests was identical to the "pre-field" stiffness tests. Finally, two strength tests—one on each span of the deck—were conducted. A summary of the test program for each deck is contained in *Table 4.*1, and *Figure 4.1* shows a timeline of all events associated with Deck 2.

4.2 Laboratory Test Setup

Similar test setups were used for all of the laboratory tests. Each deck was supported by three W18X40 steel beams (AISC, 1994, Vol. I), each spaced 6 feet 6 inches apart (*Figure 4.2*). Deck 1 was fastened to the supports using ½-inch diameter A325 bolts. *Figure 4.3* shows the locations of each bolted connection while *Figure 4.4* shows a detail of the connection. It was intended that the fasteners of Deck 1 would bear on the metal sleeve (*Figure 4.4*). Instead, when the fasteners were tightened, they beared directly on the FRP tube. This caused the top surface of the tube to become locally debonded from the top plate (*Figure 4.7*). Because of the apparent flaw in this connection detail, Deck 2 was fastened using ¾-inch diameter A325 bolts in a manner shown in *Figure 4.6.* The location of these connections is shown in *Figure 4.5*.

Load was applied to each deck by hydraulic cylinders that were mounted on a load frame (*Figure 4.8*). 100-kip and 400-kip hydraulic cylinders were used. Hydraulic fluid was delivered to the cylinders by either (1) an electric pump or (2) a hand pump. For those tests that utilized two cylinders, the cylinders were connected in parallel to one pump.

Load was transferred to the deck through a stack of steel plates (*Figures 4.9, 4.18, and 4.19*) that were welded together. The base plate of this assembly measured 11 inches (traffic direction) by 20 inches. The base plate dimensions represented the tire contact area of an HS25 wheel plus impact (26 kips) as specified in AASHTO (1998, Section 3.6.1.2.5). The purpose of welding two steel plates to the base plate was to stiffen the base plate so that bending of the base plate was minimized during loading, thereby ensuring a nearly uniform distribution of load over the base plate contact area.

Neoprene rubber pads were inserted in-between the steel plate and the surface of the deck to prevent the steel plate from locally damaging the wearing surface of the deck during testing. The combination of the steel plate resting on neoprene rubber pads will herein be referred to as a "tire patch".

4.3 Instrumentation

4.3.1 Introduction

Instrumentation was located over eight distinct locations (in plan view) of the deck. These eight locations were given names based on compass directions (*Figure 4.10*). The compass directions corresponded to the *intended* orientation of Deck 1 and the *actual* orientation of Deck 2 at the weigh station test sight.

Strains were measured using ¼-inch long, uniaxial electrical resistance strain gages, model number CEA-13-250UW-350 by Measurements Group, Inc. Deflections recorded during the laboratory tests were measured using cable-extension position transducers (model PT101 by Celesco Transducer Products, Inc.), also referred to as "wirepots".

Deflections recorded during Field Test 2 were measured using "deflectometers" made at Virginia Tech. Each deflectometer consisted of a 1/4-inch cantilevered aluminum plate clamped between two 3/8-inch thick aluminum blocks that were bolted together. Four strain gages (adhesively bonded to the underside of the cantilevered plate) were wired to create a full bridge. A threaded rod was attached to the end of the cantilevered plate; the top of this rod made contact with the underside of the deck (*Figure 4.11*). As the deck deflected, it would push down the rod and bend the cantilevered plate, thereby inducing a change in signal measured by the full bridge of strain gages.

Load was measured with dog-bone-shaped strain gage load cells made at Virginia Tech. A summary of the instrumentation that was used during each test is presented in *Table 4.1*.

4.3.2 Deck 1

Strain gages were not used in Tests 1 through 5. One longitudinal strain gage was used in Test 6. It was positioned on the underside of the bottom plate at the west region (strain gage designation BP_W_L, *Figure 4.14*). If a strain gage is designated as "longitudinal", it means that the gage measured strain in the longitudinal direction (as defined in *Figure 4.10*).

Wirepots were used in all tests. *Figure 4.15* shows (1) the location of each wirepot and (2) the designation given to each wirepot. *Table 4.1* indicates which wirepots were "active" for each test. If a particular wirepot was classified as "active" for a particular test, it means that deflection was recorded for that particular wirepot for that particular test.

4.3.3 Deck 2

Strain gages were used for all the tests conducted on Deck 2. The gages were put on the top and bottom of the FRP tubes (prior to bonding the FRP plates to the tubes). The strain gages on the tubes measured strain in the longitudinal direction (*Figure 4.10*) of the deck. Additional strain gages were put on the underside of the bottom plates. Half of these gages were oriented such that they would measure strains in the longitudinal direction while the other half were oriented such that they would measure strains in the transverse direction (*Figure 4.10*). The designation given to each gage is based on the location of the gage. For example, gage TT_E is located on the Top side of the Tubes in the East region, while gage BP_NE_L is located on the Bottom Plate in the NorthEast region, and it measures strain in the Longitudinal direction. *Figures 4.12* through *4.14* show (1) the location of each strain gage and (2) the designation given to each strain gage. The relative uncertainty of strains measured in the bottom plate was computed to be 3%. This was based on the cumulative effect of the following relative uncertainties: (1) 1% in the voltage gain (2) 1% in the excitation voltage (3) .5% in the strain gage factor (4) .15% in the alignment of the gage and (5) 2% for the shunt calibration. Shunt calibration factors were not used to adjust the strains because they were very close to 1.0. They ranged between .960 and .990, and so 2% seemed like a conservative estimate for relative uncertainty in the shunt factor.

Table 4.1 indicates which strain gages were "active" for each test. If a particular strain gage was classified as "active" for a particular test, it means that strain was recorded for that particular strain gage during that particular test.

Prior to installing Deck 2 at the weigh station test facility, the gages on the bottom plates were weatherproofed using M-Coat F strain gaging kits made by Measurements Group, Inc. After transporting Deck 2 back into the lab for the post-field stiffness tests and strength tests, the strain gages on the bottom plate were removed and new strain gages were installed.

Deflections recorded during the laboratory tests were measured using the wirepots. *Figure 4.15* shows (1) the location of each wirepot and (2) the designation given to each wirepot. *Table 4.1* indicates which wirepots were "active" for each test. If a particular wirepot was classified as "active" for a particular test, it means that deflection was recorded for that particular wirepot for that particular test.

Deflections recorded during field tests were measured using six deflectometers. The deflectometers were located in the same six positions as the wirepots were located in the laboratory (*Figure 4.15*).

4.4 Laboratory Testing Program

4.4.1 Introduction

For Deck 1, four stiffness tests were conducted, followed by two strength tests. Prior to installing Deck 2 at the weigh station test site, four "pre-field" stiffness tests (similar to the Deck 1 stiffness tests) were conducted. After removing the deck from the weigh station, four "post-field" stiffness tests (identical loading pattern to the "pre-field" tests) were conducted, followed by two strength tests.

Table 4.1 shows which tire patches were "active" for each test, while *Figure 4.16* shows the location of the tire patches. If a tire patch is listed in the "active" column in *Table 4.1*, it means that this particular patch was loaded during a test. If two tire patches were designated as "active", it means they were loaded (simultaneously) to the same load.

The location of the tire patches, as well as the determination of which patches would be loaded in each test, was not arbitrary. For example, the intent of simultaneously loading the East and West tire patches was to simulate an axle loading. The axle of an AASHTO design truck has its wheels spaced 6 feet apart; however, the East and West tire patches were spaced 6 feet 6

inches apart to allow each tire patch to be placed in the middle of each span. With each tire patch positioned in the middle of each span, it was expected that the deck would experience higher strains (over the middle support) compared with tire patches spaced 6 feet apart. The orientation of the tire patches in other tests were selected to investigate the expected "worst-case" scenarios with respect to strains and deflections. These other orientations, and the reasoning behind each orientation, are shown in *Figure 4.17*. Cases (b) and (d) in *Figure 4.17* could not be duplicated in the testing of Deck 2 because the load frame would not accommodate hydraulic cylinders that were positioned directly over the edges of the FRP deck.

4.4.2 Stiffness Tests

The stiffness tests for each deck were conducted in a similar manner. Three of the tests will be discussed briefly (to serve as illustrative examples), while the reader can reference *Table 4.1* for the details related to the other stiffness tests.

For Test 1 of Deck 1, the SE tire patch was loaded monotonically to 10 kips (*Figure 4.18*), after which the load was removed. This was done in every test and for a number of reasons: (1) to ensure that all sensors (strain gages, wirepots, and load cells) were generating output (2) to ensure that there were no loose connections in the system (3) to observe the deck's behavior before advancing to higher loads.

After loading to 10 kips and unloading, the tire patch was loaded to 26 kips, which was the equivalent of an HS25 wheel plus impact (20 kips plus 30%). During the test, data from the sensors was recorded. *Table 4.1* lists which sensors were "active" for each test.

For Test 2 of Deck 1, the SE and SW tire patches were each loaded to 10 kips, and then unloaded. Next, each tire patch was simultaneously loaded to 26 kips (using two hydraulic cylinders connected in parallel) while sensor data was recorded.

For Test 2 of Deck 2, the NE and SE tire patches were each loaded to 10 kips, after which the load was removed. Then the tire patches were each loaded to 26 kips while sensor data was recorded. Load was delivered from one hydraulic cylinder to the tire patches by a spreader beam (*Figure 4.19*). Test 4 of Deck 2 was the only other test where a spreader beam was used.

Two runs were conducted for every stiffness test. In every one of those tests, the results of the second run were virtually identical to the results of the second test. Therefore, in the context of this paper, no distinction will be made between the first and second run of any test.

4.4.3 Strength Tests

For the first strength test of Deck 1 (Test 5), load was applied to the E tire patch. The tire patch was loaded to 10 kips in the first cycle—by definition, a load cycle consisted of loading the deck to a specified level, and then back to zero. For the second (and final) cycle, the author had intended to load the deck to failure, but the capacity of the hydraulic cylinder (100 kips) was reached before failure of the deck had occurred.

For the second strength test of Deck 1(Test 6), load was applied to the W tire patch. Several cycles of load were applied to the deck (summarized in *Table 4.2*) prior to failure of the deck (Cycle 10).

For the first strength test of Deck 2 (Test 9), load was applied to the E tire patch, while for the second strength test of Deck 2 (Test 10), load was applied to the SW tire patch. Several cycles of load were applied in each test (*Table 4.2*) prior to failure of each span of the deck.

Upon completion of Test 9 and Test 10 of Deck 2, the deck was sawed into pieces, and pictures were taken to assess damage and to assess the failure mode(s).

4.5 Field Test Program

4.5.1 Field Test 1

The first test at the weigh station facility was conducted on December 16, 1999 (approximately 1 month after installation of Deck 2). Prior to testing, the FRP deck and steel access panels were visually inspected as trucks traveled over the test facility towards the weigh-in scales. Once it was clear that the deck and the access panels were behaving as expected (based on the visual inspection), strains were recorded (*Table 4.1*) for 124 truck crossings. The purpose of this exercise was to (1) gain some knowledge of the in-service strains in the deck (under normal truck traffic) and (2) to ensure that these in-service strains were well below the ultimate strain of the FRP.

Most of the trucks appeared to be crossing over the deck such that the left and right wheel lines were located slightly east of the west and center supports, respectively (*Figure 4.20*). It was felt that this axle location was not producing the highest possible strains in the deck. Therefore, a traffic cone was positioned to divert the trucks so that they would travel over the middle of the deck (i.e. each wheel line positioned approximately in the middle of each span), thereby inducing

the maximum possible strains in the FRP deck. This was done for ten trucks (truck crossings 60 through 69). From this point on, these ten truck crossings will be referred to as the bias truck crossings, while the other 114 crossings will be referred to as the random truck crossings.

4.5.2 Field Test 2

The second field test was conducted on April 13, 2000 after closing the weigh station for the day. The testing consisted of having a VDOT dump truck—the weight and axle spacing of the truck were known (*Figure 4.21*)—make several truck crossings over the FRP deck. Six sets of tests were conducted, with each test set consisting of 5-7 test runs. For each test set, the truck traveled (in the same direction as the normal truck traffic) over a different location of the deck. Lines were marked on the deck (using spray paint) that served as "wheel paths" for the truck to follow as it was driven over the deck. *Figure 4.22* shows the orientation of the front axle of the dump truck for each of the six test sets. *Table 4.3* contains a summary of the six sets of tests. In *Table 4.3*, if the column titled "Description" contains an entry of "O.K.", it means that the truck was driven accurately over the painted lines of the deck. If the entry is other than "O.K." it means that the truck was off-center of the painted lines. Data was only used from the test runs that were described as "O.K." in *Table 4.3*.

Test sets 1 through 4 and test set 6 were essentially static tests—the truck was traveling less than 5 mile per hour—whereas test set 5 consisted of "speed runs" in which the truck was traveling at 15 miles per hour. It was intended that the truck travel over the deck at approximately 40 miles per hour—the posted speed requirement at the weigh station—but this was impossible because of two concrete barriers that were within 50 feet of the test facility. These barriers prevented the truck from backing up far enough from the deck to allow the truck to accelerate up to 40 miles per hour by the time it crossed over the deck. During each truck crossing, strains and deflections were recorded (*Table 4.1*).

4.6 Tables and Figures

Table 4.1 Summary of test program

Deck 1			
Test Description	Active Tire Patches	Active Strain Gages	Active Deflection Sensors
1 service-load	SE	N.M.	WP_SE
2 service-load	SE, SW	N.M.	WP_SE, WP_SW
3 service-load	E	N.M.	WP_E
4 service load	E,W	N.M.	WP_E, WP_W
5 strength	E	N.M.	WP_E
6 strength	W	BP_E_L	WP_W
Deck 2			
Test Description	Active Tire Patches	Active Strain Gages	Active Deflection Sensors
1 “pre-field” service load	E	TT, BT, and BP_L	WP_SE, WP_E, WP_NE
2 “pre-field” service load	NE, SE	TT, BT, and BP_L	WP_SE, WP_E, WP_NE
3 “pre-field” service load	E, W	TT, BT, and BP_L	WP_E, WP_W, WP_SE
4 “pre-field” service load	NW, SW	TT, BT, and BP_L	WP_W, WP_SW
Field Test 1	N.A.	All gages	N.M.
Field Test 2	N.A. (see *Table 4.3*)	All gages	All deflectometers
5 “post-field” service load	E	BP_L, BP_T	WP_SE, WP_E, WP_NE
6 “post-field” service load	NE, SE	BP_L, BP_T	WP_SE, WP_E, WP_NE
7 “post-field” service load	E, W	BP_L, BP_T	WP_SE, WP_E, WP_NE, WP_SW, WP_W, WP_NW
8 “post-field” service load	NW, SW	BP_L, BP_T	WP_NW, WP_W, WP_SW
9 strength	E	BP_L, BP_T	WP_SE, WP_E, WP_NE
10 strength	SW	BP_L, BP_T	WP_SW, WP_W, WP_NW

N.M. = not measured
N.A. = not applicable
BP_E_L = strain gage on bottom plate, at east region, measuring strain in the longitudinal direction
TT = strain gages on the top surface of the tubes
BT = strain gages on bottom surface of the tubes
BP_L = all strain gages on the bottom plate that measure strain in the longitudinal direction
BP_T = all strain gages on the bottom plate that measure strain in the transverse direction

Table 4.2 Test program for laboratory strength tests (Deck 1 and Deck 2)

Deck 1		
Test	Cycle	Peak Load (kips)
5	1	approximately 100
6	1	15
	2	25
	3	35
	4	45
	5	55
	6	70
	7	80
	8	90
	9	100
	10	failure
	11	residual strength
Deck 2		
Test	Cycle	Peak Load (kips)
9	1	25
	2	50
	3	75
	4	100
	5	failure
10	1	25
	2	50
	3	failure
	4	residual strength

Table 4.3 Summary of tests conducted for Field Test 2

Run #	Test Set	Description
1	1 – "centered"; static test	east, half a wheel width
2		east, one wheel width
3		O.K.
4		O.K.
5		west, one wheel width
6		O.K.
7		west, half a wheel width
8	2 – 1-foot east-of-center; static test	east, one wheel width
9		O.K.
10		east, one wheel width
11		west, half a wheel width
12		O.K.
13		O.K.
14		O.K.
15	3 – 1-foot west-of-center; static test	east, half a wheel width
16		east, half a wheel width
17		O.K.
18		west, half a wheel width
19		O.K.
20		O.K.
21	4 – 1-foot east-of-middle support; static test	east, one wheel width
22		O.K.
23		east, half a wheel width
24		east, half a wheel width
25		O.K.
26		east, half a wheel width
27		O.K.
28	5 – "centered"; speed test	O.K.
29		O.K.
30		west, half a wheel width
31		O.K.
32		west, half a wheel width
33	6 – left wheel centered over middle of east span; static test	west, half a wheel width
34		O.K.
35		O.K.
36		O.K.
37		O.K.
See Figure 4.22 for schematic of axle crossings		

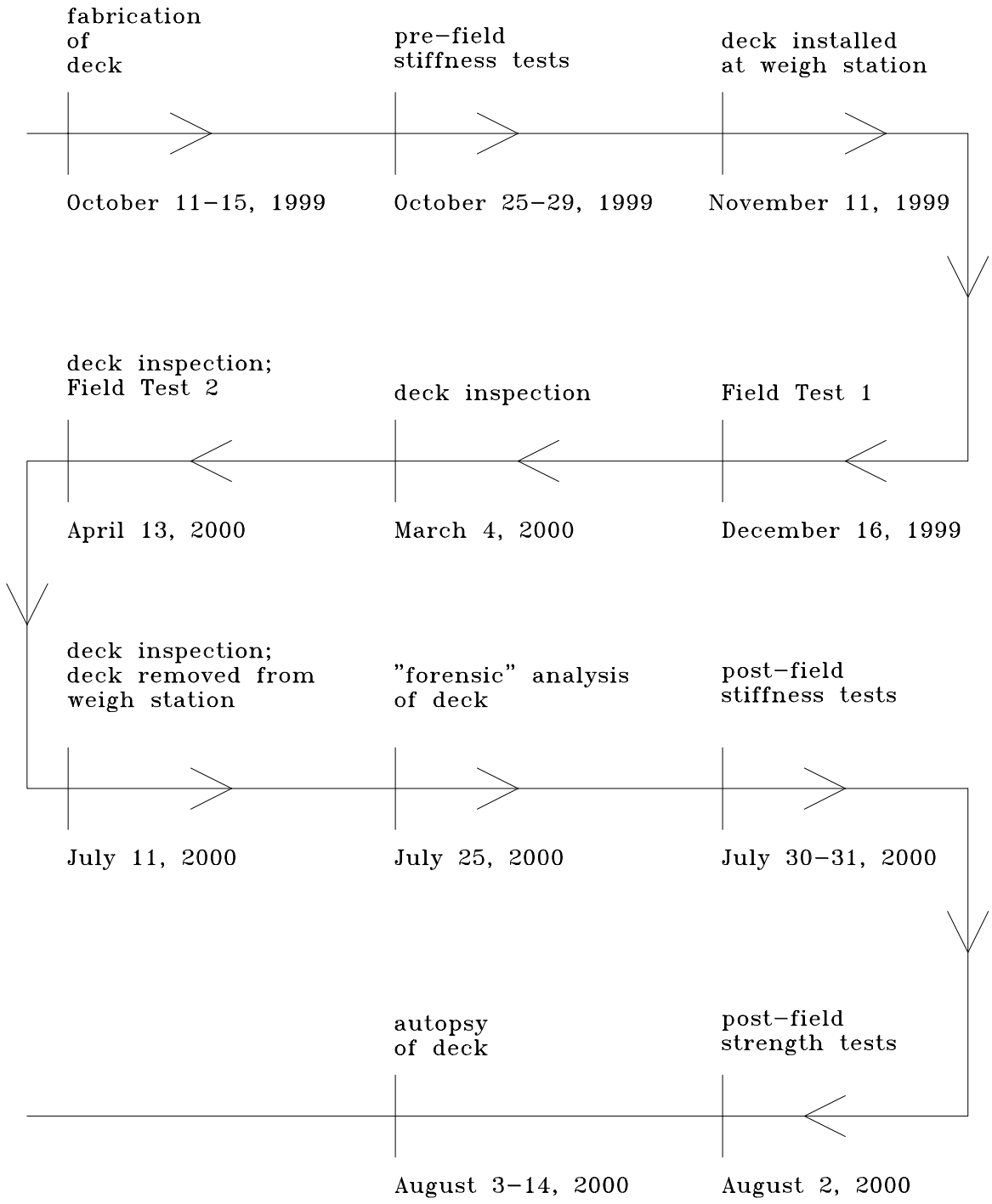

Figure 4.1 History of Deck 2

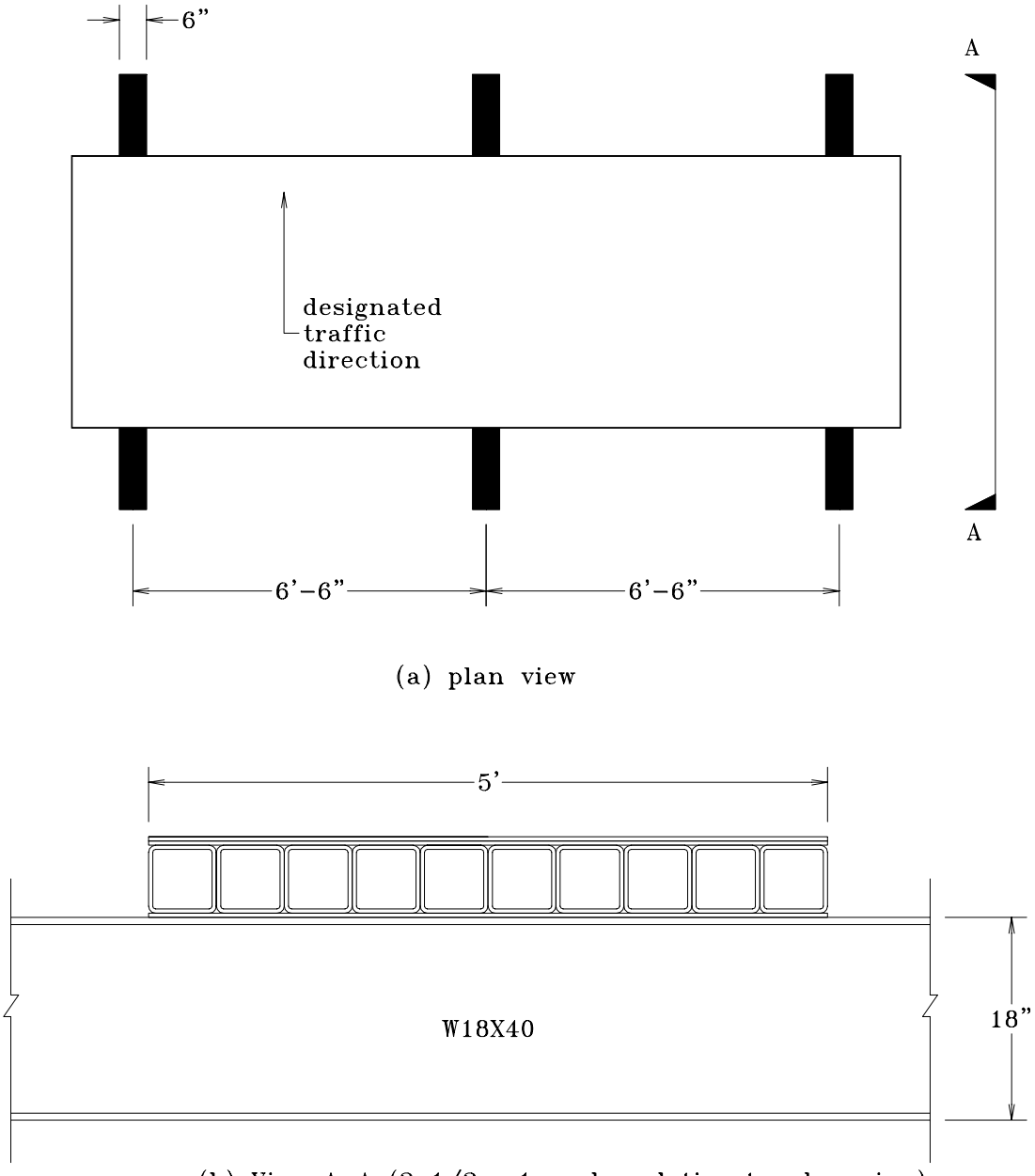

Figure 4.2 Test setup for all laboratory tests

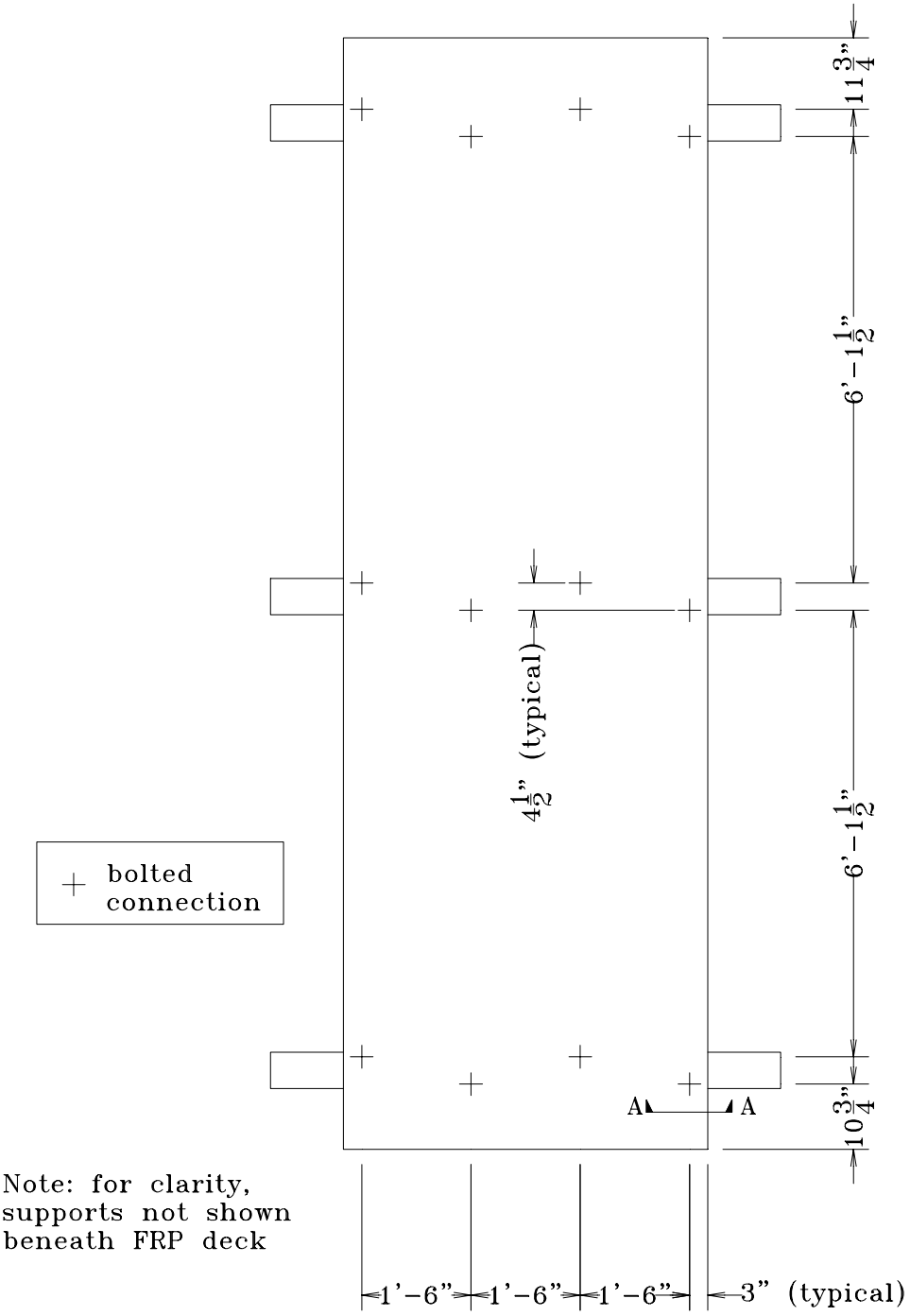

Figure 4.3 Layout of Deck 1 connections

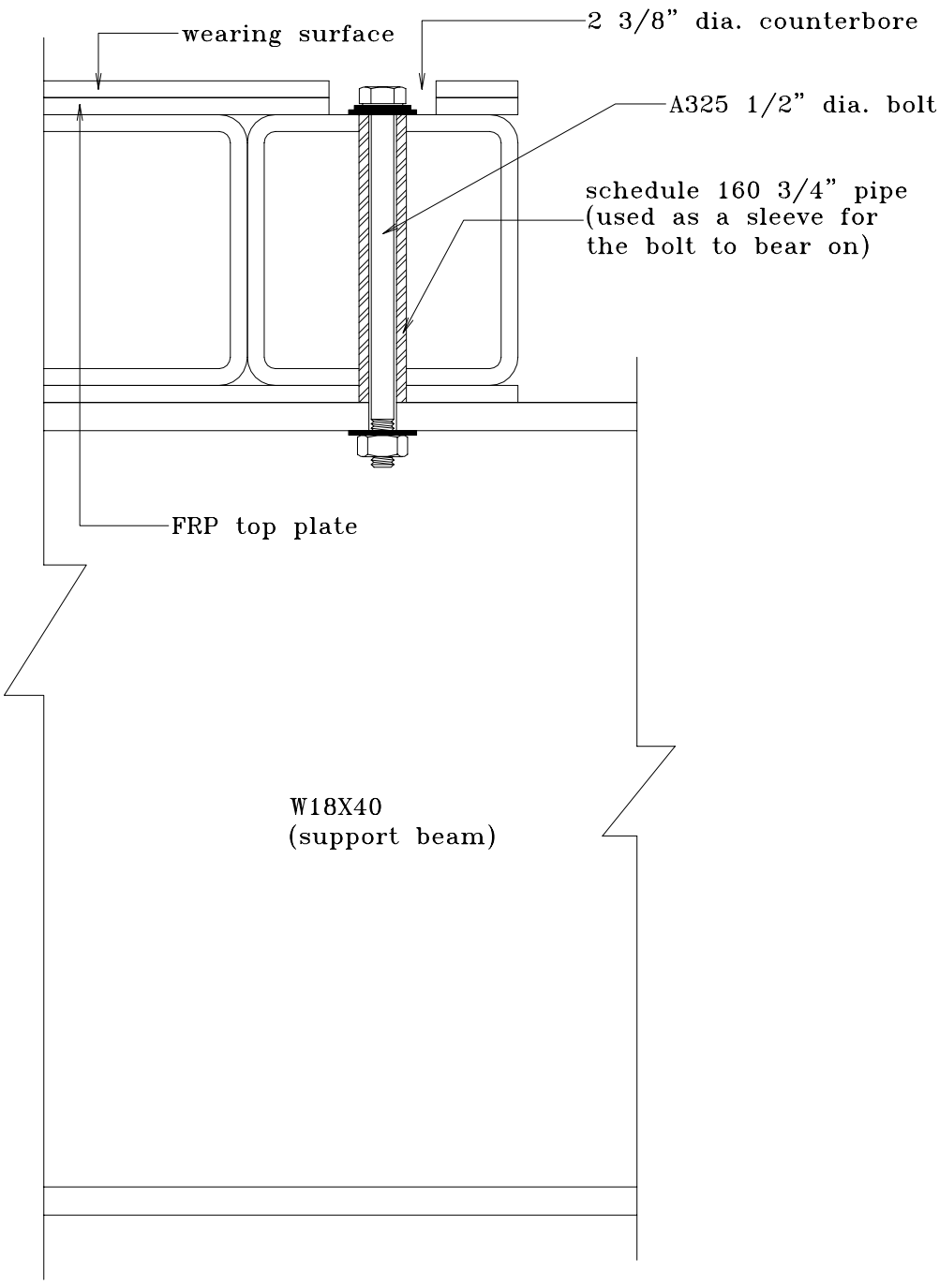

Figure 4.4 Deck 1 connection detail

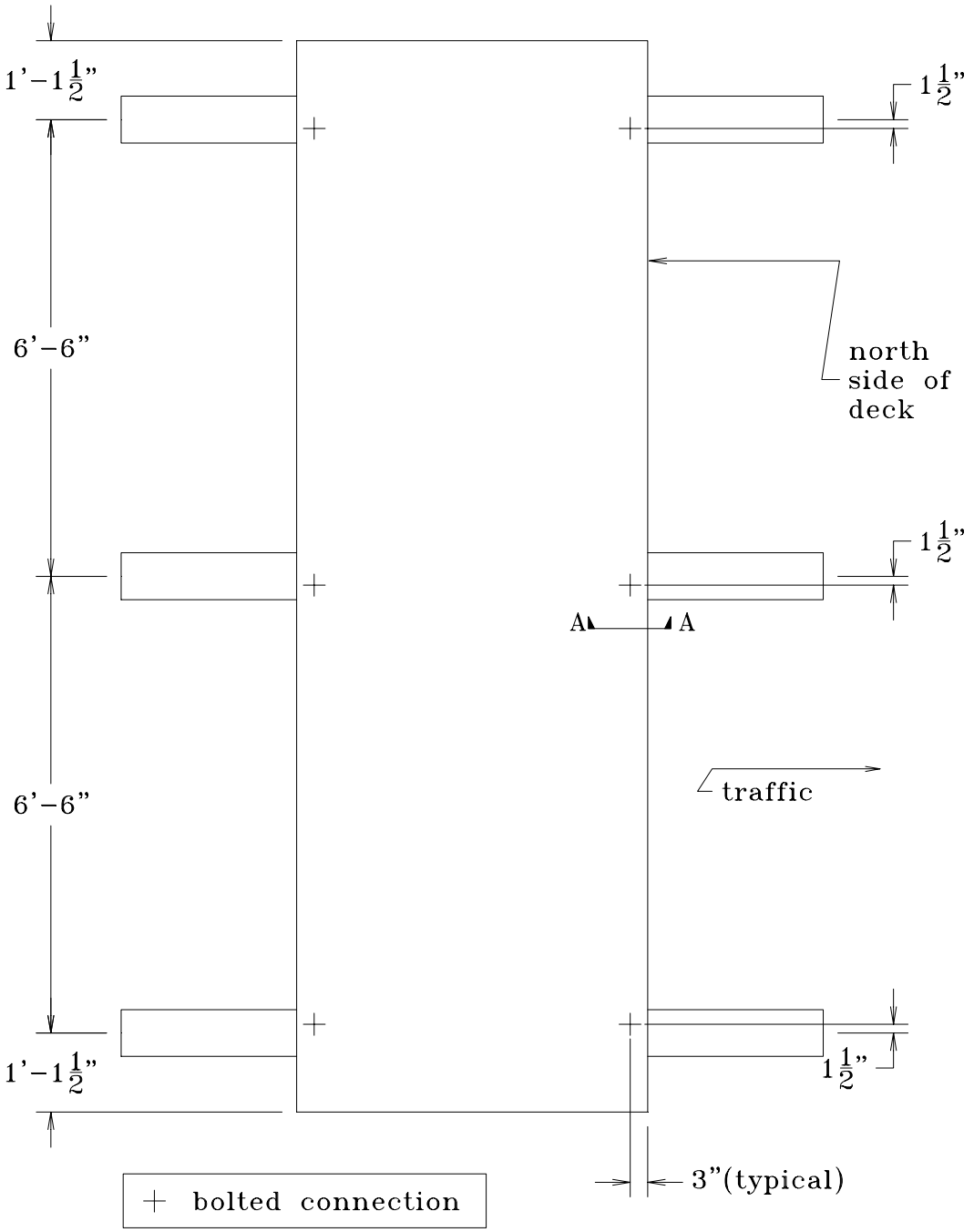

Notes:
1. For clarity, supports not shown beneath the FRP deck

Figure 4.5 Layout of Deck 2 connections

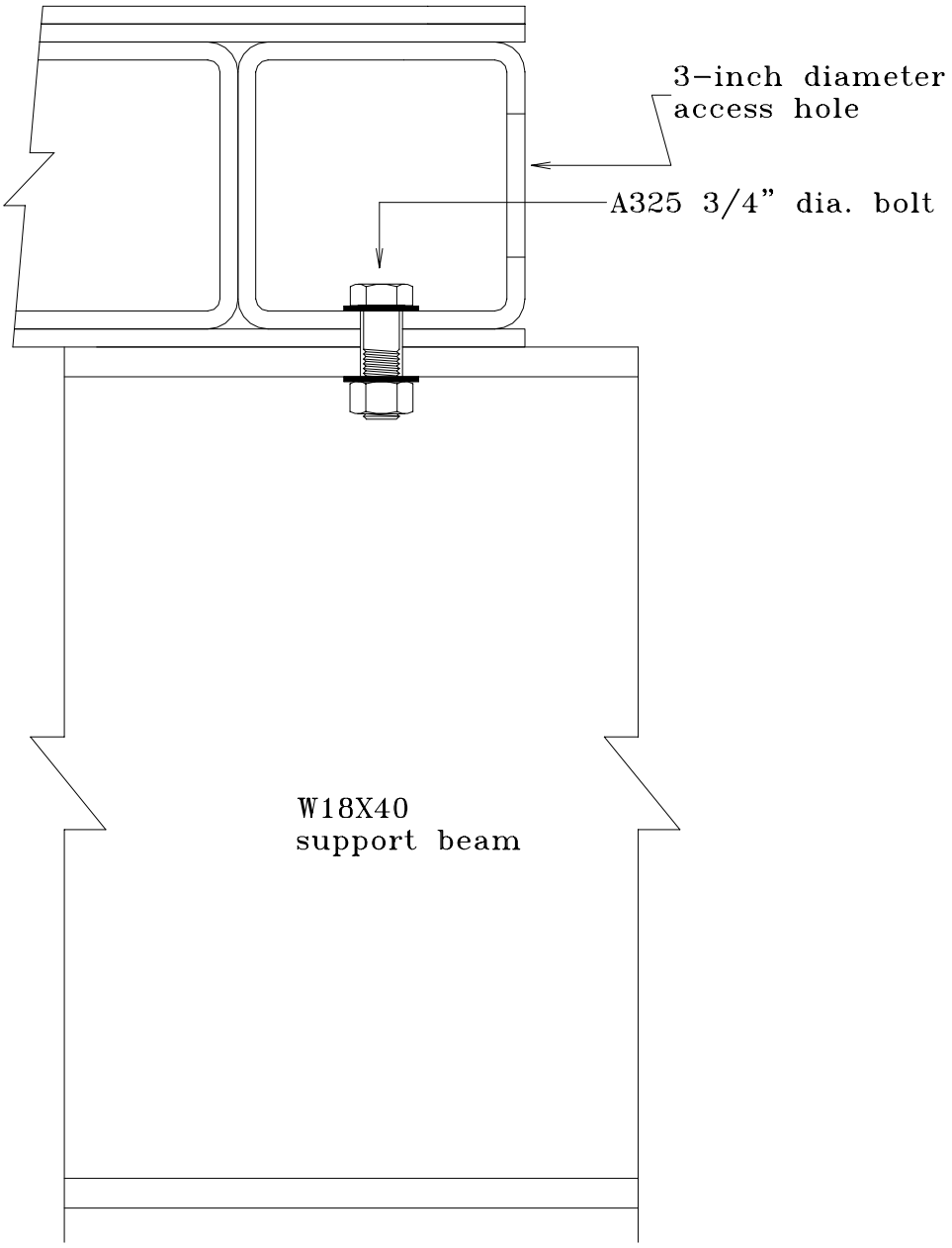

Figure 4.6 Deck 2 connection detail

Figure 4.7 Close-up of Deck 1 fastener bearing on top of FRP tube

Figure 4.8 Hydraulic cylinder mounted on a simple frame and positioned above the FRP deck

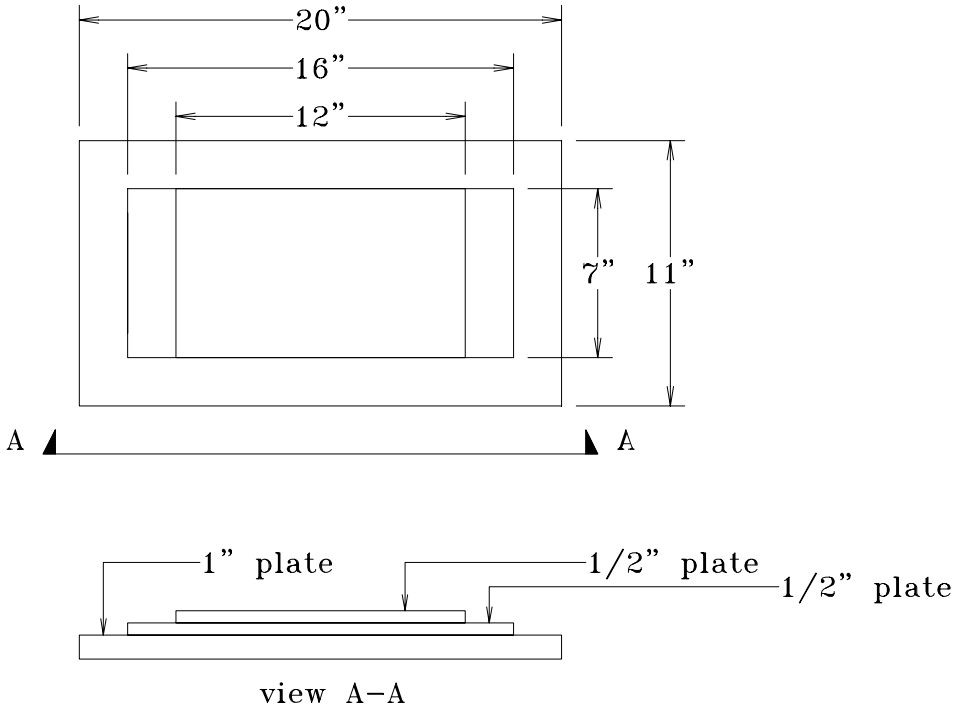

Figure 4.9 Geometry of tire patch plate

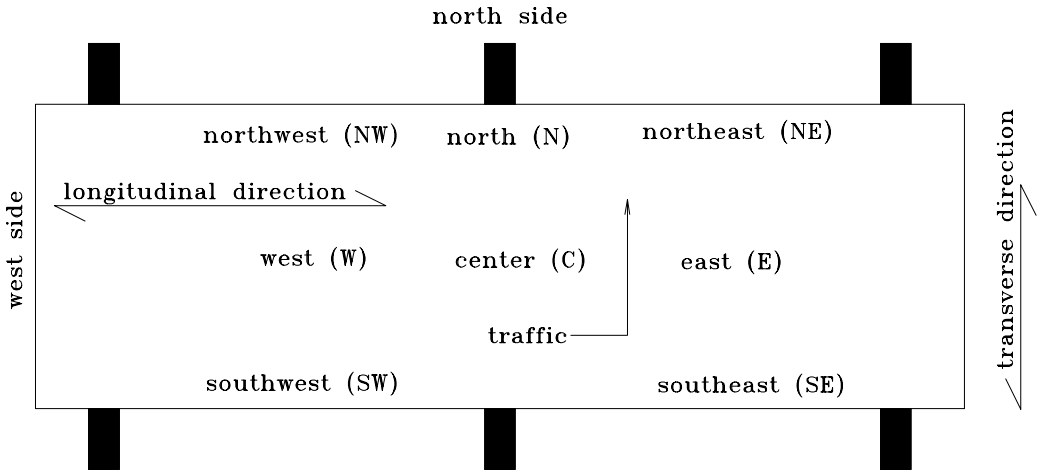

Figure 4.10 Instrumentation regions on the FRP deck

Figure 4.11 Deflectometer positioned beneath FRP deck during Field Test 2

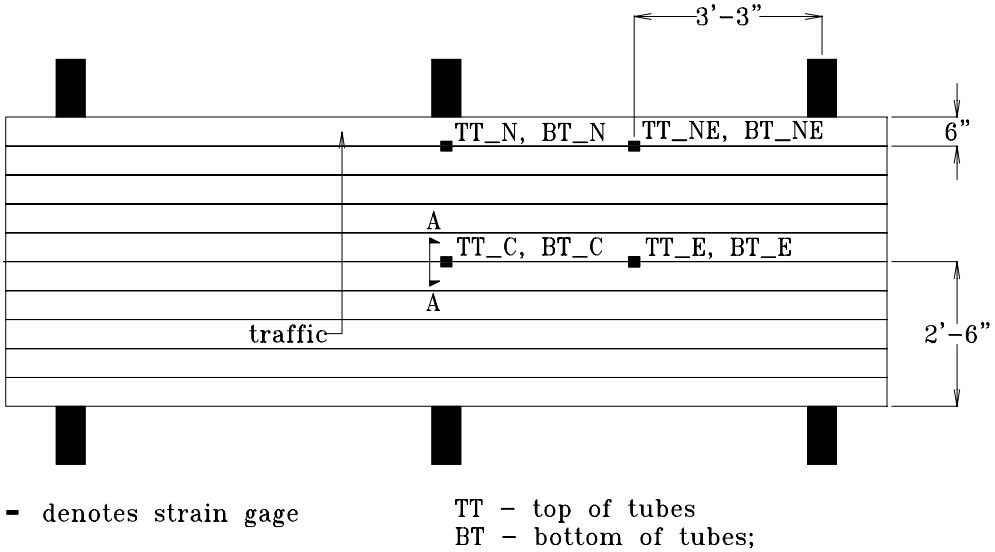

Figure 4.12 Internal strain gage layout on top and bottom of FRP tubes

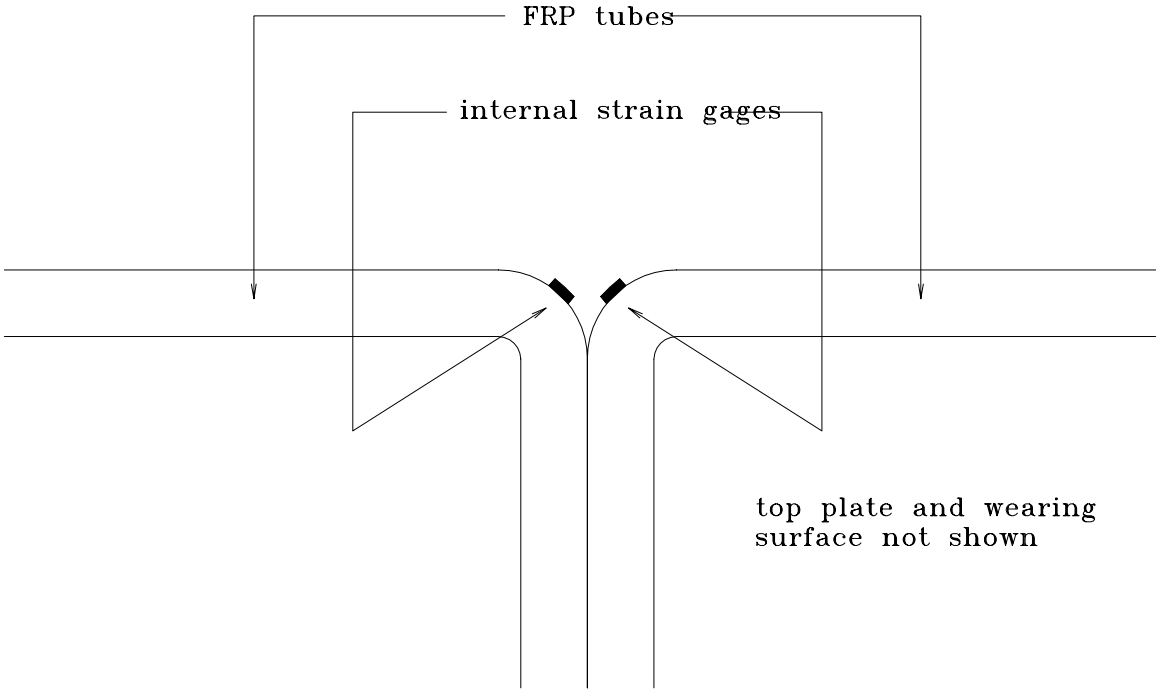

Figure 4.13 View A-A (from Figure 4.12) of internal strain gages on top surface of tubes (gage orientation on bottom surface of tubes is identical)

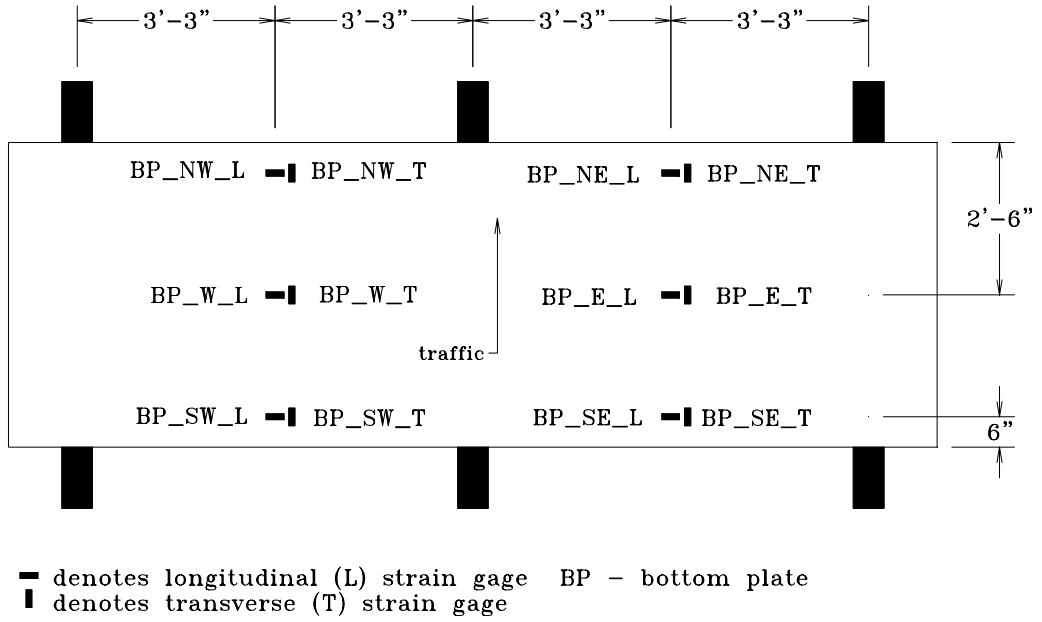

Figure 4.14 Longitudinal and transverse strain gages located on the bottom plate of the FRP deck

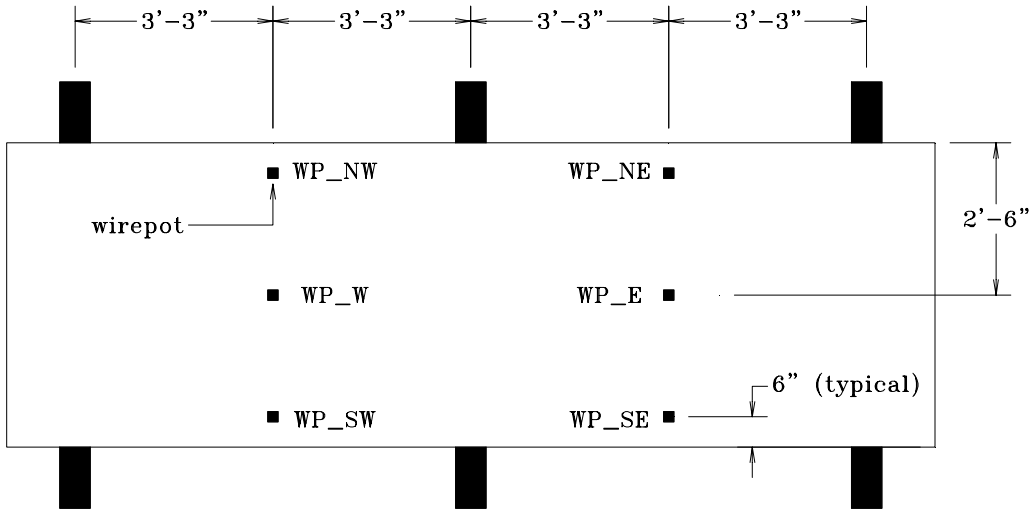

Figure 4.15 Locations and designations of deflection instrumentation (wirepots)

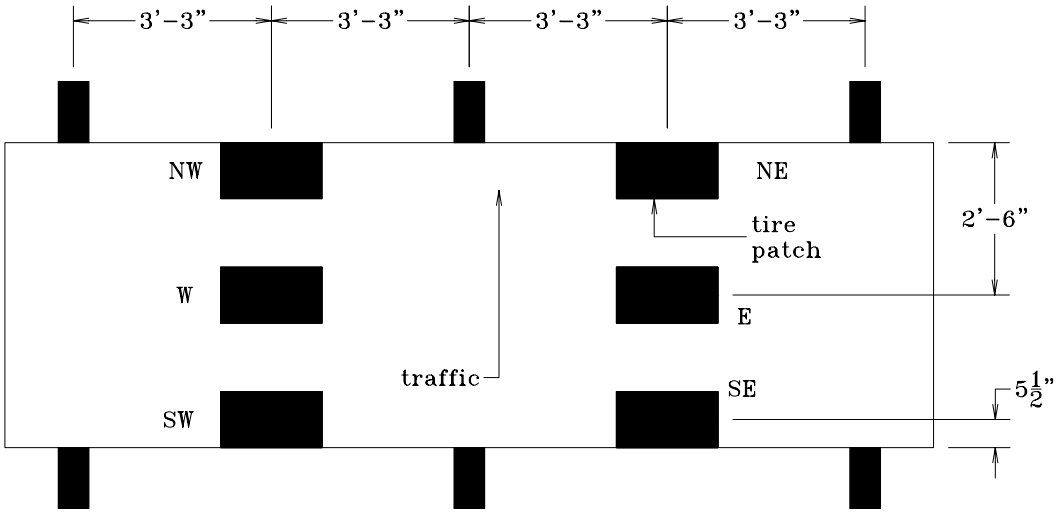

Figure 4.16 Locations and designations of tire patches

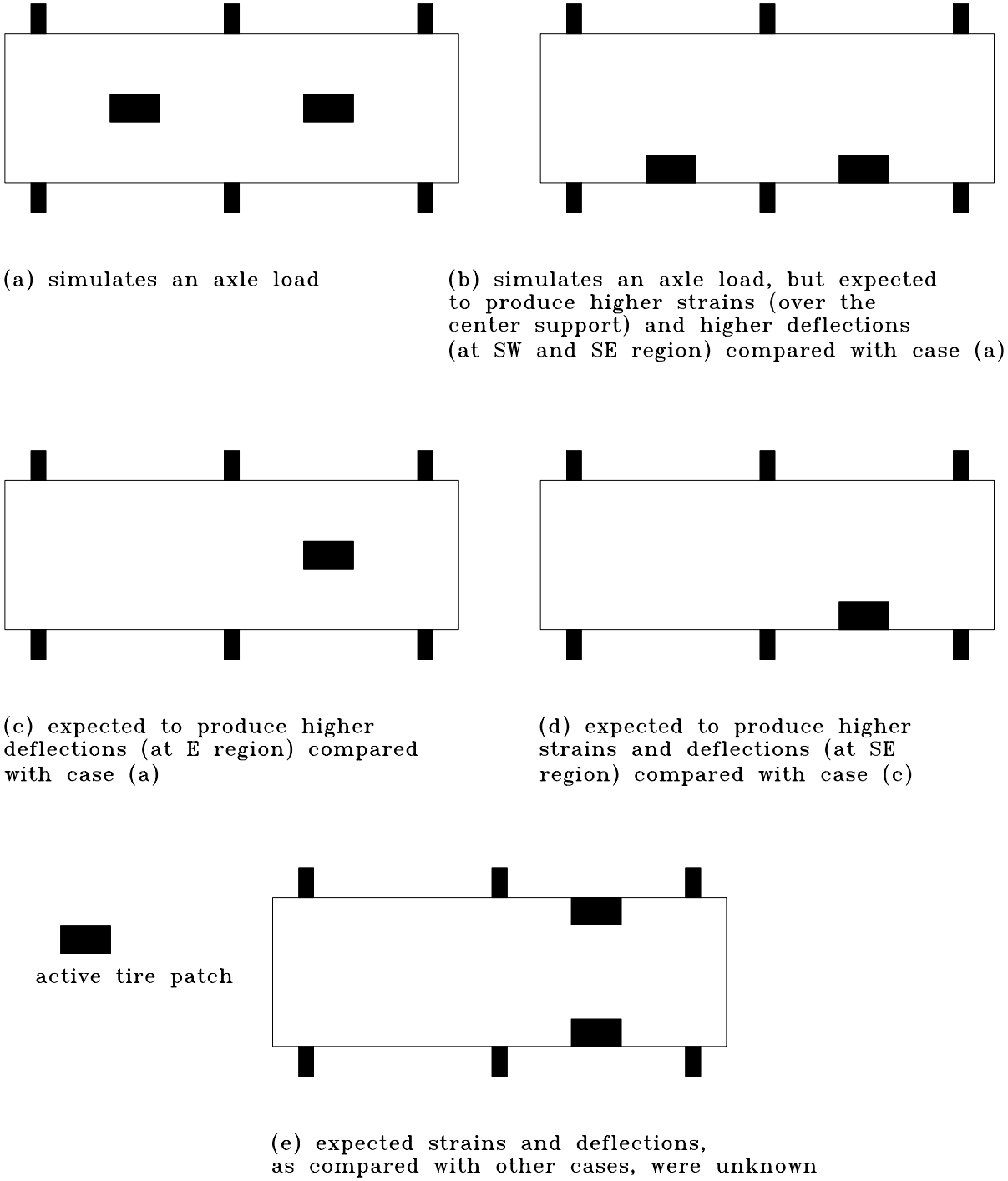

Figure 4.17 The five different loading conditions used in the laboratory stiffness tests

Figure 4.18 Single tire patch loading

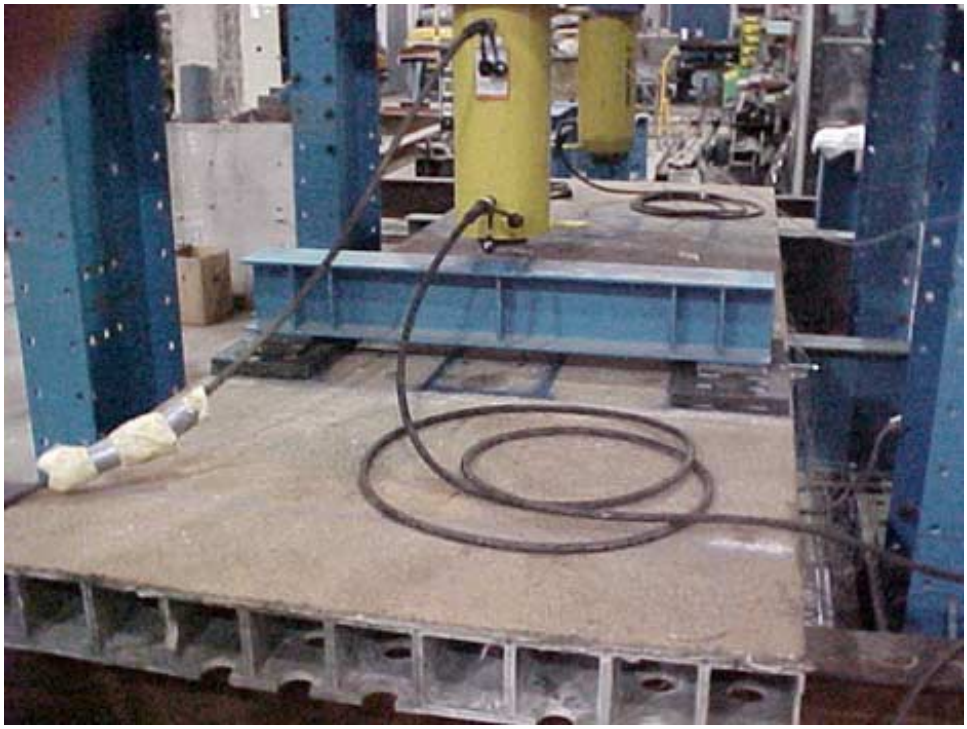

Figure 4.19 Two tire patches loaded with a spreader beam

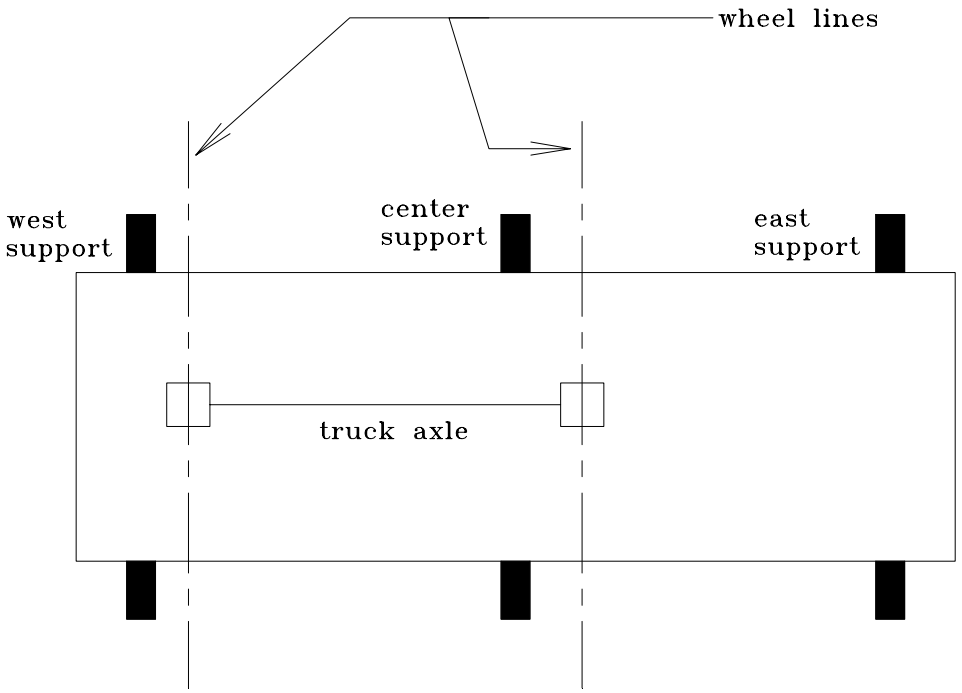

Figure 4.20 Typical orientation of truck wheel lines of random truck crossings (Field Test 1)

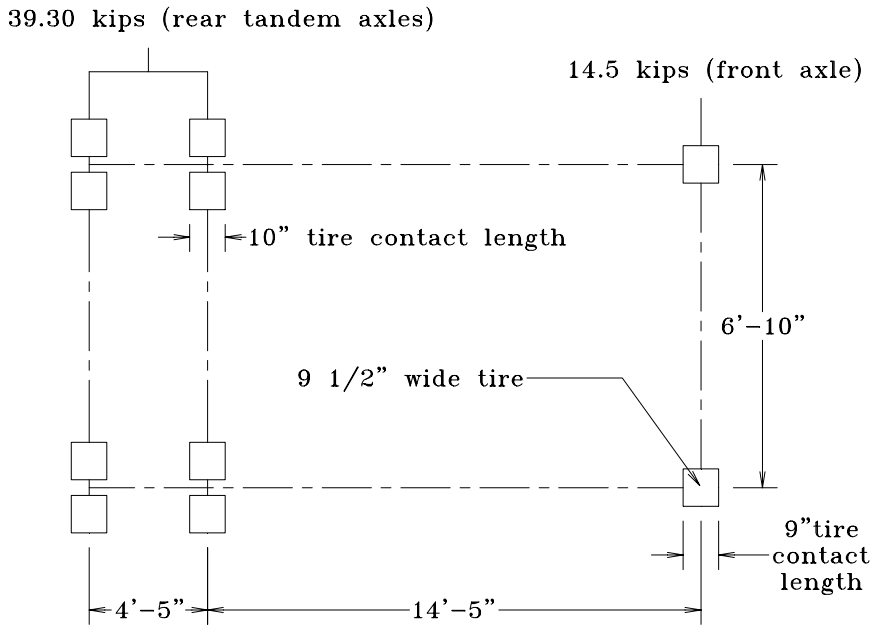

Figure 4.21 Axle weights and spacing of the VDOT dump truck used in Field Test 2

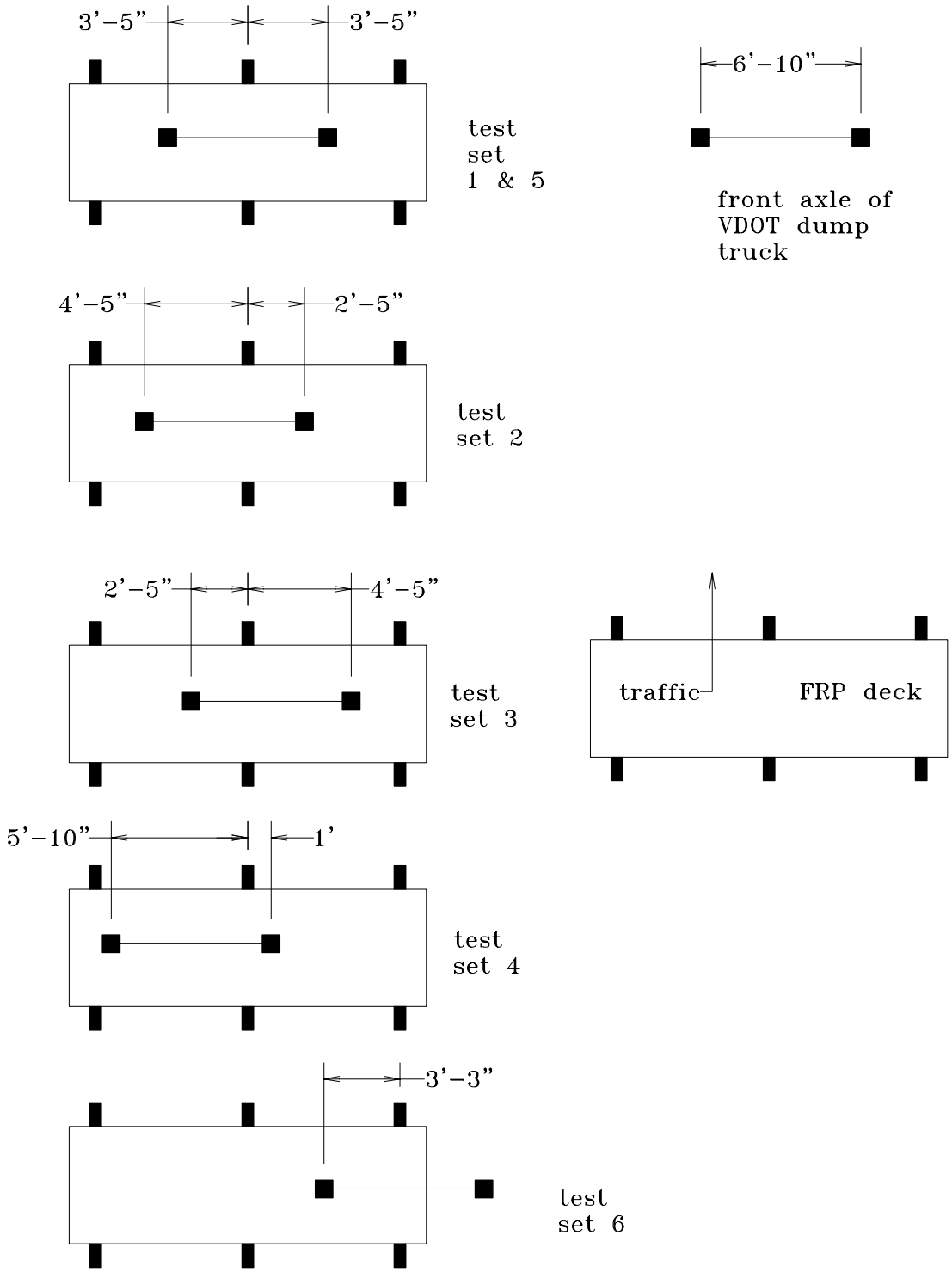

Figure 4.22 Orientation of the front axle (of the VDOT truck) on the FRP deck in Field Test 2

Chapter 5: Results and Discussion

5.1 Deck 1

5.1.1 Stiffness Tests

Results of the Deck 1 tests are shown in *Table 5.1*. Deflections are given at loads of 20.8 kips (HS20 wheel plus 30% impact) and 26.0 kips (HS25 wheel plus 30% impact). The deflections listed in the table were obtained from data that was created by using a 30-point running average of the raw data.

The running average method was used because there was some "bounce" in the raw data, as shown in *Figure 5.2*. This was attributed primarily to the wirepots, and was probably a result of the rate at which the deck was loaded. When operating the pump, it was difficult to apply load in small increments. One "click" of the pump would send fluid into the hydraulic cylinder at such a high rate that as much as 1 to 2 kips of load was instantaneously delivered to the deck. This high rate of application of load produced a large—but short term—acceleration in deck deflection. This acceleration would cause the cable (which is normally kept in tension) of the wirepot (see in *Figure 5.1*) to go slack, thereby leading to the "bounce" in the recorded deflection.

Figure 5.3 contains a load-deflection plot of the same data that was presented in *Figure 5.2*, except that this load-deflection plot was generated using a 30-point running average. From *Figure 5.3* it can be seen that the running-average method does not alter the overall trend in the data (as long as the overall trend of the raw data is linear). Rather, it "smooths out" the data and allows more accurate values of deflection to be obtained.

There were quality control concerns with Deck 1. The primary concern was that the top and bottom plates were not uniformly bonded to the tubes. This most likely produced a deck that was less stiff than one in which the tubes and plates were uniformly bonded. As a result, the deflections of Deck 1 should be considered a lower bound representation of deflections for FRP decks with similar material and section properties.

The deck experienced the largest deflections in Test 1 (WP_SE deflection of 0.315 inches 26.0 kips, for a deflection index of L/247). The lowest deflections were observed during Test 4, where the WP_E deflection at 26.0 kips was 0.167 inches, for a deflection index of L/467. In all four stiffness tests, the deck appeared to exhibit linear elastic behavior.

It is fair to question whether a bridge deck would ever be subjected to the loading conditions of Tests 1 and 2 (i.e. loads applied at a free edge). In typical stringer or girder bridges, the unsupported transverse edges of the deck are usually supported by diaphragms. In fact, AASHTO stipulates that the unsupported transverse edges must be supported (AASHTO, 1996, 3.24.9); otherwise some of the design assumptions in AASHTO would not be applicable. However, it is uncertain how this type of deck panel would be installed on a bridge, and there's the possibility that an FRP deck could be installed in a bridge in which the transverse edges were unsupported. One example of this was cited in a report by the Ohio Department of Transportation (ODOT, 2000), which indicated that problems were experienced with FRP deck panel systems that had unsupported edges. One of the "lessons learned" that was cited in the report was that end support (diaphragms) should be provided for any non-structural deck joints.

5.1.2 Strength Tests

5.1.2.1 Lab Test 5

A load-deflection plot of Test 5 (East tire patch loading, *Figure 4.16*) is shown in *Figure 5.4*. At the maximum load of 102 kips, the WP_E deflection was 0.91 inches. The reader will recall from Chapter 4 that the deck did not fail at 102 kips; rather the capacity of the hydraulic cylinder had been reached. From *Figure 5.4* it appears that the deck began to exhibit non-linear behavior at approximately 60 kips. This is 6 times larger than half of a legal axle (10 kips), giving some indication that the deck behavior is well within the linear range under legal truckloads. From this point on half of a legal axle (10 kips) will be referred to as a legal wheel. After completing the Test 5, an inspection of the deck did not reveal any damage.

5.1.2.2 Lab Test 6

A load-deflection plot of Cycle 7 (80 kips) through Cycle 10 (failure cycle) in Test 6 (West tire patch loading, *Figure 4.16*) is shown in *Figure 5.5*, while a load-strain plot is shown in *Figure 5.6*. The maximum load sustained by the deck was 107 kips (over 10 times larger than the maximum legal wheel load). The WP_W deflection and the BP_W_L strain at this load were 1.24 inches and 5200 microstrain (compared with the reported ultimate coupon strain of 12000 microstrain in the lengthwise direction, *Table 2.1*), respectively. Failure of the deck was attributed to punching shear (*Figure 5.7*), although it is uncertain whether any internal damage

had occurred prior to the punching failure. It can also be seen from *Figure 5.5* and *5.6* that the deck did exhibit ductile behavior—prior to reaching the peak load, there was a pronounced nonlinear region in the load-strain and load-deflection curves of Cycle 10.

No loss in stiffness was observed through at least the 70-kip load cycle. This is evident in *Table 5.2* (discussed further below), which contains flexibility coefficients for deflection (denoted as f_D, units of inches/kip) and flexibility coefficients for strain (denoted as f_ε, units of microstrain/kip). In the context of this research, and unless otherwise stated, a flexibility coefficient is computed as the inverse of the slope at a point on a 2^{nd} order polynomial that has been "fitted" to a load-deflection curve or a load-strain curve. For all cycles up to and including the 70-kip cycle, the computed flexibility at 30 kips remained at or below .00844 inches/kip and 42.0 microstrain/kip (*Table 5.2*), which indicates that the deck behavior remained elastic through at least 55 kips, which is 7 times larger than a legal wheel load.

5.2 Deck 2

5.2.1 Pre-Field Stiffness Tests

Deflections and strains at applied loads of 20.8 kips and 26.0 kips are summarized in *Table 5.3*. The deflections of Deck 2 were similar to the deflections of Deck 1. In Test 3 of Deck 1, the WP_E deflection was .170 inches at 20.8 kips, whereas in Test 1 of Deck 2, the WP_E deflection was .147 inches. The Deck 1 deflection was 15% higher than the Deck 2 deflection. Further comparison shows that in Test 4 of Deck 1, the WP_E and WP_W deflections were .139 inches and .129 inches, respectively, at 20.8 kips. In Test 3 of Deck 2, the WP_E and WP_W deflections were .136 inches and .130 inches—virtually identical to the deflections observed in Deck 1. The reader will recall that there were some differences in fabrication between Deck 1 and Deck 2 (discussed in Chapter 2). It was thought that because the quality control was higher for Deck 2, that it would be a stiffer deck compared with Deck 1. The only reasonable conclusion would seem to be that the two decks had comparable stiffnesses (based solely on deflections). For the remainder of this section, only the results for Deck 2 will be discussed.

The largest measured strains and deflections of Deck 2 were observed in Test 2 and Test 4. In Test 2, the WP_SE deflection at 26.0 kips was 0.290 inches (L/268) while the WP_NE deflection at 26.0 kips was 0.268 inches (L/291). The WP_SE deflection was 8.2 % larger than the WP_NW deflection. Theoretically, it would be expected that these two deflections would be

equal, but it was uncertain as to why these deflections did not more closely match each other. In Test 4, the WP_SW deflection at 26.0 kips was 0.285 inches. This is 1.8 % less than the WP_SE deflection recorded in Test 2. It would be expected that these two values be close together, considering that the loading case of Test 4 was the same as the loading case of Test 2 (except that the loads were placed on the opposite span). In Test 2, the strain pattern was opposite that of the deflection pattern. The BP_NE_L strain (1074 microstrain) was larger than the BP_SE_L strain (976 microstrain), yet the WP_NE deflection (.216 inches) was smaller than the WP_SE deflection (.237 inches); it was uncertain as to why this was the case.

A plot of load vs. strain for Test 1 (East Tire Patch loading) is shown in *Figure 5.8*. The deck appeared to exhibit fairly linear behavior. However, a closer look at the plot reveals that the deck appeared to get stiffer as it was loaded. A plot of load vs. flexibility (*Figure 5.9*) shows that as the load on the deck increases, the measured flexibility of the deck decreases. This was probably a result of loose elements in the system (such as connections), which eventually stiffened as the applied load increased. Upon unloading, the curve returned to zero, so that it can be concluded that the deck's behavior, while perhaps non-linear, is elastic up to at least 26.0 kips (over 2 ½ times larger than a legal wheel load).

Plots of load vs. deflection and load vs. strain for Test 3 (East and West tire patch loading) are shown in *Figures 5.10* and *5.11*, respectively. The load-strain data in *Figure 5.11* indicates that the deck exhibited linear behavior. However, the load-deflection data in *Figure 5.10* indicates otherwise. This was a result of the inability of the wirepots to accurately record deflection (and not a reflection of the actual behavior of the deck). The BP_E_L and BP_W_L strains match closely, indicating that the deck was behaving symmetrically about its center support. In the zero-to-five kip range, there were "bumps" in the load-deflection and load-strain data (*Figures 5.10* and *5.11*). This was a result of one of the hydraulic cylinders initially lagging behind the other during the initial stages of loading. Other than this short-term anomaly, the general structural response seen in *Figure 5.11* was fairly representative of the response observed in all the pre-field stiffness tests—i.e. the behavior was linear elastic, and the test results were repeatable.

One uncertainty prior to conducting the stiffness tests was whether the plates and tubes would exhibit composite behavior. In this context, the word "composite" is used in a structural sense to denote that the plates and tubes were acting as an integral unit. One way of ascertaining

whether the tubes and plates were acting compositely was to observe the strains at a particular cross section of the deck. For example, consider the strains in the center of the East span of the deck for Test 1 (East tire patch loading). At approximately 20.8 kips, the TT_E1 and TT_E2 (*Figure 5.12*) strains were used to compute an average strain at the top surface of the tubes. Next, the BT_E1 and BT_E2 strains (*Figure 5.12*) were used to compute an average strain at the bottom surface of the tubes. Given these two strain averages, and assuming plane sections remain plane, a linear strain distribution could be drawn through the cross section of the deck where the East tire patch was located. This strain distribution could be used to extrapolate a value of strain at the bottom surface of the bottom plate. This extrapolated value could then be compared with the actual value of strain recorded by the BP_E_L strain gage (*Figures 4.12* through *4.14* show where the 5 strains were measured). *Figure 5.12* shows the strain distribution through the thickness of the deck at the center of the East span. It can be seen that the strain distribution based on the tube strains extrapolated to 854 microstrain. The measured BP_E_L strain was 892 microstrain, which is 4.4% more than the extrapolated strain. This is very close to the relative uncertainty (3%, see Section 4.3.3) of the measured strain in the bottom plate strain gages, which is a good indication that the tubes and plates were behaving as an integral unit. *Figure 5.13* shows a strain distribution through the deck thickness at the center of the East span for Test 3 (East and West tire patches loaded simultaneously). The extrapolated strain on the bottom plate was 724 microstrain, while the measured strain was 768 microstrain (6.1% more than the extrapolated strain). This reinforces the idea that the plates and tubes were behaving compositely, indicating that the tube-to-plate adhesive was performing adequately prior to field installation of the deck.

5.2.2 Field Test 1

Prior to conducting Field Test 1, the deck was visually inspected. Next, the deck was observed for a short period of time as several random trucks crossed over it. The deck did not appear to be undergoing excessive deflections or vibrations, and there was no visible damage to the deck.

An arbitrary strain-time-time plot of a longitudinally oriented strain gage (BP_E_L, see *Figure 4.14*) is shown in *Figure 5.14*. The first “hump” was the result of the first (i.e. front) axle of a truck crossing the deck. The peak of the first hump was the maximum strain induced by the

first axle of the truck. That there are five humps indicates that this particular truck had five axles. All of the trucks for which data was recorded were five-axle trucks because it was felt that the five-axle trucks would induce the highest strains in the deck. In *Figure 5.14*, note that the strains at this particular location of the deck were positive (i.e. tensile strains) for the entire duration of the truck crossing. In other words, there did not appear to be any strain reversal at this point on the deck. This was true of all the longitudinally oriented strain gages on the bottom plate, but was not true of every strain gage (as discussed below).

An arbitrary strain-time-time plot for a transversely oriented gage (BP_E_T, see *Figure 4.14*) is shown in *Figure 5.15*. Each axle that crossed over the deck produced positive (tensile) as well as negative (compressive) strains. This was a result of plate behavior. For example, when the front axle initiated contact with the deck (south edge of the deck), a compressive strain was induced in the BP_E_T strain gage, but by the time the axle was directly over the gage, the strain had become tensile. When the axle was on the far edge of the deck (north edge), compression was once again induced in the gage. This strain-reversal pattern was characteristic of all the transverse gages on the bottom plate. The point to keep in mind is that there were two typical patterns of "strain-time-time" behavior for each truck crossing; at some points in the deck, only tensile strains were induced, while at other locations in the deck both tensile and compressive strains were induced. These patterns were a function of the location and orientation of the strain gage.

The reader is reminded that strains in the deck were observed under two different "sets" of truck crossings—random truck crossings and bias truck crossings. During the random truck crossings, the trucks traveled over the deck in a random fashion (i.e. no attempt was made to alter the traveling path of the truck). However, for ten of the truck crossings, a traffic cone was positioned to divert the trucks so that they would travel over the middle of the deck (i.e. each wheel line positioned approximately in the middle of each span). It was thought that by traveling over the middle of the deck, the trucks would induce the maximum possible strains in the FRP deck. This was done for ten trucks (truck crossings 60 through 69).

Plots that summarize the data from Field Test 1 are shown in *Figure 5.16* and *5.17*. Before discussing the results, the features of these plots will be discussed. As an example, consider the first vertical bar (strain gage TT_N1) in *Figure 5.16*. The vertical bar shows the range of TT_N1 strains induced by the random truck crossings (the strain ranges from the 10 bias truck crossings

were not used to develop the strain ranges in these plots, as explained later). From inspection of the vertical bar, it is seen that the TT_N1 strains ranged from a maximum of approximately 500 microstrain (tension) to a minimum of 350 microstrain (compression). Also shown for each gage are four data points. Two of these points are the average measured maximum tensile strain and the average measured maximum compressive strain induced during the random truck crossings. The other two points are the maximum measured tensile strain and the maximum measured compressive strain induced by one of the bias truck crossings. Finally, the plots show a horizontal line that represents the maximum expected tensile strain—600 microstrain in this instance. This maximum expected tensile strain was estimated using engineering judgment based on two factors: (1) the strains observed in the lab tests under known loads and (2) the expected truck loads based on legal load limits (discussed in Chapter 1).

Some general observations that can be made from *Figures 5.16* and *5.17* are as follows: (1) the measured strains in the bottom plate were typically higher than the measured strains in the tubes (2) the *range* of strain in any transverse gage was always larger than the range of strain in its accompanying longitudinal gage, which is plausible because of plate behavior and the fact that the FRP deck was orthotropic (flexural stiffness in the longitudinal direction [per foot width] is approximately 2 times larger than the flexural stiffness in the transverse direction [per foot width]). (3) the *average* strain in any transverse gage was always larger than the average strain in its accompanying longitudinal gage (which, again, is plausible because the FRP deck was orthotropic) (4) the average measured strains near the free edges of the deck were larger than the measured strains in the middle regions of the deck. Other observations that were made are discussed in more detail below.

From *Figures 5.16* and *5.17*, it is seen that the maximum recorded tensile strains induced by the random truck crossings were below the maximum expected tensile strain, providing some confidence that the behavior of the deck in the field bore some relationship to the behavior of the deck in the lab. For example, had the maximum recorded strains in the field been substantially higher than the expected maximum strain, it would lead one to believe that either (1) a mistake was made in the prediction of the deck strains in the field or (2) the laboratory tests that were conducted were not a good predictor of the field behavior.

It is interesting to note that in almost all of the strain gages, the tensile strains induced by the bias truck crossing (Truck 65) were higher than the average strains induced by the random truck

crossings. This was a direct result of the orientation of the "wheel lines" as the bias truck crossed the deck. The TT_N1 strain induced by the bias truck crossing was even higher than the maximum expected strain. The measured tensile strains induced by the other 9 bias truck crossings were also typically higher than the average measured tensile strains induced by the random truck crossings. If the orientation of the random truck crossings observed during Field Test 1 (see *Figure 4.20*) were typical of the orientation of the "everyday" truck crossings, then it can be concluded that the everyday truck crossings were not inducing the maximum possible strains in those areas that were instrumented with gages. But it's important to realize that the strain gages were located at points of expected maximum *flexural* strains. Strain gages were not put on any areas of maximum expected *shear* strains (e.g. on the webs of tubes and near the deck supports). While the truck orientation shown in *Figure 4.20* may not have been producing the worst possible flexural strains in the deck, it's quite possible that this orientation was inducing very high shear strains near the middle and west supports. This possibility is discussed further in section 5.2.4.

After crossing the deck, all ten bias trucks were weighed on the weigh station scales. The results of the "weigh-ins" are shown in *Table 5*.4. The maximum gross vehicle weight, as well as maximum permissible axle and tandem weights allowed without a permit are shown in *Table 5.4* (and were also discussed in Chapter 1).

Now compare the strains observed in Lab Test 6 (West tire patch loading) of Deck 1, and the strains observed in Field Test 1 (from Truck 65) of Deck 2. From *Table 5.4*, it can be seen that both tandems on Truck 65 weighed approximately 98% of the legal tandem. Truck 65 induced a maximum recorded strain of approximately 350 microstrain in the BP_W_L strain gage (*Figure 5.17*), and in Test 6 of Deck 1 the strain at the BP_W_L location of the deck was 5200 microstrain at an ultimate load of 107 kips (which is over 3 times the legal weight of a truck tandem). At the very least, it appears that when the deck was loaded by a truck whose tandems approached the legal limit, the strains that were induced were nowhere close to the strains that would be induced in the deck at failure. This comparison was used at the time of testing to ensure that there wouldn't be a failure of the deck due to overload from trucks exceeding the maximum legal weights.

5.2.3 Field Test 2

A summary of the absolute maximum (i.e. highest magnitude regardless of sign) strains that were recorded for each test set of Field Test 2 is shown in *Table 5.5*. Data for some of the strain gages has not been shown because the gages were not functioning (BT_N1, BT_N2, BT_NE1, and BT_NE2). Several general observations can be made: (1) Similar to what was observed in Field Test 1, the transverse strains on the bottom plate were very close in magnitude to the longitudinal strains (once again, this is due to the orthotropy of the deck). (2) recorded strains in the bottom plate were generally much higher than the recorded strains in the tubes. (3) recorded strains near the edges of the deck were significantly larger than the recorded strains in the middle regions of the deck. (4) The strains exhibited during Test Set 5 (the speed run, front axle crossing the middle of the deck) were no higher than the strains exhibited during Test Set 1. This does not mean that the FRP deck is immune to dynamic loading effects, only that these effects were not observed when the truck was traveling at 15 mile per hour. (5) The largest recorded tensile strains occurred in the bottom plate of the east span during Test Set 6 (see *Figure 4.22* for truck wheel orientation). High tensile strains were also recorded in the bottom plate of both spans during Test Sets 1 and 5. It is possible that the deck was experiencing higher tensile strains in the top plate over the middle support, but since it wasn't possible to provide strain gages on the top plate, the magnitude of the strains in this region was unknown.

In looking over *Table 5.5*, it is evident that the deck exhibited significantly lower strains during Test Sets 2, 3 and 4. Of these three test sets, Test Set 4 induced the lowest recorded tensile strains in the bottom plate. The relationship between Test Set 4 and Test Set 6 is analogous to the relationship between the bias truck crossings of Field Test 1 and the random truck crossings of Field Test 1. The strains induced in the deck during Test Set 6 were significantly higher than the strains induced in Test Set 4. Similarly, the strains induced by the bias truck crossings were significantly higher than the average strains induced by the random truck traffic. It would appear that the highest *flexural* strains are induced in the bottom plate when a truck straddles the middle support. A truck that is offset from this position, such as shown in *Figure 4.20* or *Figure 4.22* (Test Sets 2 through 4), produces markedly lower tensile strains in the deck. For example, the maximum BP_E_L tensile strain recorded in Test Set 1 was approximately 197% larger than the maximum BP_E_L strain recorded in Test Set 2 (*Table 5.6*). The maximum BP_E_L tensile strain recorded in Test Set 1 was approximately 716% larger than

that the maximum BP_E_L strain recorded in Test Set 4 (*Table 5.6*). In general, as the offset (relative to the middle of the deck) of the VDOT truck became larger, the strains in the bottom plate gages became smaller. This is shown by the results presented in *Table 5.6*, which shows how much larger (by a percent) the bottom plate strains were in Test Set 1 compared with Test Sets 2, 3 and 4.

The weight of the front axle of the VDOT dump truck was 14.5 kips, while the weight of the rear tandem axle was 39.3 kips (*Figure 4.21*). The rear tandem axle was approximately 15% higher than the legal limit. Consider that the largest strain recorded in Field Test 2 was 583 microstrain (BP_NE_L). The highest strains observed in Field Test 1 (*Figures 5.16* and *5.17*) were a little under 600 microstrain. This would seem to indicate that the deck had not lost any appreciable stiffness since Field Test 1. However, a direct comparison between the strains induced by the bias trucks of Field Test 1 and the VDOT truck would be difficult, because the exact orientation and the axle spacing of the bias trucks were not known.

The deflections and strains measured in Field Test 2 were higher than expected because of rocking of the supports. As the first axle of the truck made contact with the first access panel, the supports not only experienced a vertical reaction, but also experienced some twisting ("rocking"), as depicted in *Figure 5.19*. *Figure 5.20* shows a plot of deflection vs. time from that field test. Note where the truck tires first make contact with the FRP deck. There are visible deflections—though small—that appear prior to this. It is apparent from this figure that the deflectometers were recording small levels of deflection prior to the truck wheels making contact with the FRP deck. In order to eliminate this problem, the deck, access panels, and supports were removed, and grout was poured on those areas of the concrete slab where the support beams would rest. Prior to hardening of the grout, the access panels and support beams were dropped back in the test pit, and the support beams were fastened to the slab while the grout was wet. Subsequent testing of another deck (not discussed in this paper) in the weigh station showed that the grouting eliminated the rocking of the supports, and thereby produced more reliable deflection data.

5.2.4. Field Inspection of Deck 2

The north and south faces of the deck were first inspected on March 3, 2000 (with the deck having been in service approx. 4 months). The inspection revealed that cracks had developed on

the north face over the middle support (*Figure 5.21*); these cracks most likely initiated at the access hole. Two other cracks were observed inside the access hole—a crack along the bottom wall of the tube and a crack along one of the bottom fillets of the tube (*Figure 5.22* and *5.23*). No cracks were observed at any other location on the deck.

Another inspection was done on April 13, 2000 (5 months in service) immediately prior to Field Test 2. The inspection revealed that the cracks on the north face of the deck over the middle support had grown since they were first observed on March 3. It was not possible to conclude whether the cracks inside the access hole had grown. No other cracks were observed.

A third inspection was performed after removing the deck from the weigh station on July 11, 2000 (after 8 months in service). Cracks were observed in several regions of the deck. *Figure 5.25* shows a schematic denoting those regions where cracks were detected. The regions labeled 1 through 6 were on the bottom plate of the deck. Most of the cracks on the bottom plate were oriented in the longitudinal direction of the deck. *Figure 5.24* shows a picture of the cracks that had developed in regions 4 and 5. It is uncertain how these cracks could have developed. It would seem that the strains in this region (bottom plate over mid-support) would be primarily compressive strains in the longitudinal direction, and it is uncertain how these strains could have caused cracking in this region.

The inspection revealed that the cracks on the north face over the middle support had continued to grow. In addition, several other cracks on the north and south faces were observed for the first time. Two partial elevation views of the deck (*Figure 5.27* and *5.28*) show that the cracks had formed at the access holes. *Figures 5.27* and *5.28* also show the typical location of the axles from the random truck traffic. This axle orientation induced high shear forces near the middle and west supports. It would seem that the reduced cross sectional area (due to the access holes) coupled with the high shear forces led to the initiation of cracking near these support locations.

5.2.5. Discussion of "Pre-Field" and "Post-Field" Stiffness Tests and Field Test 2

Flexibility coefficients (for strain and deflection in the bottom plate) were computed for some of the "pre-field" and "post-field" stiffness tests of Deck 2 (*Table 5.7*). Flexibility coefficients were also computed from some of the test sets of Field Test 2 (*Table 5.7*). Prior to analyzing the data, it was felt that a direct comparison could be drawn between Test Set 6 of

Field Test 2 (one line of wheels crossing middle of east span) and Lab Tests 1 and 5 (East tire patch loading). In Test Set 6 (*Fig. 4.22*), it was believed that as the truck wheel was traveling over the deck, there would be one instant when the wheel's position on the deck would be very similar to the position of the east tire patch (*Figure 4.16*) in Lab Test 1 and 5. It was also believed that this wheel position would induce the highest recorded strain in the BP_E_L strain gage (*Figure 4.14*). Therefore, it was felt that this maximum recorded strain could be used to compute a flexibility coefficient that could be directly compared to flexibility coefficients computed from the laboratory test data. Similar to the explanation just given, it was felt that a direct comparison could be made between Field Test 2, Test Set 1 (*Fig. 4.22*) and Lab Tests 3 and 7 (East and West tire patches loaded simultaneously).

Using the weight of one wheel of the VDOT truck (7.3 kips) as well as the maximum recorded BP_E_L strain, a flexibility coefficient of 67.0 microstrain/kip was computed for Test Set 6 of Field Test 2 (*Table 5.7*). This flexibility coefficient was computed by taking the inverse slope of a line whose two data points were as follows: (1) zero strain at zero load and (2) 489 microstrain, which was assumed to occur when the wheel was over the middle of the deck, at 7.3 kips (half the weight of the front axle of the VDOT truck). Recall that this method of computing the flexibility coefficient is different than the method used to compute flexibility coefficients in the lab tests (discussed previously in Section 5.1.2.2).

The author expected that the flexibility coefficient computed for Test Set 6 of Field Test 2 would fall somewhere between the flexibility coefficients for Lab Test 1 and 5. It was expected that Test 1 would exhibit the lowest flexibility coefficients (i.e. the highest stiffness) and that Test 5 would exhibit the highest flexibility coefficients (i.e. the lowest stiffness). It was reasoned that the deck would exhibit the least flexibility in the "pre-field" stiffness tests because it had not been subjected to any prior load. Similarly, it was reasoned that the deck would exhibit the most flexibility in the "post-field" stiffness tests because it had been subjected to approximately 4 million cycles of load (i.e. 4 million axle crossings) over a period of 8 months. Additionally, several areas of damage had been observed (see section 5.2.4), and it was felt that this would increase the deck's flexibility.

As previously mentioned, the flexibility computed in the BP_E_L strain gage for Field Test 2, Test Set 6 (explained in the table) was 67.0 microstrain/kip, while the flexibility coefficients computed for Lab Tests 1 and 5 were 43.3 microstrain/kip and 40.4 microstrain/kip, respectively

(*Table 5.7*). Also, the flexibility computed in the BP_E_L strain gage for Field Test 2, Test Set 1 (explained in the table) was 50.5 microstrain/kip, while the flexibility coefficients computed for Lab Tests 3 and 7 were 37.0 microstrain/kip and 44.7 microstrain/kip, respectively. In both cases, the flexibility coefficient computed for Field Test 2 was higher than the flexibility coefficients in either the "pre-field" or "post-field" stiffness tests. The flexibility coefficients for deflection also exhibit this pattern (*Table 5.7*). The higher flexibility observed in the field was probably a result of several factors. First, the support beam-to-slab connections (in the field) were probably not as stiff as the support beam-to-reaction floor connections (in the lab). Second, the supports in the field had a tendency to "rock", as discussed in section 5.2.3. These first two factors had the effect of allowing the supports to twist inward when the deck was loaded (as depicted in *Figure 5.19*). This certainly caused the deck to experience higher deflections and strains in the longitudinal direction. The third factor that could explain the higher flexibility observed in the field was that the tire patch (discussed in Section 4.2) used to load the deck during the laboratory tests may not have been representative of an actual truck tire. For example, the size of the front tire of the VDOT dump truck was 9 ½ inches by 9 inches (*Figure 4.21*), whereas the base size of the tire patch used in the lab test measured 11 inches by 20 inches (*Figure 4.9*). Because the tire patch was larger, it could spread the applied load over a greater area of the deck, and perhaps reduce the load effect as compared with an actual tire. Nonetheless, because of the large discrepancy between the field and lab flexibilities, no further comparisons were drawn between the field and lab tests.

Two plots of load vs. strain comparing the "pre-field" stiffness tests and "post-field" stiffness tests are shown in *Figure 5.26* and *5.30*. The "post-field" behavior appeared to be very similar to the "pre-field" behavior. The deck exhibited linear behavior up to 26.0 kips. Deflections and strains for the "post-field" stiffness tests are shown in *Table 5.3*. Similar to the results of the "pre-field" tests, the highest measured deflections and the highest measured bottom plate longitudinal strains occurred when the deck was loaded at its free edges (Tests 6 and 8). Also, the transverse strains on the bottom plate were very comparable—though typically slightly less—than the longitudinal strains on the bottom plate.

In Test 1 (Pre-Field Stiffness), the WP_E deflection at 26.0 kips was .183 inches, while in Test 5 (Post-Field Stiffness) the WP_E deflection was .209 inches (14% larger). This would seem to indicate that the deck had lost stiffness after being in the field for 8 months. However,

the BP_E_L strain at 26.0 kips was 1084 microstrain for Test 1 and 1001 microstrain (7 % smaller) for Test 5. These two sets of results conflict with one another—the deflection data indicated that the deck had lost stiffness, while the strain data indicated that the deck had gained stiffness. However, computation of flexibility coefficients at 20 kips yielded a Pre-Field flexibility for deflection of .00750 inches/kip compared with a Post-Field flexibility for deflection of .00740 inches/kip (*Table 5.8*). The computed flexibility coefficients for strain were 39.0 microstrain/kip (Pre-Field) compared with 31.7 microstrain/kip (Post-Field). In both cases, the computed flexibility is lower in the Post-Field Stiffness test. This is shown more clearly in *Figure 5.29,* which shows that at all levels of load, the Post-Field flexibility for strain was lower than the Pre-Field flexibility for strain.

Another interesting result is seen when comparing flexibility coefficients for Test 3 (Pre-Field Stiffness) and Test 7 (Post-Field Stiffness), as shown in (*Table 5.9*). The BP_E_L and BP_W_L flexibility coefficients (at 20 kips) for Test 3 were 35.0 microstrain/kip and 35.8 microstrain/kip, respectively. The BP_E_L and BP_W_L flexibility coefficients (at 20 kips) for Test 7 were 29.9 microstrain/kip and 42.8 microstrain/kip, respectively. These results seemed to indicate that the west side of the deck had become more flexible relative to the east side of the deck. This is shown more clearly in *Figure 5.31* and *5.32,* which show that at all levels of load, the Post-Field flexibility of the east span (based on the BP_E_L strain) was lower than the Pre-Field flexibility of the east span, which is opposite the relationship between the Pre-Field and Post-Field flexibility of the west span (based on the BP_W_L strain). However, the visual inspection of the deck did not yield any evidence that the west side of the deck had suffered more damage compared with the east side of the deck. It is possible that truck traffic at the weigh station may have caused more internal damage to the west side of the deck, but this is only speculation. In general, the changes in strain and deflection (from the pre-field stiffness tests to the post-field stiffness tests) were not significant enough to conclude that the deck had lost appreciable stiffness.

5.2.6. Strength Tests

5.2.6.1 Lab Test 9

A plot of load (East tire patch, *Figure 4.16*) vs. BP_E_L strain (*Figure 4.14*) is shown in *Figure 5.33,* while *Figure 5.34* contains a plot of load vs. WP_E deflection. The deck appeared

to exhibit linear elastic behavior (in the loading portion of the curve) well beyond 26.0 kips. The maximum load sustained by the deck was 132.4 kips (over 13 times larger than a legal wheel load). At this load, the BP_E_L strain was approximately 6800 microstrain (compared with a reported ultimate coupon strain in the lengthwise direction of 12000 microstrain, *Table 2.1*), the BP_E_T strain was approximately 6680 microstrain (compared with an ultimate strain in the crosswise direction of 8750 microstrain), and the WP_E deflection was approximately1.27 inches. The strains recorded in these two strain gages were significantly larger than the other strains in the bottom plate. Failure of the deck was attributed to a combination of punching shear (*Figure 5.35*) and shear failure of the tube walls (*Figure 5.36*).

The deck did exhibit some ductility, as it continued to deform under load—albeit lower load—without experiencing an abrupt drop in load carrying capacity. Immediately before unloading the deck, a strain of 10850 microstrain (BP_E_L) and a deflection of 1.43 inches were recorded.

The deck did not appear to lose significant stiffness through the first three cycles of load, as evident in *Table 5.10*. In the 50-kip load cycle, flexibility coefficients of .00782 inches/kip and 41.1 microstrain/kip were computed at 30 kips. In the 100-kip cycle, the computed flexibility coefficients at 30 kips were .00730 inches/kip and 37.1 microstrain/kip. While it's unlikely that the deck *gained* stiffness as higher magnitudes of load were applied, the results seem to indicate that the deck behavior remained elastic at least up to 75 kips, which is over 7 times larger than the legal wheel load. Each time the deck was unloaded, the unloading portion of the load-strain curve (or load-deflection curve) did not trace back over the loading path. It's unclear as to why the deck behaved in this manner.

It should be kept in mind that the fractures in the deck occurred in locations other than where strain gages were located. Therefore, it would be incorrect to label any of the strains on the bottom plate as "failure strains" for the FRP material. The strains on the bottom plate served as indicators as to when the strains at the failure locations were nearing critical levels. For example, the BP_E_L strain—at the time of failure—was 6800 microstrain. The maximum recorded BP_E_L strain observed in Field Test 1 and Field Test 2 was approximately 600 microstrain, which is less than 10% of 6800 microstrain. What can be concluded here is that the measured strains that were induced in the FRP deck under service condition were well below the measured levels of strain that were induced in the deck as it was nearing its ultimate capacity.

The effect of the thru rods on the deck's behavior is uncertain. It is possible that the thru rods lead to an increase in strength and stiffness, though the only way to determine this would be to test FRP decks without thru rods.

5.2.6.2 Lab Test 10

A plot of load (Southwest tire patch) vs. BP_SW_L strain (*Figure 4.14*) is shown in *Figure 5.37*, while *Figure 5.38* contains a plot of load vs. WP_SW deflection. The maximum load sustained by the deck was 85 kips (over 8 times larger than a legal wheel load). At this load, the BP_SW_L strain was approximately 5900 microstrain, and the WP_SW deflection was approximately 1.15 inches. Failure of the deck was attributed to shear fracture of the tube wall (*Figure 5.39*), with these cracks having propagated from existing cracks—the lower right hand corner of *Figure 5.39* shows tick marks where the existing cracks had extended prior to Test 10.

5.3 Tables and Figures

Table 5.1 Deflections at AASHTO design loads, Deck 1, Tests 1 through 4 (Stiffness Tests)

Test	Active Tire Patch(es)[1]	Load, kips	Deflection (sensor in parentheses)[2], inches	Deflection Index
1	SE	20.8	0.247 (WP_SE)	L/315
		26.0	0.315 (WP_SE)	L/247
2	SE and SW	20.8	0.232 (WP_SE) 0.232 (WP_SW)	L/336 L/336
		26.0	0.284 (WP_SE) 0.279 (WP_SW)	L/274 L/279
3	E	20.8	0.170 (WP_E)	L/458
		26.0	0.196[3] (WP_E)	L/398
4	E and W	20.8	0.139 (WP_E) 0.129 (WP_W)	L/561 L/604
		26.0	0.167 (WP_E) 0.161 (WP_W)	L/467 L/484

[1] Location of tire patches shown in Fig. 4.16
[2] Location of deflection sensors shown in Fig. 4.15
[3] Extrapolated from 0.181 inches at 24.0 kips (maximum test load)

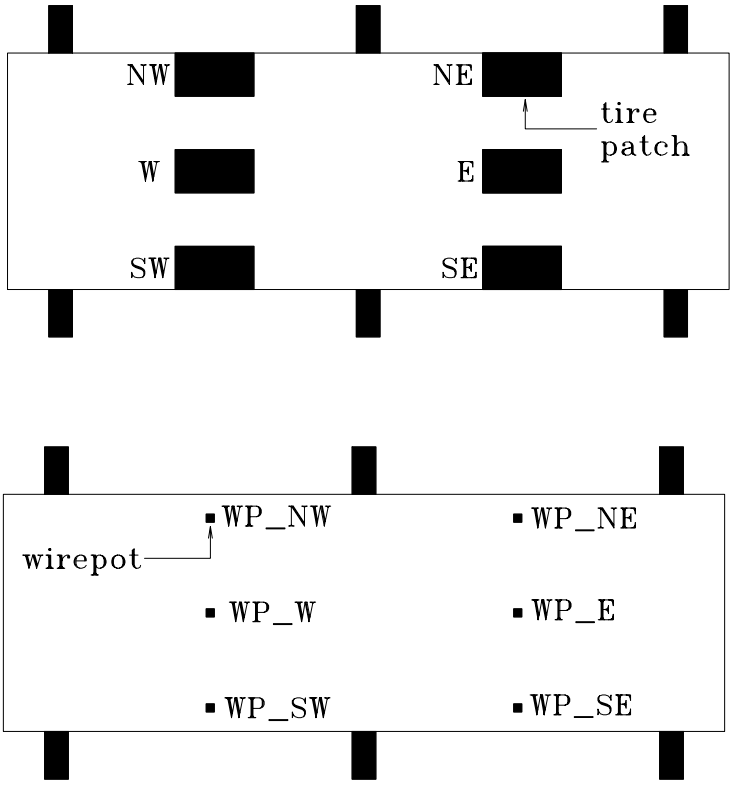

Table 5.2 Deck 1 flexibility coefficients at 30 kips, Test 6 (Strength), West tire patch loading (Fig. 4.16)

Cycle	f_D[1] (in./kip)	f_ε[2] (με/kip)
35 kips	0.00844	42.0
45 kips	0.00816	40.6
55 kips	0.00796	39.7
70 kips	0.00842	41.1
80 kips	0.00850	40.7
90 kips	0.00890	42.1
100 kips	0.00894	42.6
107 kips	0.00946	45.0

[1] Flexibility coefficient based on data from deflection sensor WP_W (see Fig. 4.15)
[2] Flexibility coefficient based on data from strain gage BP_W_L (see Fig. 4.14)

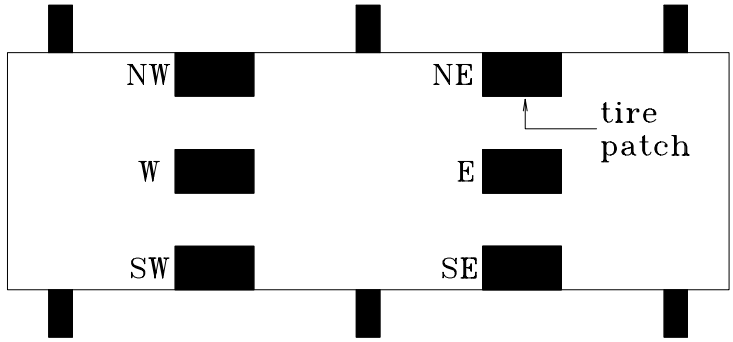

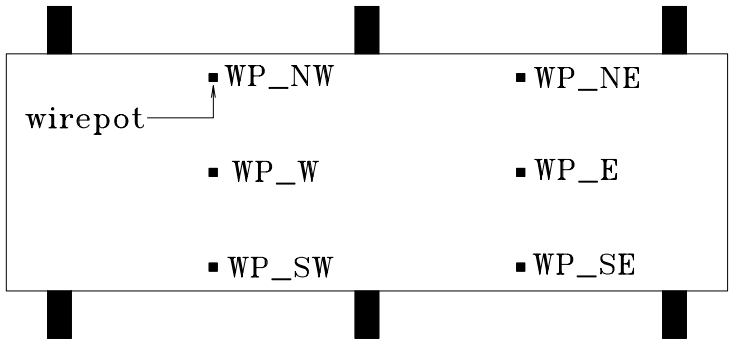

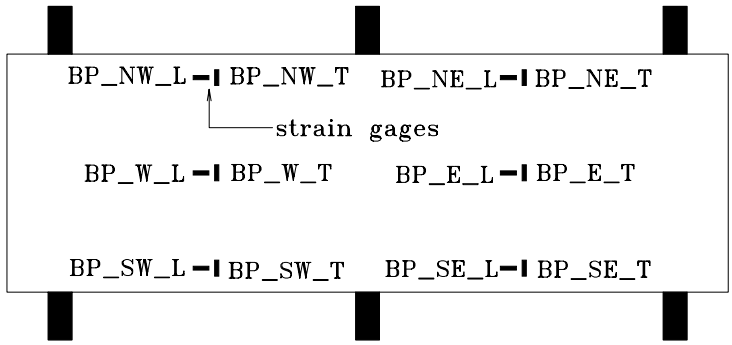

Table 5.3 Deck 2 deflections and strains at AASHTO design loads, Pre-Field and Post Field Stiffness Tests

Test	Active Tire Patch(es)[1]	Load; kips	Deflection (sensor in parentheses)[2]; inches	Deflection Index	Strain (sensor in parentheses)[3]; microstrain
1	E	20.8	0.147 (WP_E)	L/530	887 (BP_E_L)
		26.0	0.183 (WP_E)	L/426	1084 (BP_E_L)
2	NE and SE	20.8	0.237 (WP_SE) 0.216 (WP_NE)	L/329 L/361	976 (BP_SE_L) 1074 (BP_NE_L)
		26.0	0.290 (WP_SE) 0.268 (WP_NE)	L/268 L/291	1226 (BP_SE_L) 1349 (BP_NE_L)
3	E and W	20.8	0.136 (WP_E) 0.130 (WP_W)	L/573 L/600	765 (BP_E_L) 776 (BP_W_L)
		26.0	0.167 (WP_E) 0.160 (WP_W)	L/467 L/487	947 (BP_E_L) 956 (BP_W_L)
4	NW and SW	20.8	0.236 (WP_SW)	L/330	(BP_SW_L)[4] 1105 (BP_NW_L)
		26.0	0.285 (WP_SW)	L/273	(BP_SW_L)[4] 1373 (BP_NW_L)
5	E	20.8	0.171 (WP_E)	L/456	842 (BP_E_L) 891 (BP_E_T)
		26.0	0.209 (WP_E)	L/373	1001 (BP_E_L) 1100 (BP_E_T)
6	NE and SE	20.8	0.280 (WP_SE) 0.246 (WP_NE)	L/278 L/317	1126 (BP_SE_L) 1141 (BP_NE_L) 134 (BP_SE_T) 708 (BP_NE_T)
		26.0	0.340 (WP_SE) 0.301 (WP_NE)	L/229 L/259	1409 (BP_SE_L) 1418 (BP_NE_L) 142 (BP_SE_T) 812 (BP_NE_T)
7	E and W	20.8	0.153 (WP_E) 0.163 (WP_W)	L/509 L/478	718 (BP_E_L) 951 (BP_W_L) 792 (BP_E_T) 828 (BP_W_T)
		26.0	0.196 (WP_E) 0.194 (WP_W)	L/397 L/402	876 (BP_E_L) 1168 (BP_W_L) 982 (BP_E_T) 1013 (BP_W_T)
8	NW and SW	20.8	0.309 (WP_SW) 0.248 (WP_NW)	L/252 L/314	1557 (BP_SW_L) 1142 (BP_NW_L) 1533 (BP_SW_T) 806 (BP_NW_T)
		26.0	0.371 (WP_SW) 0.315 (WP_NW)	L/210 L/248	1886 (BP_SW_L) 1421 (BP_NW_L) 1781 (BP_SW_T) 894 (BP_NW_T)

[1] Location of tire patches shown in Fig. 4.16
[2] Location of deflection sensors shown in Fig. 4.15
[3] Location of strain gages shown in Fig. 4.14
[4] Gage was malfunctioning during testing

Table 5.4 Summary of axle and tandem weights for the 10 bias trucks that crossed over Deck 2 during Field Test 1

		Axle and Tandem Weights (kips)							
Truck Crossing	Truck Type[1]	Axle 1	Tandem 1	Tandem 2	Axle 2	Axle 3	Axle 4	Axle 5	Total
60	3S-2	10.88	32.28	32.68					75.84
61	2S1-2	9.84			16.62	15.26	10.74	11.02	63.48
62	3S-2	11.10	34.38[2]	32.86					78.34
63	2S1-2	10.52			13.84	9.16	7.90	10.68	52.10
64	3S-2	9.72	13.02	8.72					31.46
65	3S-2	10.90	33.28	33.88					78.06
66	3S-2	11.60	31.26	33.86					76.72
67	3S-2	10.88	33.90	31.89					76.67
68	3S-2	12.06	24.14	19.62					55.82
69	3S-2	12.10	33.24	33.36					78.70

- Maximum axle weight allowed without an overload permit is 20 kips
- Maximum tandem weight allowed without an overload permit is 34 kips
- Maximum gross vehicle weight allowed without an overload permit is 80 kips

[1] Truck types are shown in Fig. 5.18

[2] Exceeds legal tandem weight

Table 5.5 Summary of maximum recorded strains (regardless of algebraic sign) in Deck 2, Field Test 2

strain gage[1]	Test Set 1	Test Set 2	Test Set 3	Test Set 4	Test Set 5	Test Set 6
TT_N1	117	107	104	-96	139	-85
TT_N2	183	176	151	-47	134	-47
TT_C1	85	79	79	-39	46	-43
TT_C2	78	68	77	-42	42	-44
TT_NE1	-333	-155	-174	-78	-346	-471
TT_NE2	-348	-156	-212	-107	-364	-478
TT_E1	-215	-89	-107	-52	-220	-308
TT_E2	-234	-89	-106	-41	-237	-322
BT_C1	-82	-71	-76	37	-57	29
BT_C2	-83	-71	-81	42	-60	36
BT_E1	263	119	85	32	219	339
BT_E2	262	93	111	33	238	339
BP_SW_L	521	298	215	69	474	-27
BP_SW_T	414	272	183	-61	412	24
BP_W_L	369	175	124	41	283	-28
BP_W_T	318	240	202	115	284	37
BP_NW_L	484	295	195	66	408	-27
BP_NW_T	419	314	-221	-100	380	27
BP_SE_L	446	174	213	66	422	560
BP_SE_T	403	221	260	99	412	489
BP_E_L	330	111	121	40	295	417
BP_E_T	311	200	236	113	287	342
BP_NE_L	441	210	220	87	425	583
BP_NE_T	430	282	264	110	429	532

[1] Location of strain gages shown in Fig. 4.12 – 4.14
Test Set 1 (Center of front axle positioned over middle of deck, see Fig. 4.17)
Test Set 2 (Center of front axle offset 1' west of middle of deck, see Fig. 4.17)
Test Set 3 (Center of front axle offset 2' east of middle of deck, see Fig. 4.17)
Test Set 4 (Right wheels offset 1' east of middle support, see Fig. 4.17)
Test Set 5 (same as Test Set 1, except truck moving at approximately 15 miles per hour)
Test Set 6 (Left wheels positioned over middle of east span, see Fig. 4.17)

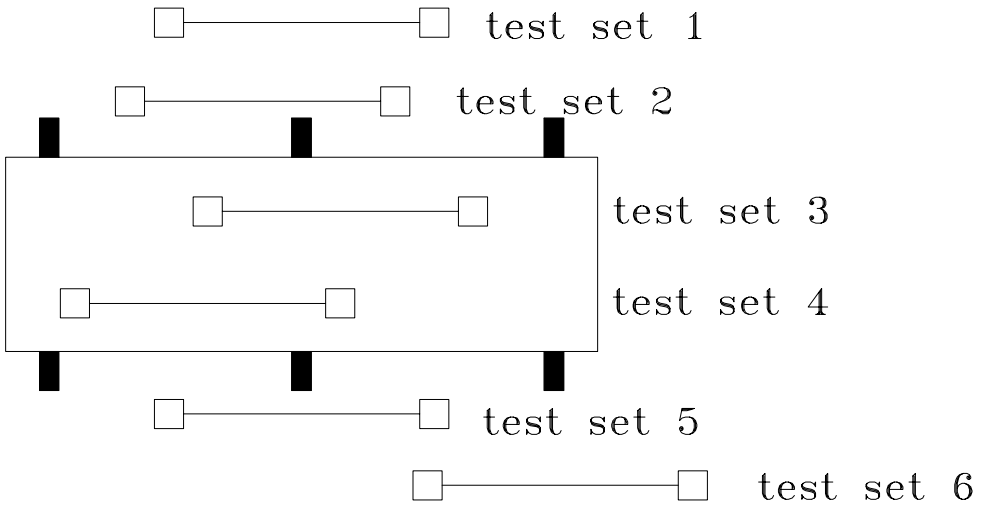

Table 5.6 Differences in maximum tensile strains of Test Sets 2, 3 and 4 relative to Test Set 1, Field Test 2 (Truck crossings made by VDOT dump truck, see Fig. 4.21)

Strain gage[1]	TS1	TS2	difference[2]	TS1	TS3	difference[3]	TS1	TS4	difference[4]
BP_SW_L	521	298	74.8%	521	215	142.5%	521	69	654.5%
BP_SW_T	414	272	52.3%	414	183	126.2%	414	61	576.5%
BP_W_L	369	175	111.2%	369	124	197.6%	369	41	789.9%
BP_W_T	318	240	32.5%	318	202	57.4%	318	115	176.5%
BP_NW_L	484	295	64.3%	484	195	148.6%	484	66	631.9%
BP_NW_T	419	314	33.4%	419	213	96.7%	419	60	595.6%
BP_SE_L	446	174	156.5%	446	213	109.5%	446	66	574.6%
BP_SE_T	403	221	82.1%	403	260	55.0%	403	99	307.3%
BP_E_L	330	111	196.8%	330	121	172.7%	330	40	715.5%
BP_E_T	311	200	55.5%	311	236	31.8%	311	113	175.2%
BP_NE_L	441	210	109.9%	441	220	100.6%	441	87	407.9%
BP_NE_T	430	282	52.9%	430	264	63.0%	430	110	292.4%

[1] Location of strain gages shown in Fig. 4.14
[2] difference = [(TS1 – TS2)/TS2]*100
[3] difference = [(TS1 – TS3)/TS3]*100
[4] difference = [(TS1 – TS4)/TS4]*100
where:
TS1 = Test Set 1; TS2 = Test Set 2; TS3 = Test Set 3; TS4 = Test Set 4
(see Table 5.5 for description of truck crossing during each test set)

Table 5.7 Deck 2 flexibility coefficients for strain and deflection at 7.3 kips, Field Test 2 vs. Lab Stiffness Tests

Sensors[1]	Test	f_ε (με/kip)	f_D (in/kip)
BP_E_L and WP_E	W2_TS6	67.0	0.01408
	T1 (Pre-Field)	43.3	0.00674
	T5 (Post-Field)	40.4	0.00791
BP_W_L and WP_W	W2_TS1	50.5	0.01507
	T3 (Pre-Field)	37.0	0.00626
	T7 (Post-Field)	44.7	0.00766
BP_E_L and WP_E	W2_TS1	45.5	0.01129
	T3 (Pre-Field)	37.3	0.00702
	T7 (Post-Field)	33.9	0.00706

[1] Location of sensors shown in Fig. 4.14 and 4.15
W2_TS6 = Field Test 2, Test Set 6 (Fig. 4.22)
T1 = Test 1, East tire patch loading (Fig. 4.16)
T5 = Test 5, East tire patch loading
W2_TS1 = Field Test 2, Test Set 1 (Fig. 4.22)
T3 = Test 3, East & West tire patch loading (Fig. 4.16)
T7 = Test 7, East & West tire patch loading

Table 5.8 Deck 2 flexibility coefficients at 20 kips, Test 1 (Pre-Field Stiffness) vs. Test 5 (Post-Field Stiffness)

Test	f_D (in./kip)	f_ε (με/kip)
Pre-Field	0.00750	39.0
Post-Field	0.00740	31.7

Test 1 and 5, East tire patch loading (Fig. 4.16)
f_D = flexibility coefficient based on data from WP_E sensor (Fig. 4.15)
f_ε = flexibility coefficient based on data from BP_E_L sensor (Fig. 4.14)

Table 5.9 Deck 2 flexibility coefficients at 20 kips, Test 3 (Pre-Field Stiffness) vs. Test 7 (Post-Field Stiffness)

Test	f_D (in/kip), WP_E	f_ε (με/kip), BP_E_L
Pre-Field	0.00600	35.0
Post-Field	0.00630	29.9
	f_D (in/kip), WP_W	f_ε (με/kip), BP_W_L
Pre-Field	0.00550	35.8
Post-Field	0.00690	42.8
Test 3 and Test 7, East & West tire patch loading (Fig. 4.16) f_D = flexibility coefficient based on data from WP_E and WP_W sensors (Fig. 4.15) f_ε = flexibility coefficient based on data from BP_E_L and BP_W_L sensors (Fig. 4.14)		

Table 5.10 Deck 2 flexibility coefficients at 30 kips, Test 9 (Strength), West tire patch loading (Fig. 4.16)

Cycle	f_D (in/kip)	f_ε (με/kip)
50 kips	0.00782	41.1
75 kips	0.00698	39.0
100 kips	0.00730	37.1
132 kips	0.00818	44.1
f_D = flexibility coefficient based on data from WP_W sensor (Fig. 4.15) f_ε = flexibility coefficient based on data from BP_W_L strain gage (Fig. 4.14)		

Table 5.11 Factors of Safety (w/ respect to legal truck loads) for Deck 1 and Deck 2 Strength Tests

Test	Maximum Tire Patch load (kips)	Legal Wheel Load (kips)[1]	Safety Factor[2]
Deck 1 (East tire patch loading)	102	10	10.2
Deck 1 (West tire patch loading)	107	10	10.7
Deck 2 (East tire patch loading)	132	10	13.2
Deck 2 (Southwest tire patch loading)	85	10	8.5
[1] Taken to be half of a legal axle (20 kips) [2] Max. tire patch load divided by legal wheel load			

Table 5.12 Factors of Safety (w/ respect to maximum field strains) for Deck 1 and Deck 2 Strength Tests

Test	Strain at Max. Load (microstrain)	Max. Field Strain (microstrain)	Safety Factor[7]
Deck 1 (West tire patch loading)	5200[1]	369[2]	14.1
Deck 2 (East tire patch loading)	6800[3]	417[4]	16.3
Deck 2 (Southwest tire patch loading)	5900[5]	547[6]	10.8
[1] BP_W_L strain at 107 kips, Deck 1, Test 6 (Strength) [2] Maximum BP_W_L strain recorded in both field tests [3] BP_E_L strain at 132 kips, Deck 2, Test 9 (Strength) [4] Maximum BP_E_L strain recorded in both field tests [5] BP_SW_L strain at 85 kips, Deck 2, Test 10 (Strength) [6] Maximum BP_SW_L strain recorded in both field tests [7] Strain at max. load divided by max. field strain			

Figure 5.1 Wirepots positioned beneath the middle of one of the deck spans during an arbitrary lab test

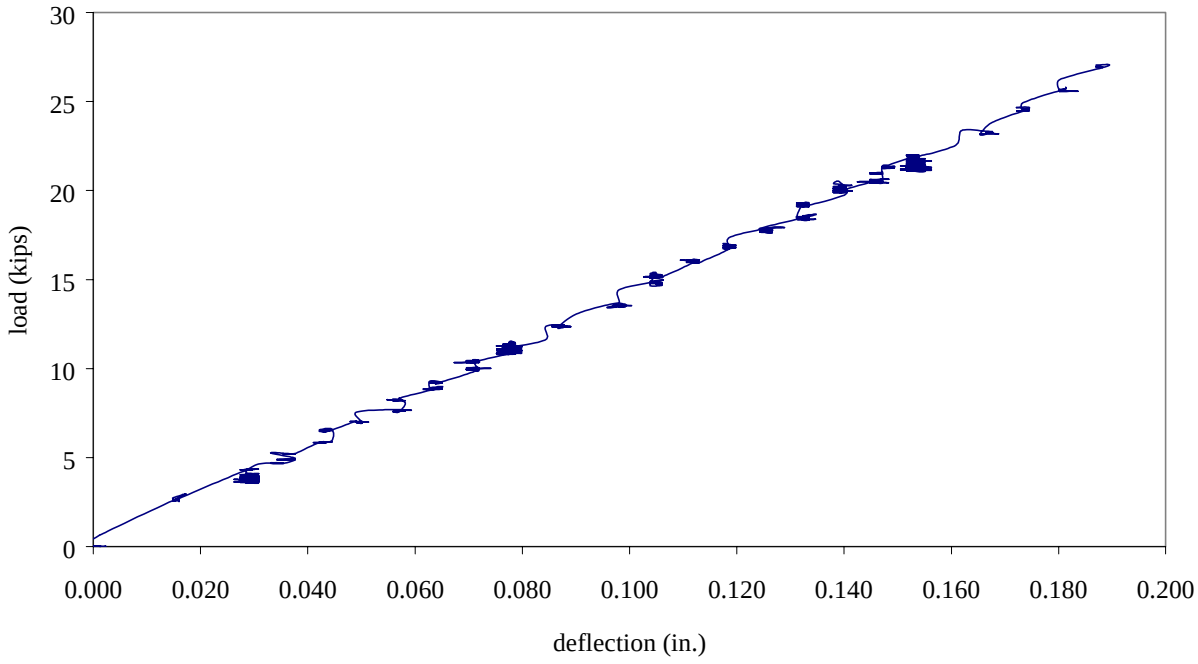

Figure 5.2 Plot of load vs. deflection, raw data from an arbitrary lab test

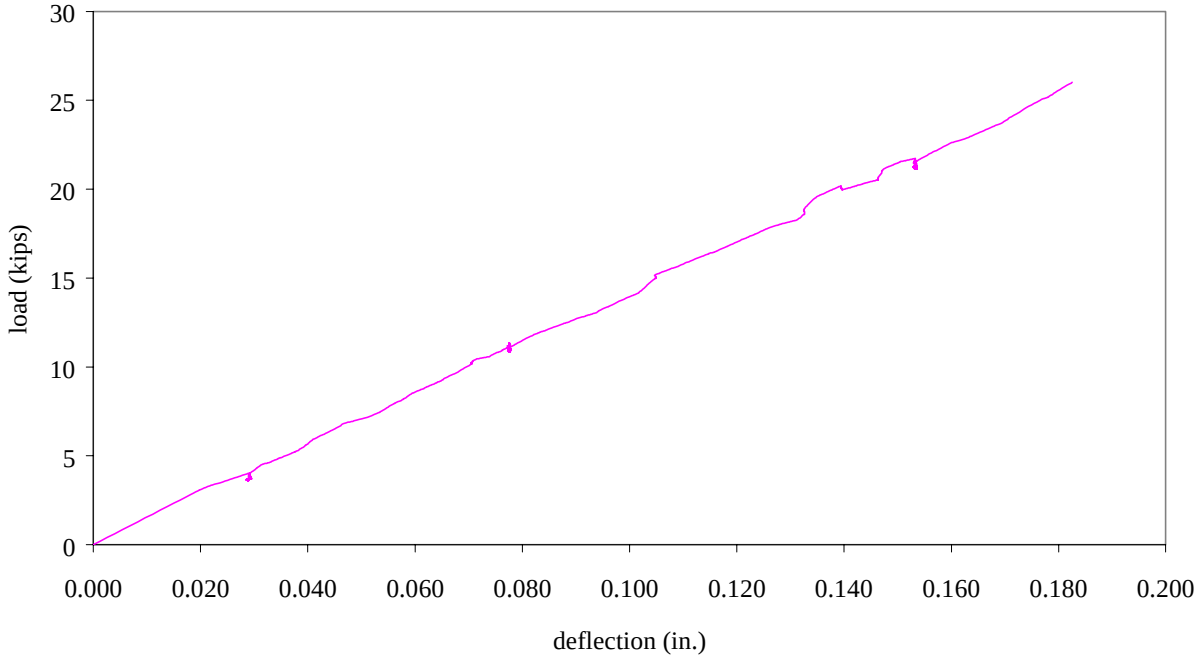

Figure 5.3 Plot of load vs. deflection, 30-point running average (raw data shown in Figure 5.2)

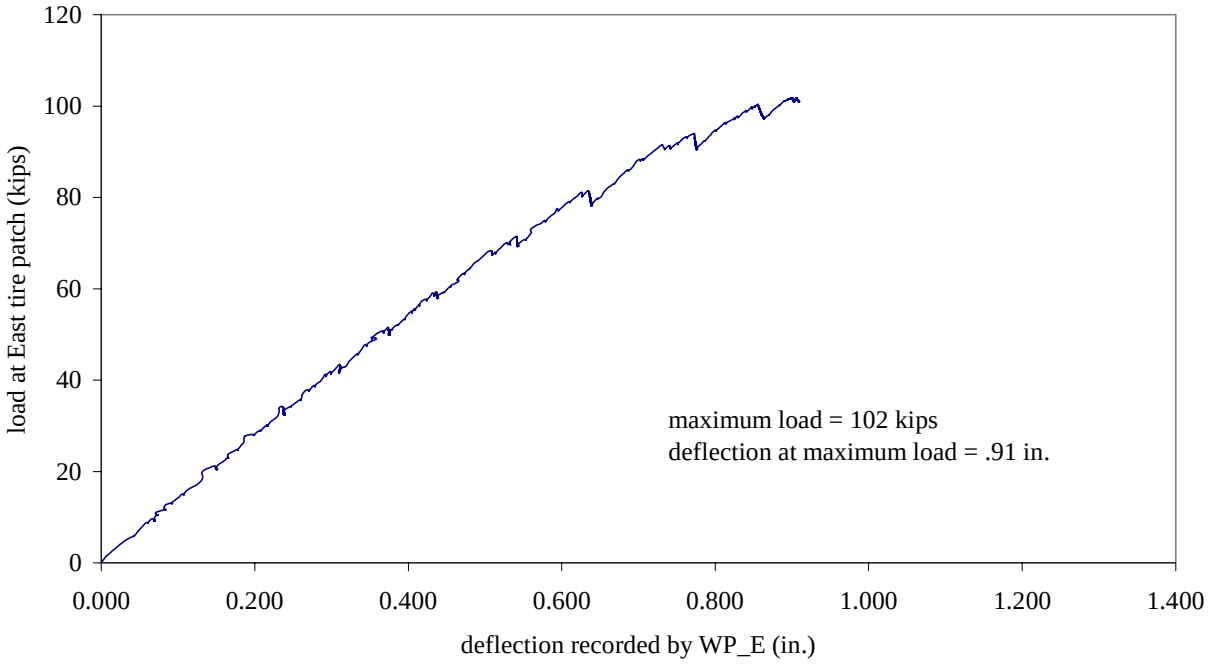

Figure 5.4 Plot of load vs. deflection, Deck 1, Test 5 (Strength), East tire patch loading (Fig. 4.16)

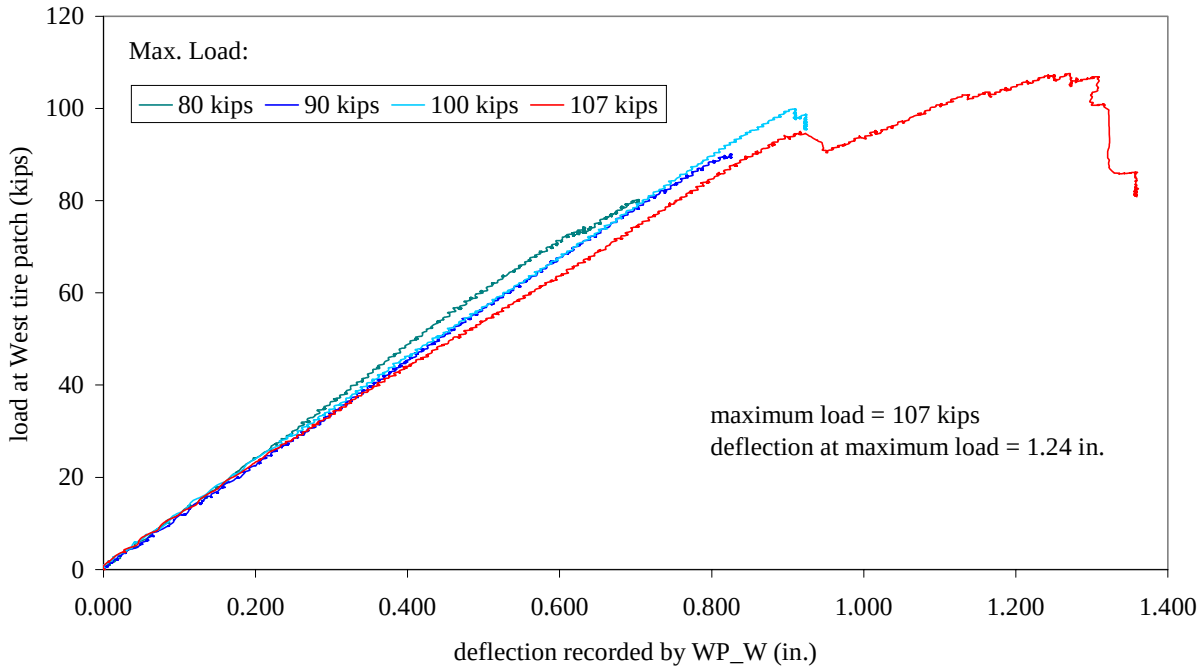

Figure 5.5 Plot of load vs. deflection, Deck 1, Test 6 (Strength), West tire patch loading (Fig. 4.16)

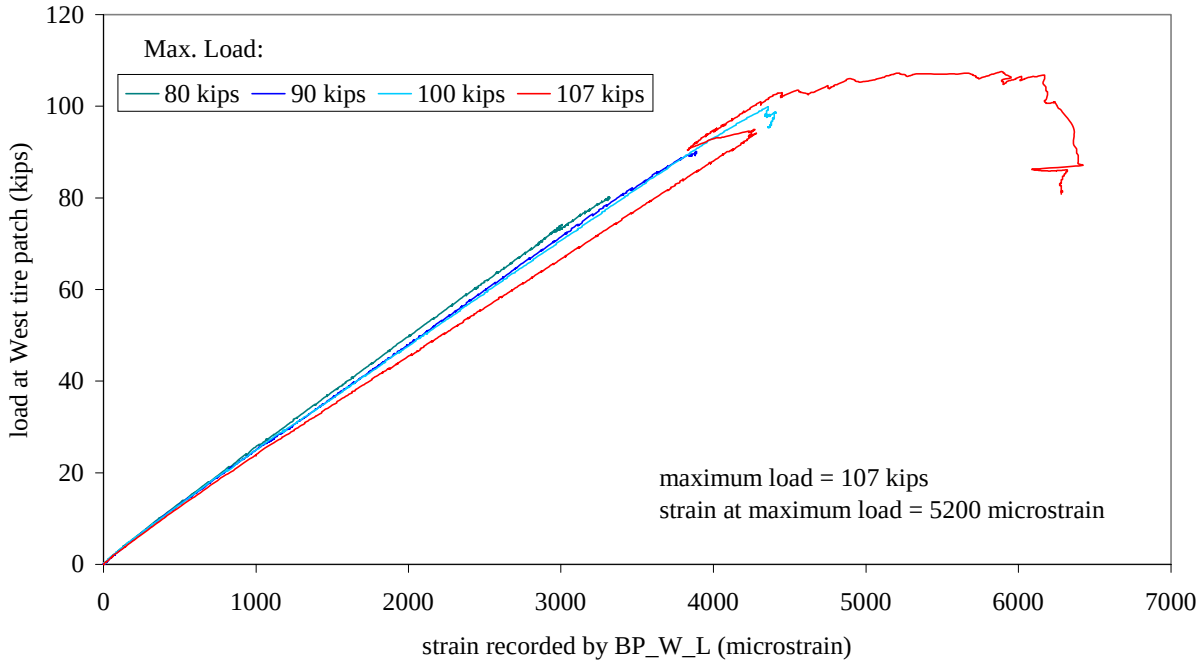

Figure 5.6 Plot of load vs. strain, Deck 1, Test 6 (Strength), West tire patch loading

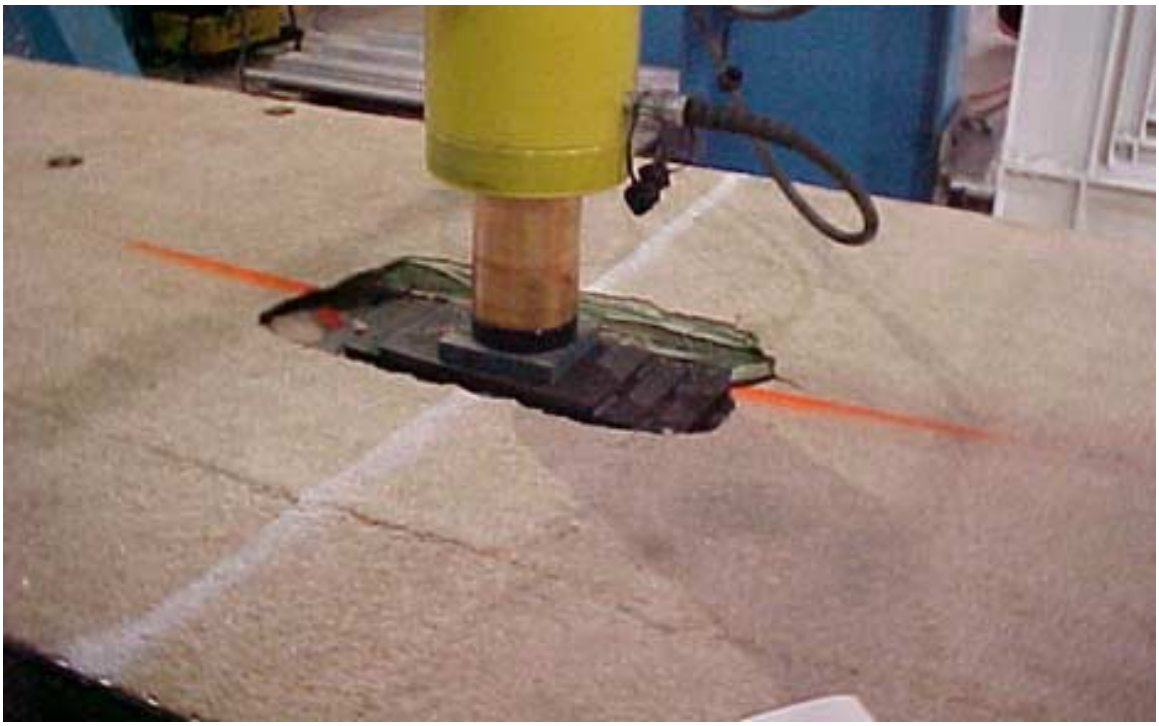

Figure 5.7 Punching failure at West span, Deck 1, Test 6 (Strength), Residual strength cycle

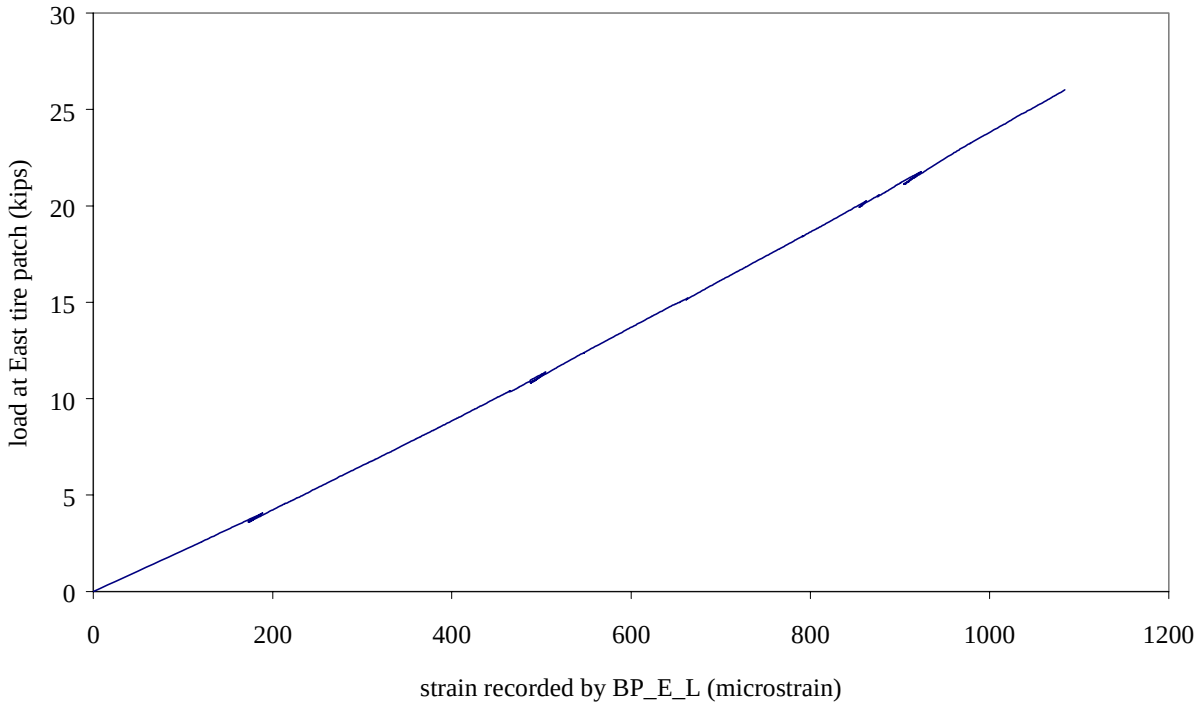

Figure 5.8 Plot of load vs. strain, Deck 2, Test 1 (Pre-Field Stiffness), East tire patch loading

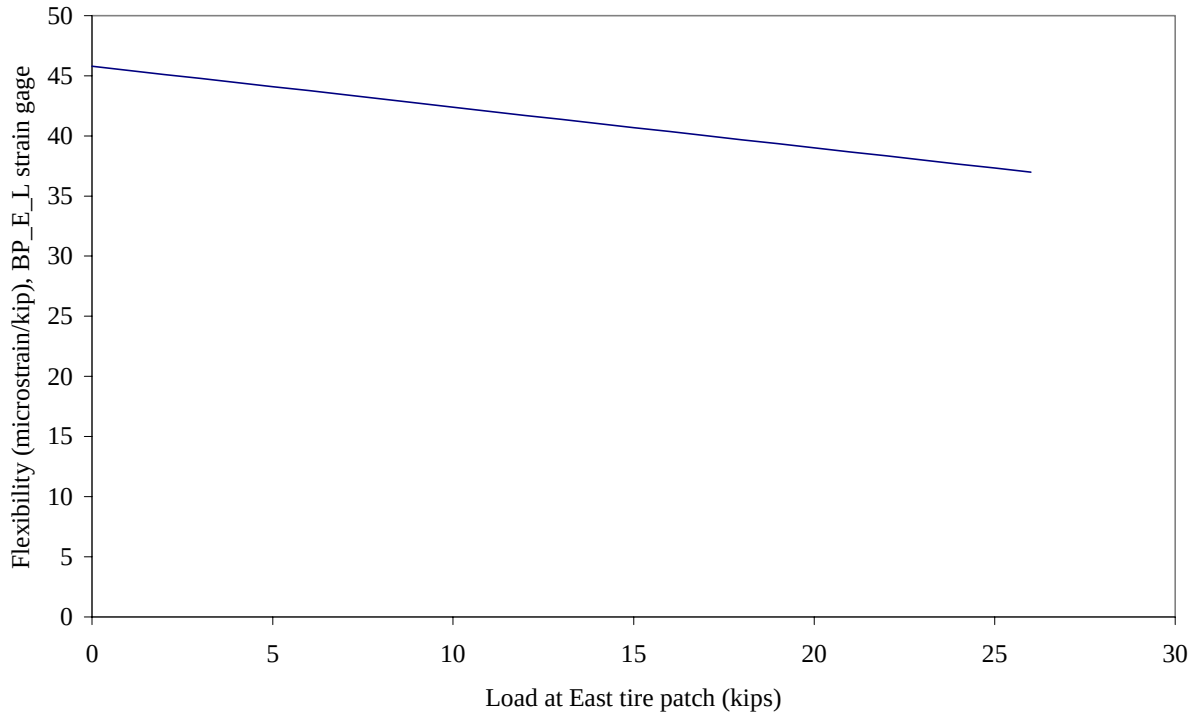

Figure 5.9 Plot of load vs. flexibility at BP_E_L strain gage, Deck 2, Test 1 (Pre-Field Stiffness)

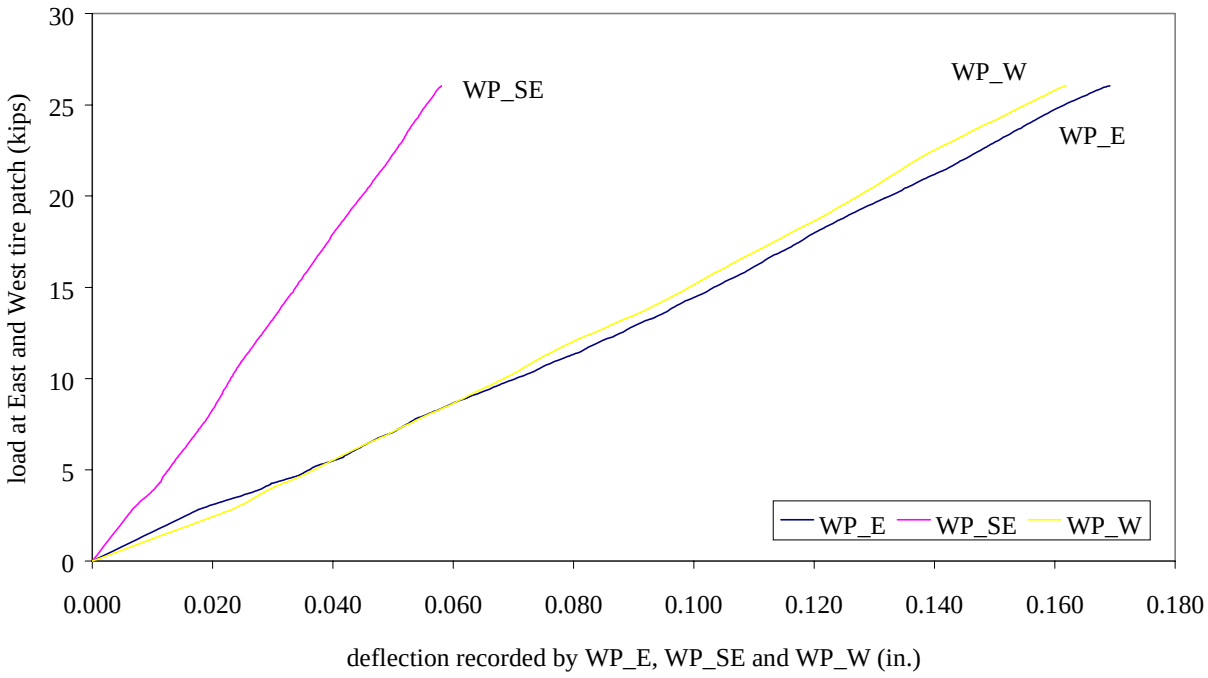

Figure 5.10 Plot of load vs. deflection, Deck 2, Test 3 (Pre-Field Stiffness), East and West tire patch loading

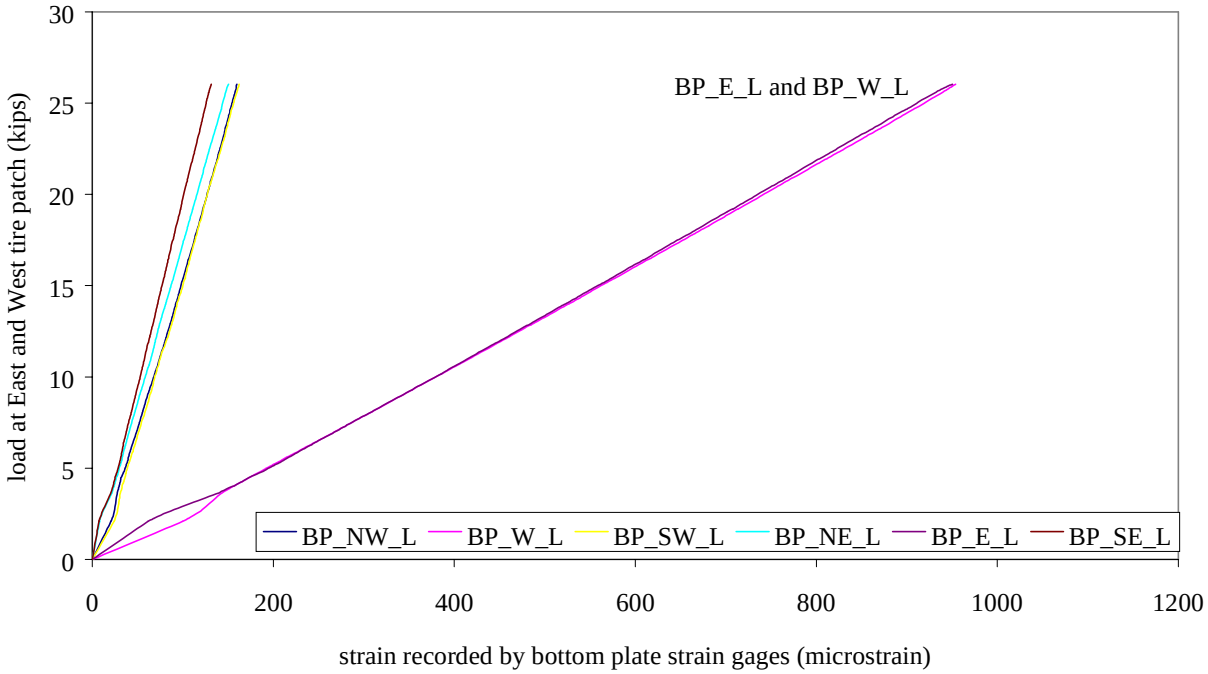

Figure 5.11 Plot of load vs. strain, Deck 2, Test 3 (Pre-Field Stiffness)

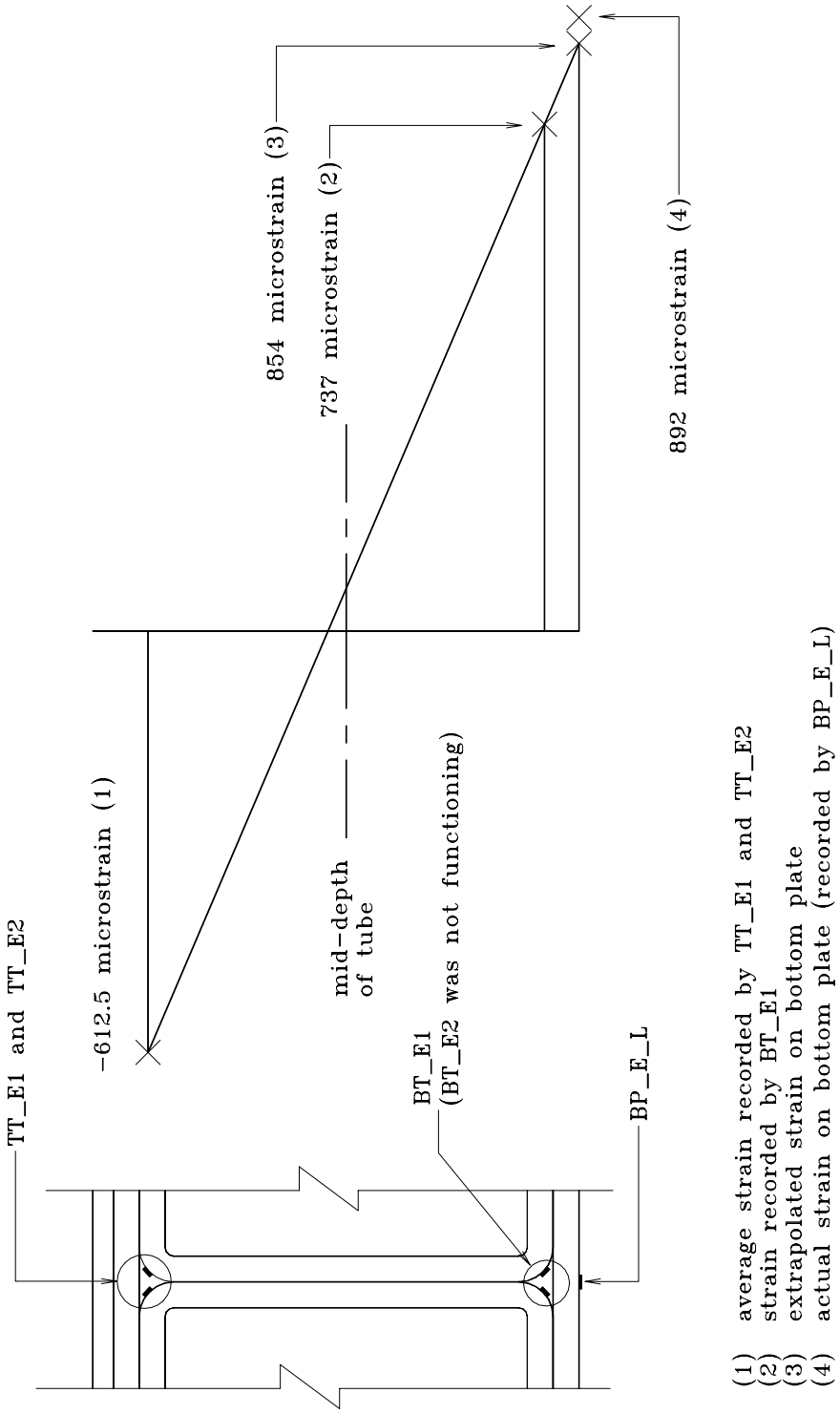

Figure 5.12 Strain distribution (at 20.8 kips) at the East region, Deck 2, Test 1 (Pre-Field Stiffness)

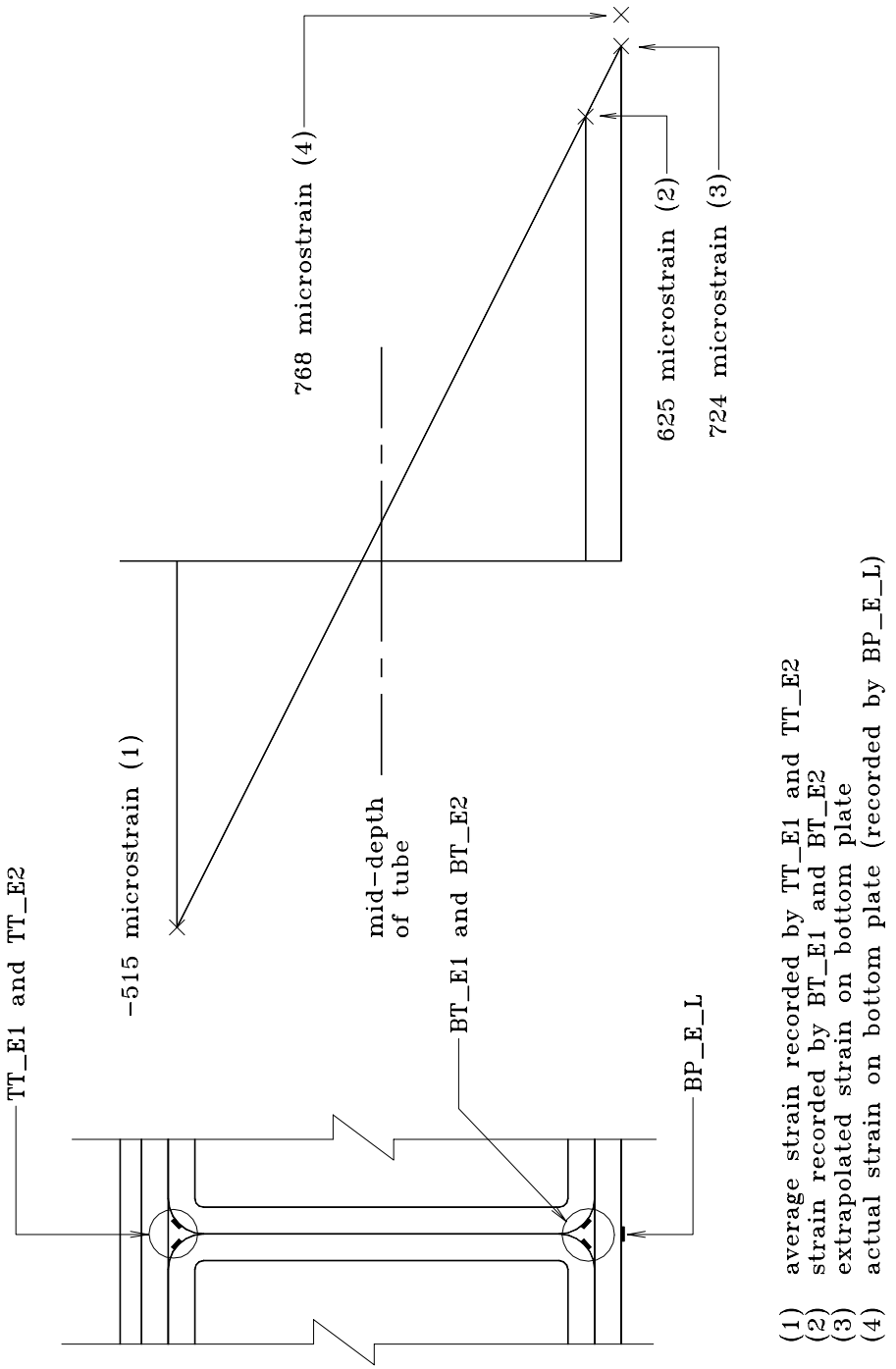

Figure 5.13 Strain distribution (at 20.8 kips) at the East region, Deck 2, Test 3 (Pre-Field Stiffness)

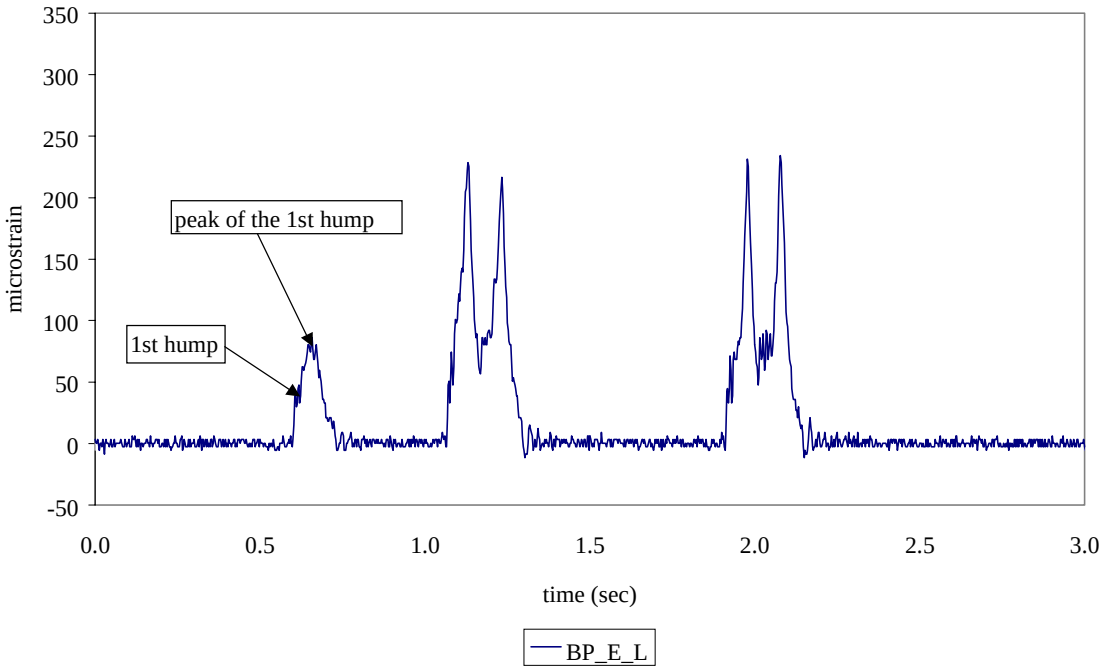

Figure 5.14 Arbitrary plot of strain vs. time for a longitudinally oriented strain gage, Field Test 1

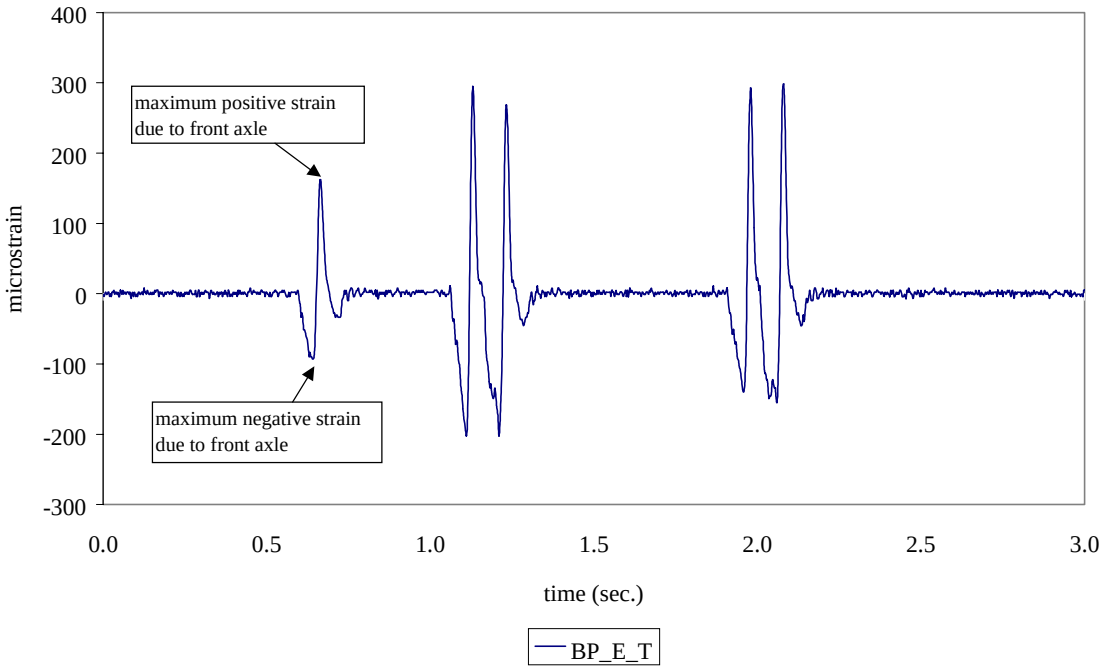

Figure 5.15 Arbitrary plot of strain vs. time for a transversely oriented strain gage, Field Test 1

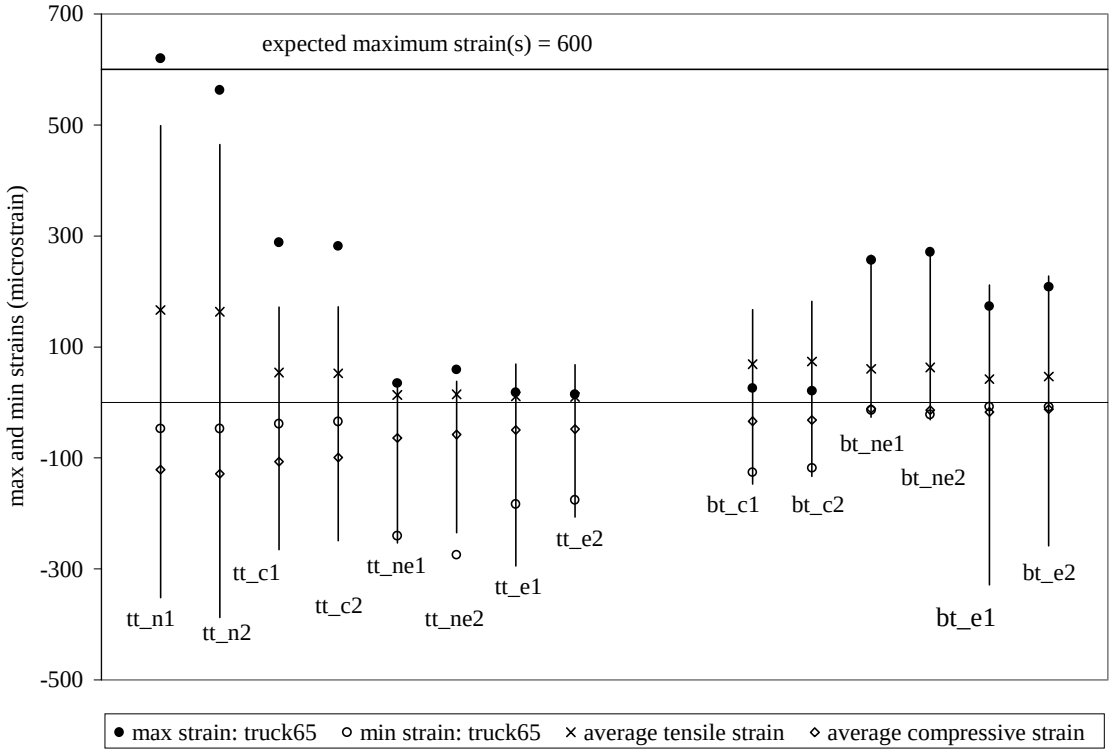

Figure 5.16 Strains due to random truck crossings, Field Test 1 (Top-of-tube and bottom-of-tube strain gages)

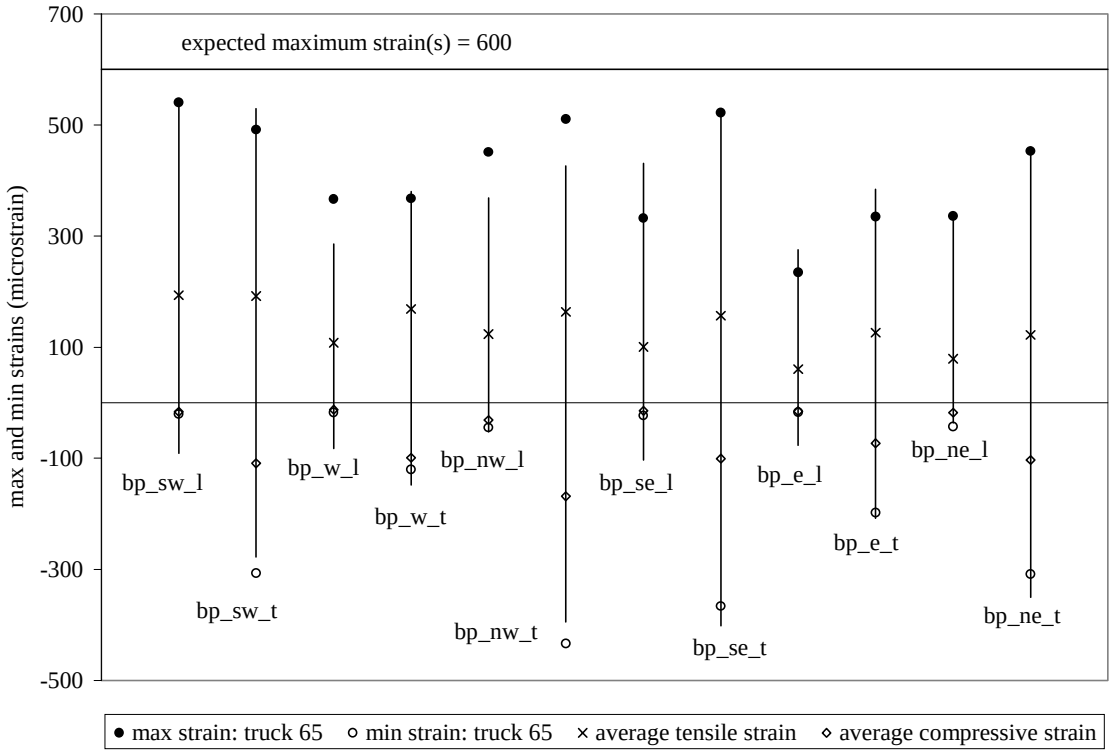

Figure 5.17 Strains due to random truck crossings, Field Test 1 (Bottom plate strain gages)

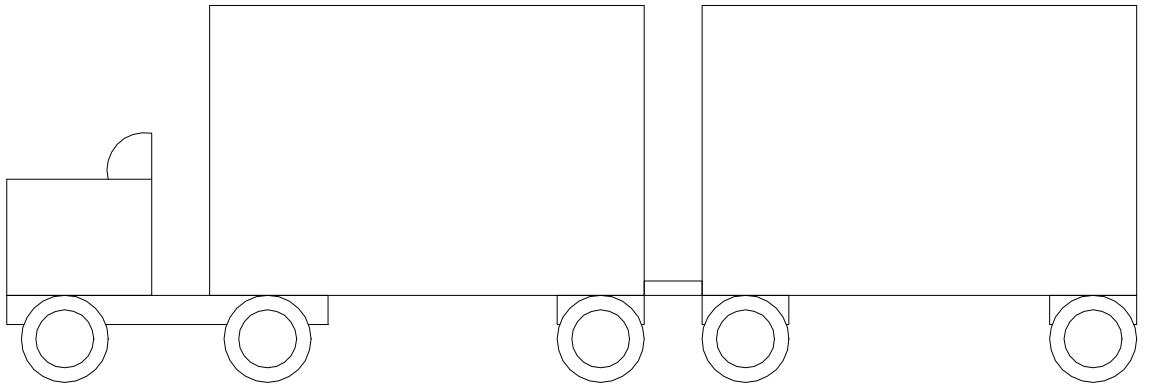

(a) Truck Type 2S1-2: 2 axle tractor with a 1 axle semi-trailer and 2 axle t

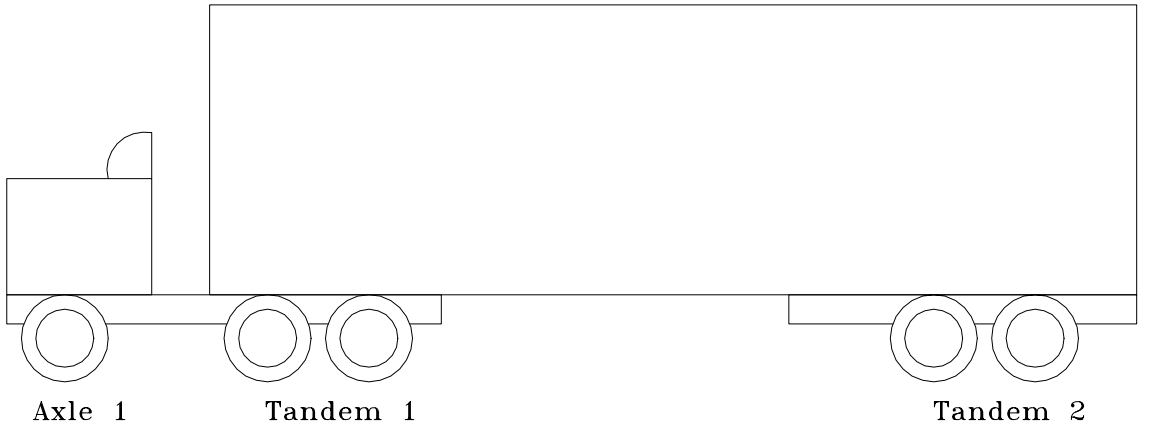

(b) Truck Type 3S-2: 3 axle tractor with 2 axle semi-trailer

Figure 5.18 Schematic showing the 2 types of bias trucks from Field Test 1

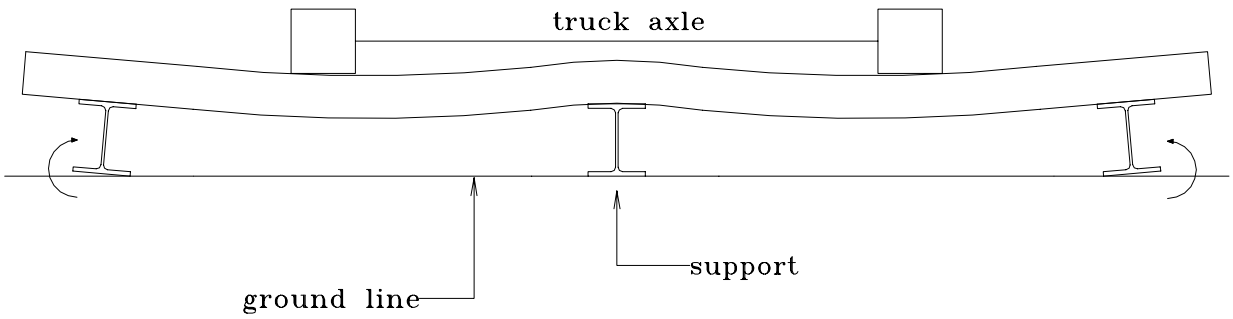

Figure 5.19 Schematic illustrating the "rocking" of supports in the weigh station test facility

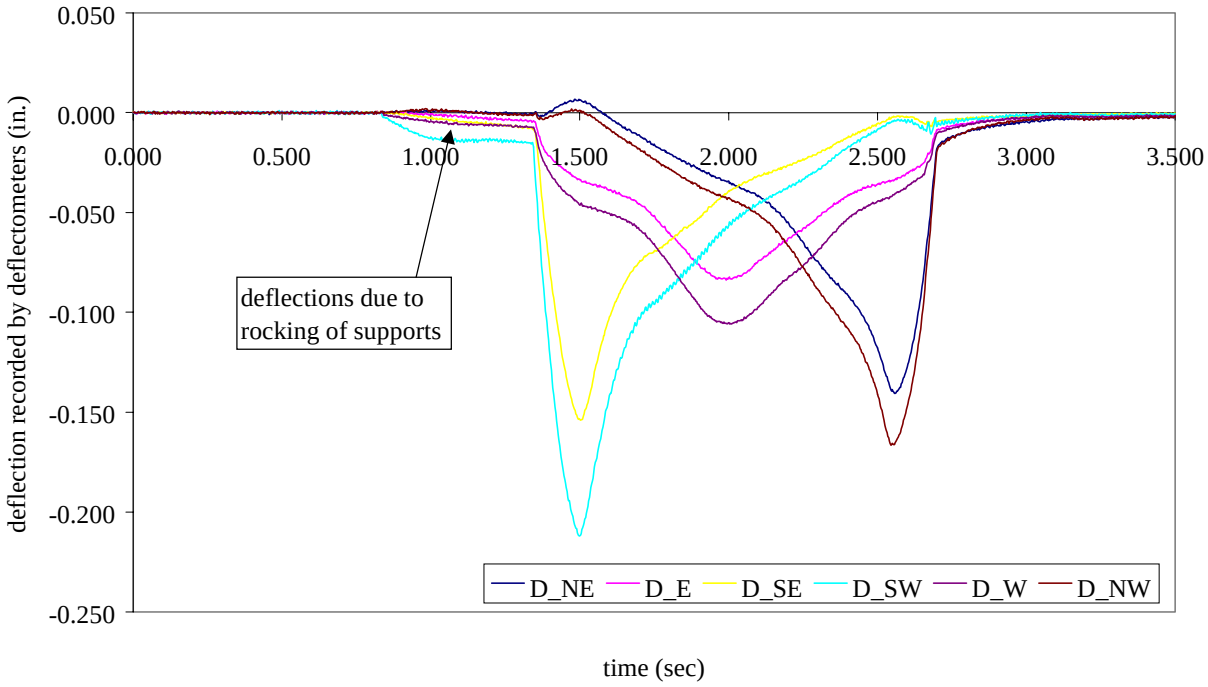

Figure 5.20 Plot of deflection vs. time, Field Test 2, Test Set 1 (front axle crossing middle of deck)

Figure 5.21 Cracks (upper left and lower right of access hole), north face of Deck 2 at weigh station test facility

Figure 5.22 Crack inside the north tube, over the middle support at weigh station test facility

Figure 5.23 Crack at fillet of north tube over the middle support at weigh station test facility (4 months in service)

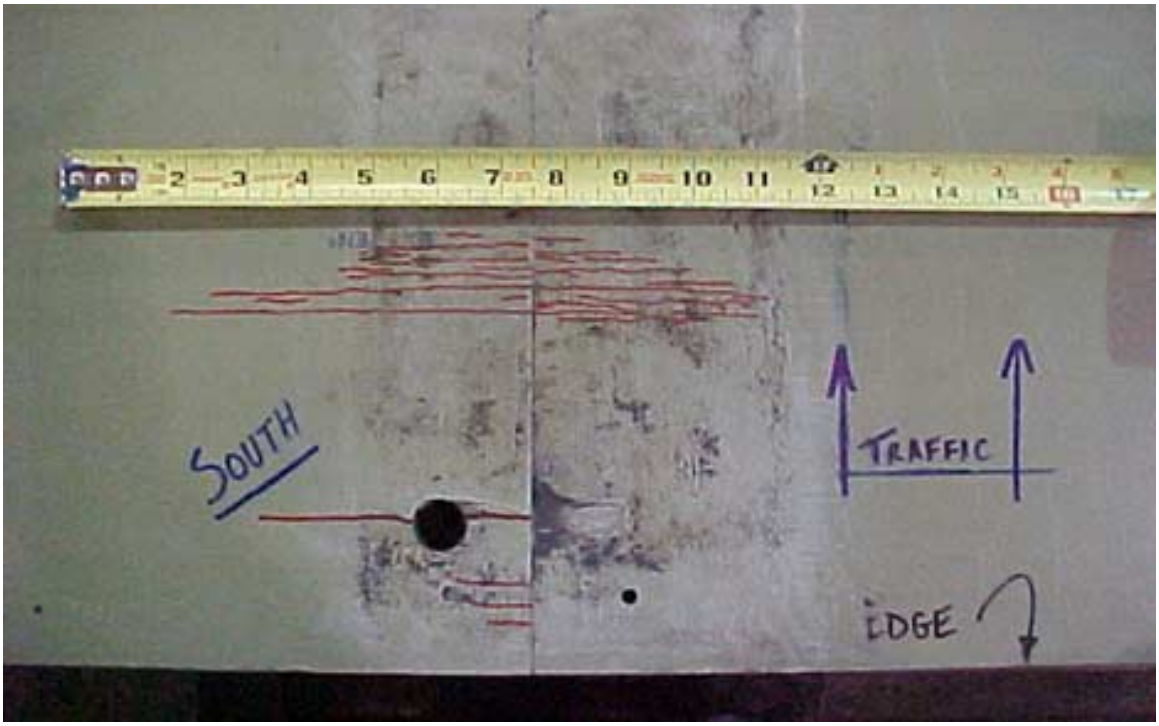

Figure 5.24 Cracks in bottom plate (where middle support had been located), after 8 months in service

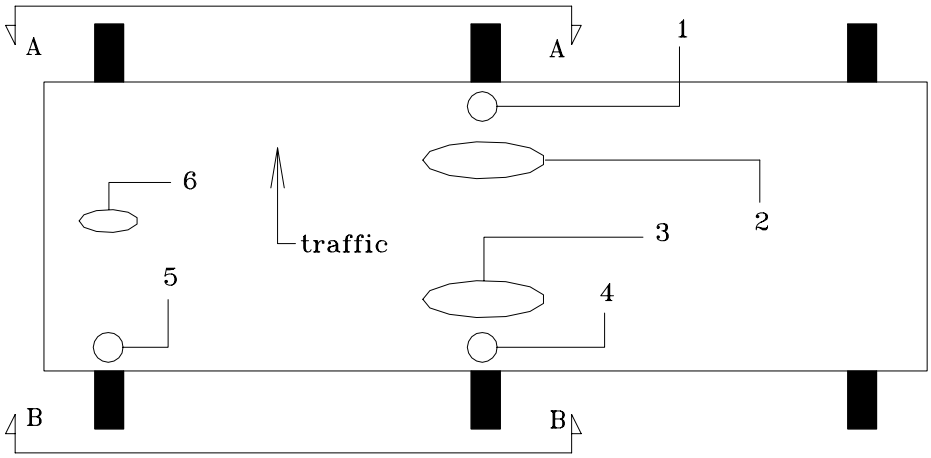

1 a few small cracks around fastener hole
2 several longitudinal cracks
3 several longitudinal cracks
4 a few small cracks around fastener hole
5 2 cracks around fastener hole
6 a few longitudinal cracks

View A–A and B–B can be see in Figure 5.27 and 5.28

Figure 5.25 Location of cracks on bottom plate of Deck 2, after 8 months in service

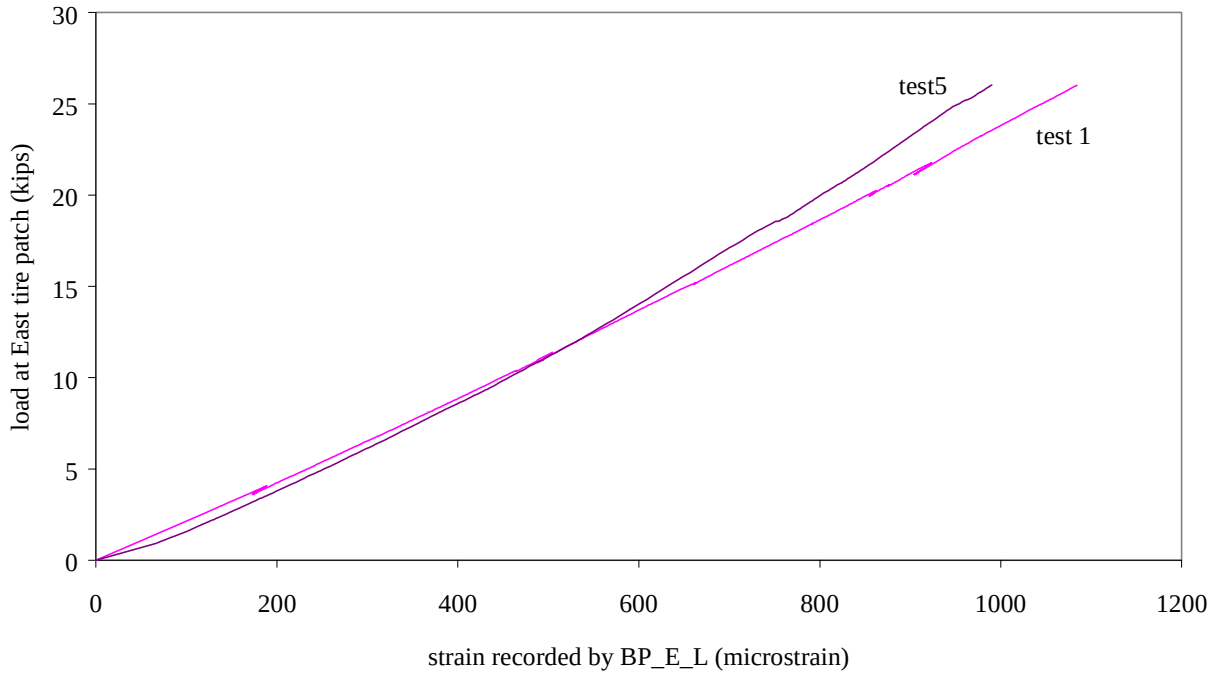

Figure 5.26 Plot of load vs strain, Deck 2, Test 1 (Pre-Field Stiffness) vs Test 5 (Post-Field Stiffness)

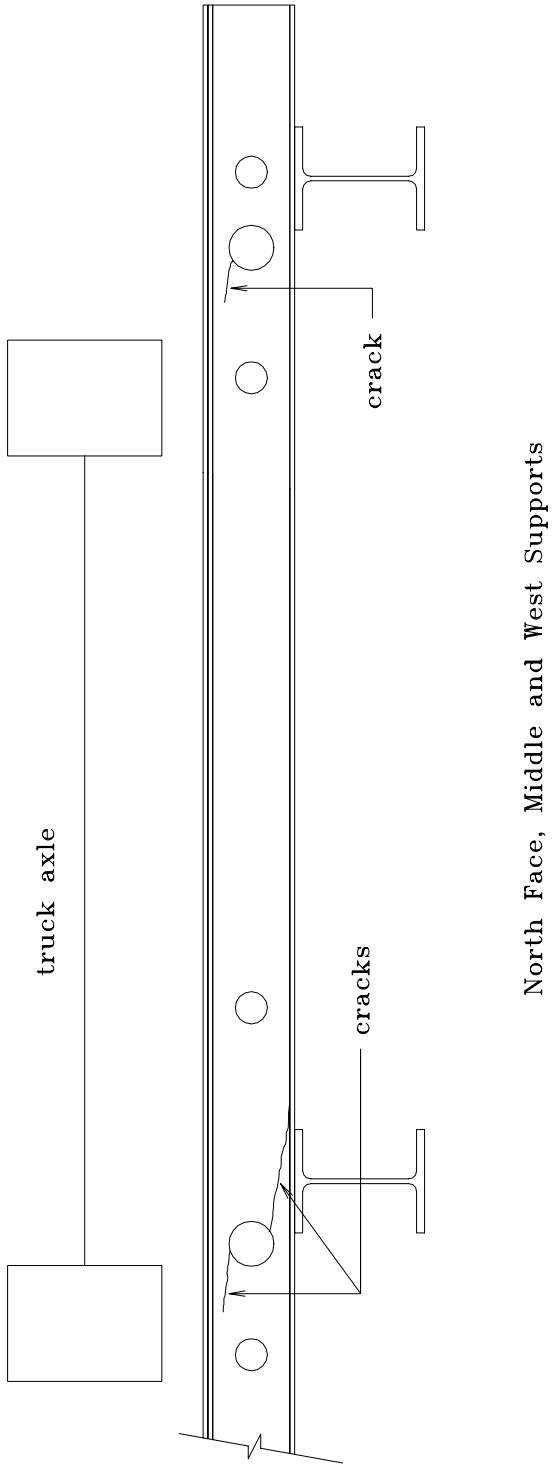

Figure 5.27 Cracks on Deck 2; View A-A from Figure 5.25

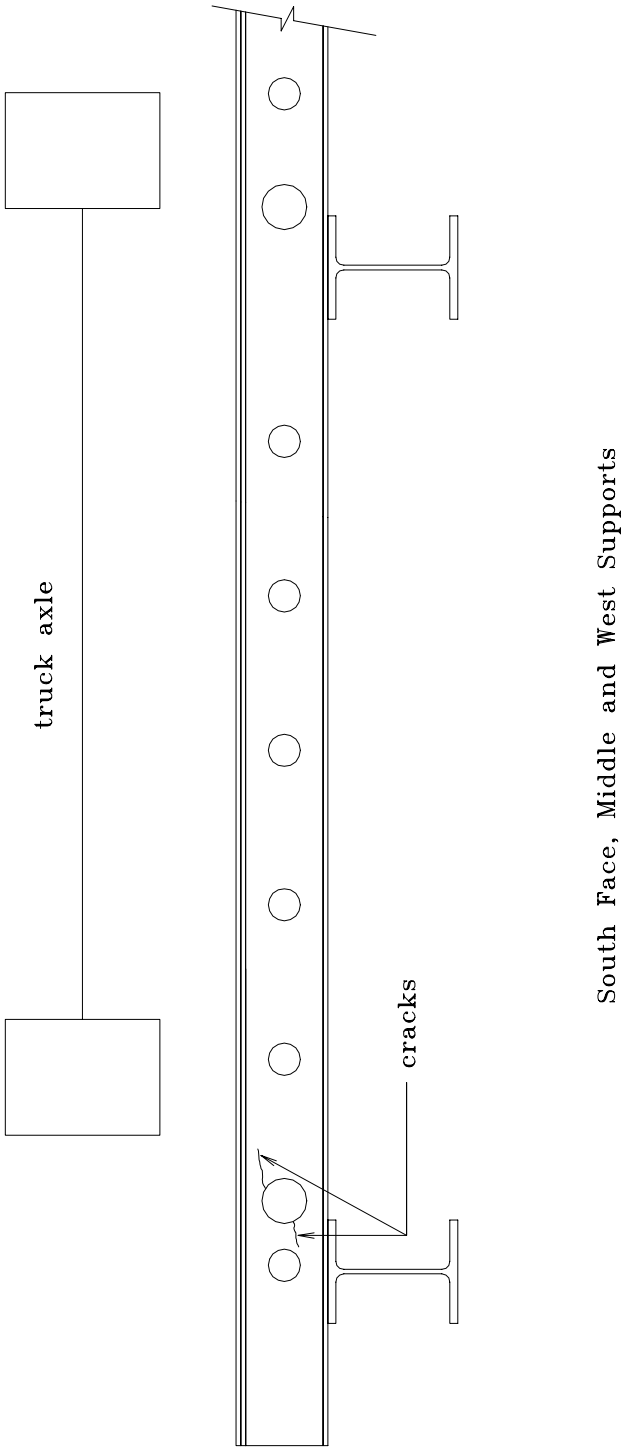

Figure 5.28 Cracks on Deck 2; View B-B from Figure 5.25

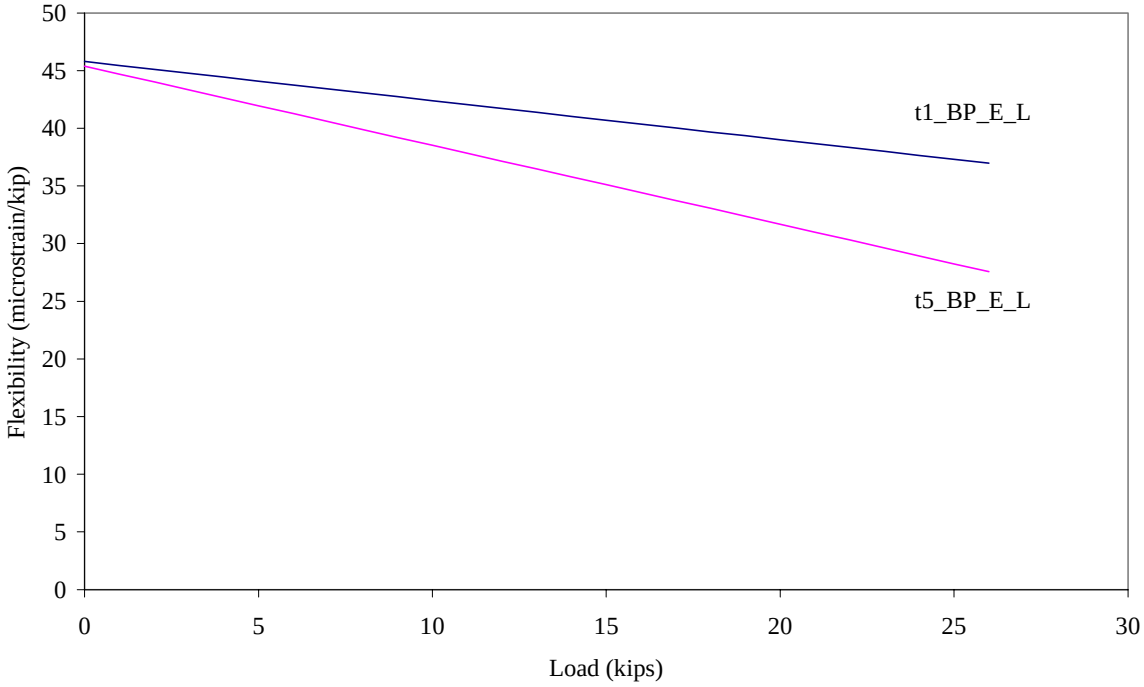

Figure 5.29 Deck 2, Load vs Flexibility, Test 1 (Pre-Field Stiffness) vs Test 5 (Post-Field Stiffness)

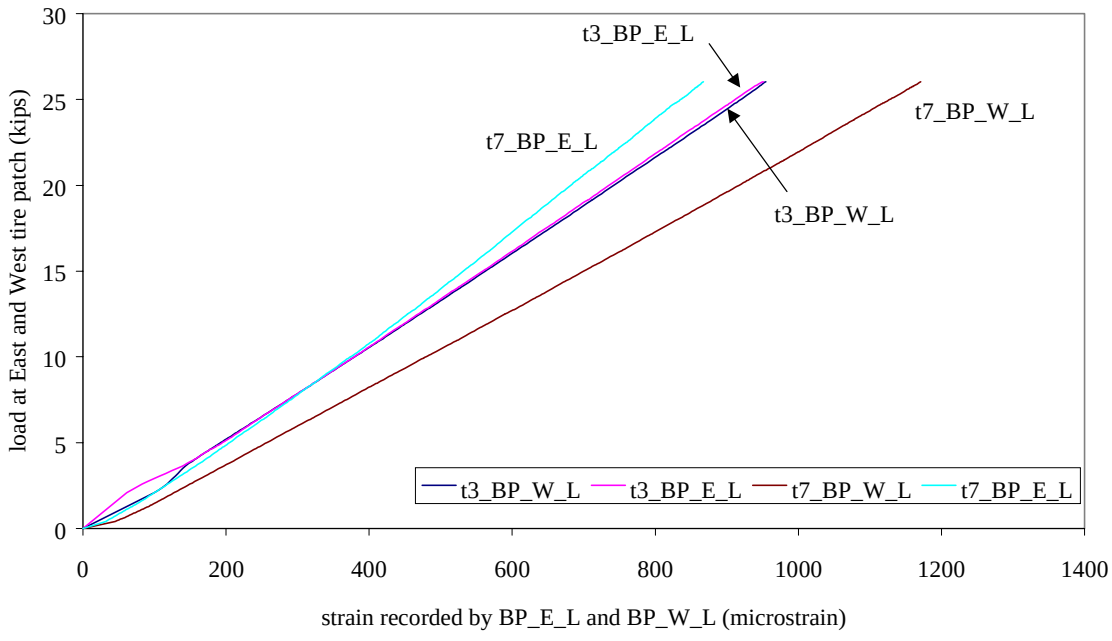

Figure 5.30 Plot of load vs strain, Deck 2, Test 3 (Pre-Field Stiffness) vs Test 7 (Post-Field Stiffness)

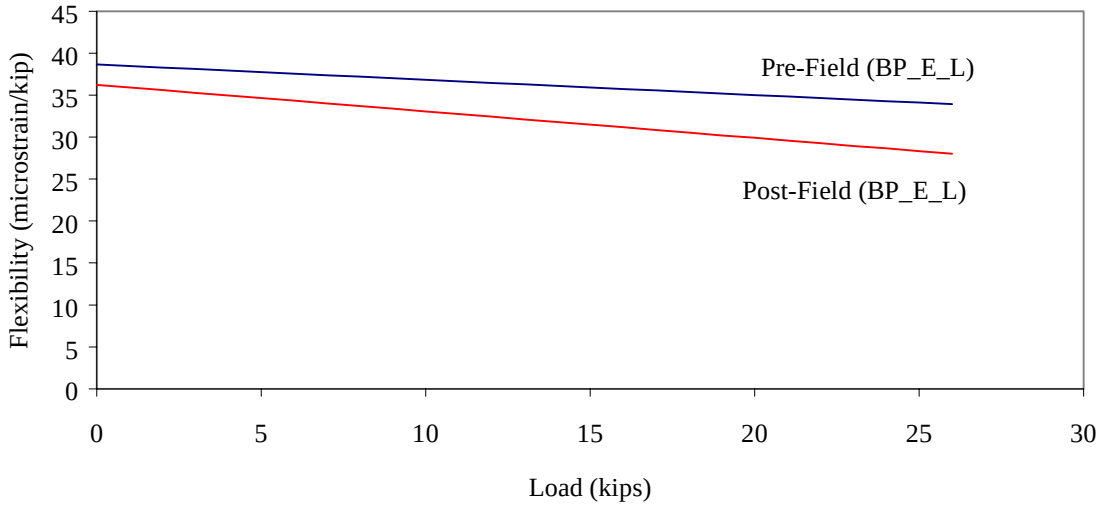

Figure 5.31 Deck 2, Load vs Flexibility, Test 3 (Pre-Field Stiffness) vs Test 7 (Post-Field Stiffness)

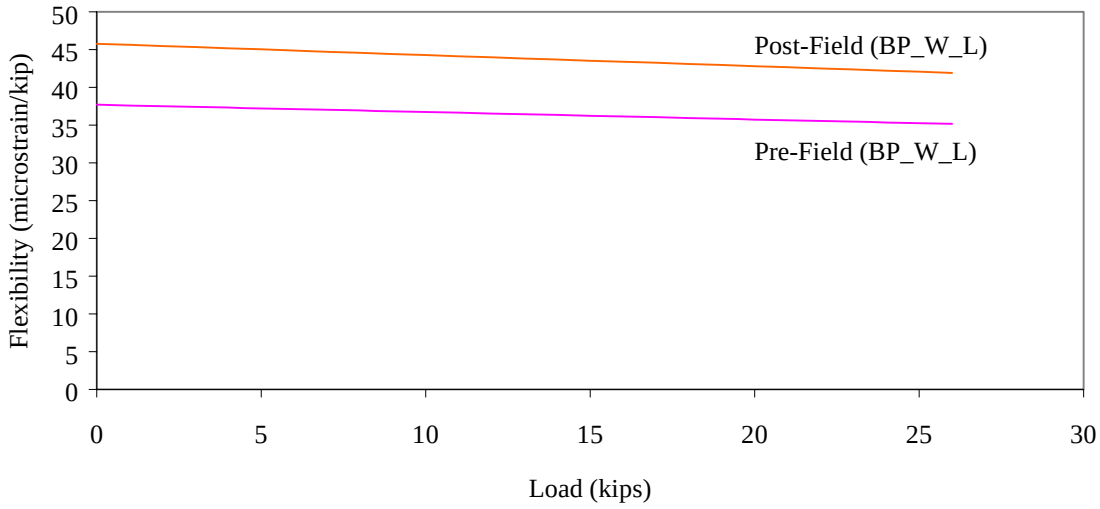

Figure 5.32 Deck 2, Load vs Flexibility, Test 3 (Pre-Field Stiffness) vs Test 7 (Post-Field Stiffness)

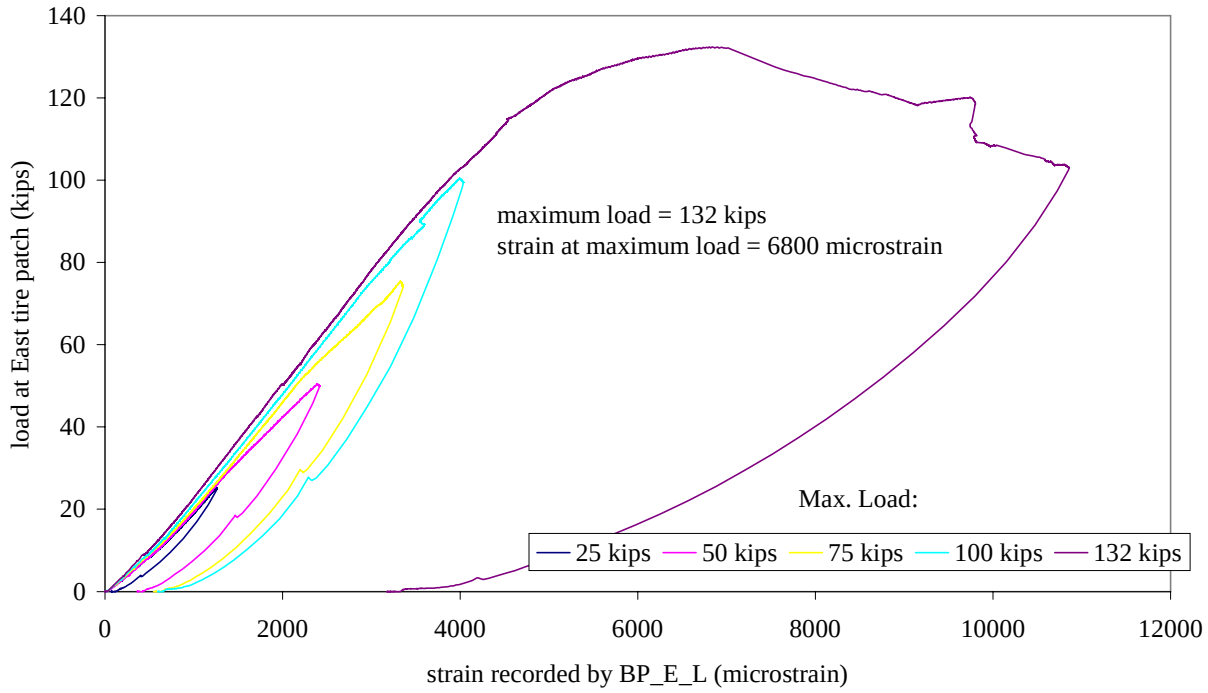

Figure 5.33 Plot of load vs strain, Deck 2, Test 9 (Strength), East tire patch loading (Fig. 4.16)

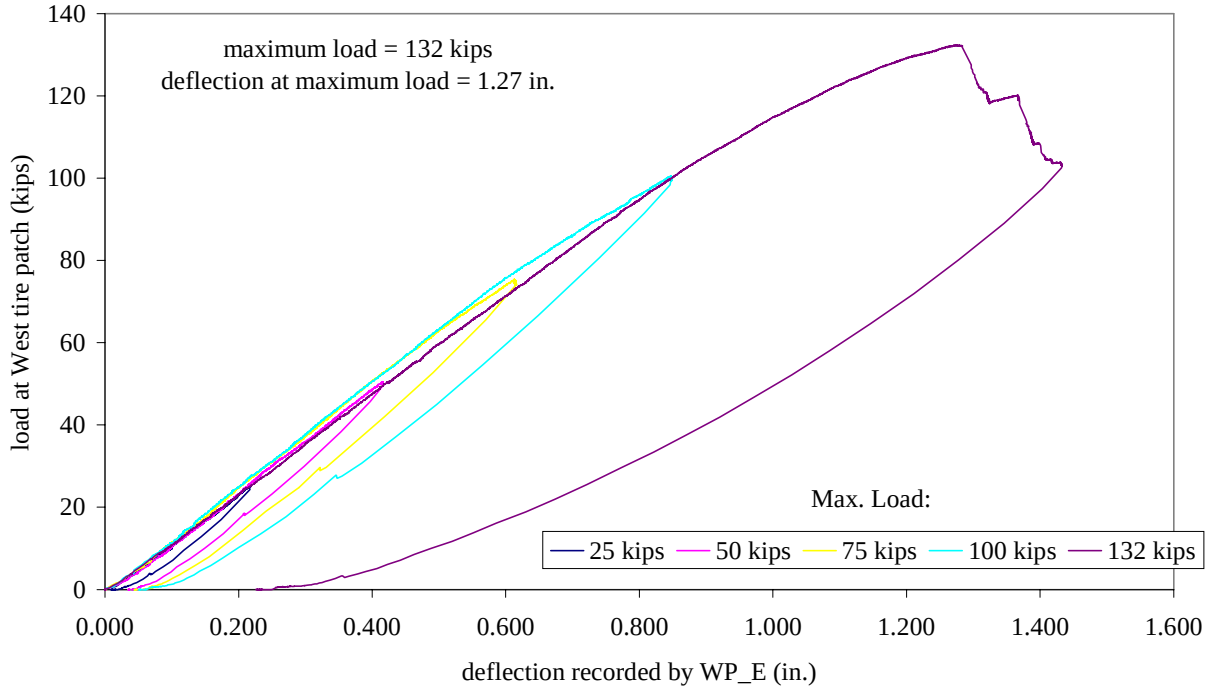

Figure 5.34 Plot of load vs deflection, Deck 2, Test 9 (Strength)

Figure 5.35 Deck 2 punching fracture damage from Test 9 (Strength)

Figure 5.36 Deck 2 shear fracture damage from Test 9 (Strength)

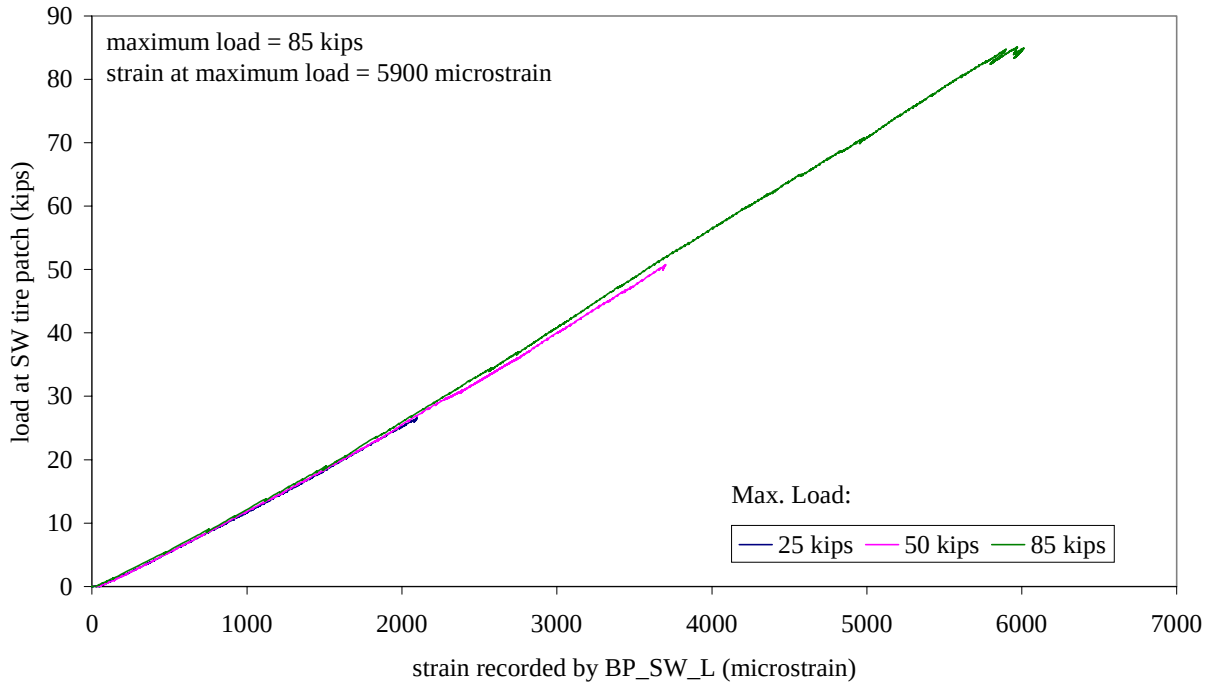

Figure 5.37 Plot of load vs strain, Deck 2, Test 10 (Strength), Southwest tire patch loading (Fig. 4.16)

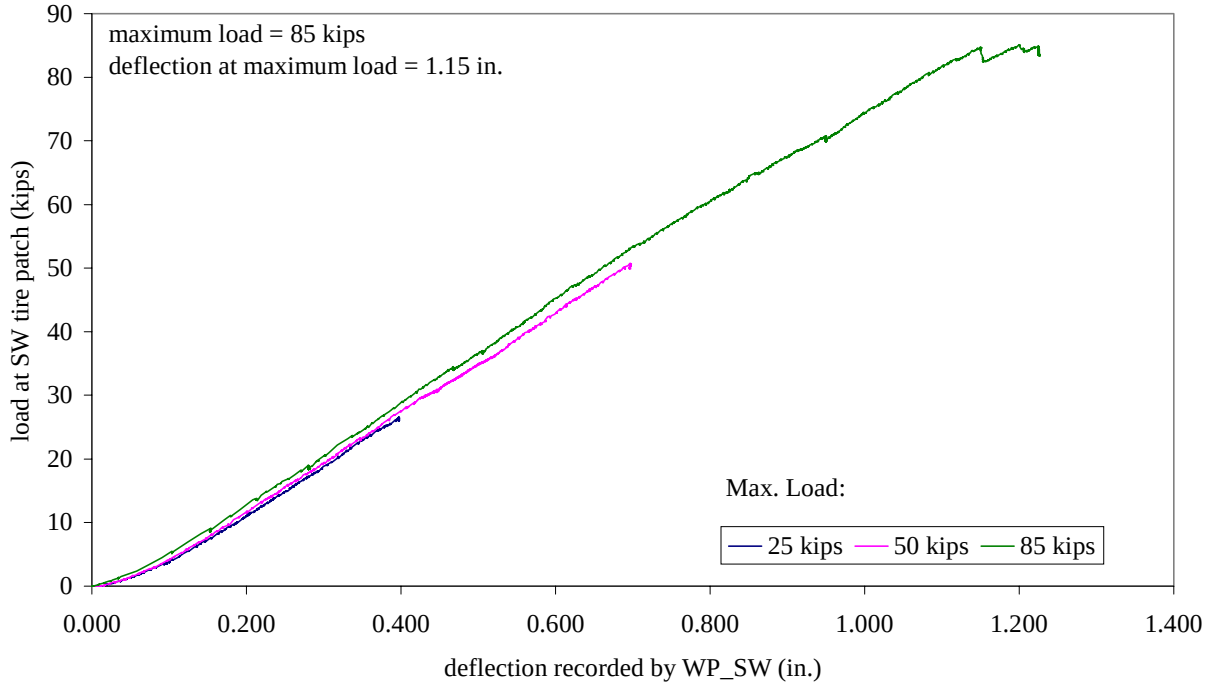

Figure 5.38 Plot of load vs deflection, Deck 2, Test 10 (Strength)

Figure 5.39 Deck 2 shear fracture damage from Test 10 (Strength)

Chapter 6: Conclusions and Recommendations

Based on the research that was outlined in this thesis, the following conclusions and recommendations are made:

- Large strides in quality control were made in going from Deck 1 to Deck 2. Though it could not be shown that the higher quality control produced a stiffer deck, it certainly produced a better product. In particular, the vacuum bagging of Deck 2 produced a much more uniform bond between the tubes and plate (compared with Deck 1).

- The testing of Deck 1 in the laboratory prior to the planned installation in the field was invaluable. It uncovered several areas that required modification. One major example was the deck-to-support connection. It was shown that the connection detail in Deck 1 led to the debonding of the tube-to-plate interface. This connection detail was modified for Deck 2, but even this detail had its shortcomings. Specifically, access holes were drilled in the sidewalls of the deck to allow installation of the bolts. These access holes were the source of several cracks that had developed in Deck 2 during its time in the weigh station facility. These two examples show how critical it is to develop a satisfactory method for connecting an FRP deck to its supporting members.

- Under a simulated HS-25 axle load plus impact, Deck 1 and Deck 2 exhibited a maximum recorded deflection of L/467.

- Both FRP decks exhibited elastic behavior well beyond legal loads. In the three strength tests in which a single tire patch was loaded in the middle of a span, elastic behavior was observed at least up to 60 kips, which is 6 times larger than a legal wheel load.

- The recorded strains in the deck during the field tests were well below the strains that were observed in the deck at failure. The factor of safety between strains recorded in the laboratory at failure and maximum recorded field strains ranged from 10.8 (deck loaded at an unsupported edge) to 16.3 (deck loaded in the middle of one of the spans). The loads sustained by the deck in the lab were well above legal loads. The factor of safety between failure loads in the lab tests and

a 10 kip legal wheel load ranged from 8.5 (deck loaded at an unsupported edge) to 13.2 (deck loaded in the middle of one of the spans).

- After being in the field for 8 months and subjected to approximately 4 million cycles of load (conservative estimate), Deck 2 showed no indication of a loss in stiffness. It would appear that the epoxy adhesive had performed adequately, otherwise a loss in stiffness would most certainly have been observed. Though there were several cracks detected in the deck, this did not appear to adversely affect the stiffness of the deck. However, the cracks that were detected in the deck showed no signs of arresting, and it is uncertain how this would have affected the behavior had the deck remained in the weigh station beyond 8 months.

- It was uncertain what effect the thru rods had on the service-load behavior of the deck. It is possible that the thru rods added significant stiffness to the deck. The only way to truly ascertain the influence of the thru rods would be to test several decks, in which some of the decks would have to be fabricated without the thru rods. It would certainly bring down the costs of the FRP deck if it could be fabricated without the thru rods.

- The author is uncertain what importance to attach to the deflection results. Currently, the criteria for deflection in AASHTO's LRFD specifications is considered optional (except for special cases). However, the current specifications do not include FRP as a design material, and it is possible that deflection criteria could be required for FRP composites, but this would certainly require further research. At present, however, it does appear that FRP decks are governed by stiffness rather than strength.

- When loaded in the middle of its span, the failure mode for the FRP decks was punching shear. It would be interesting to see at what support spacing, if any, the failure mode would change from a punching shear to some other mode of failure.

- The highest recorded strains *under service loads* were in the bottom plate, and were approximately 600 microstrain (tensile) in the longitudinal and transverse direction. This is well below the reported ultimate coupon strains (Strongwell Design Manual) in the longitudinal

direction (11100 microstrain) as well as the transverse direction (7100 microstrain). It is quite possible that local strains beneath the tire patch were higher than recorded strains in the bottom plate, but the only way to determine this would be to place strains gages on the tubes in those areas where load would be directly applied.

Cited References

AASHTO (1977). AASHTO Standard Specifications for Highway Bridges (12th ed.). Washington, D.C., Maryland, U.S.

AASHTO (1996). AASHTO Standard Specifications for Highway Bridges (16th ed.). Washington, D.C., Maryland, U.S.

AASHTO (1998). AASHTO LRFD Bridge Design Specifications (2nd ed.).

AISC (1994a). Manual of Steel Construction—Load and Resistance Factor Design (Vol. 1, 2nd ed.). Chicago, Illinois, U.S.

AISC (1994b). Manual of Steel Construction—Load and Resistance Factor Design (Vol. 2, 2nd ed.). Chicago, Illinois, U.S.

ASM (1978). Metals Handbook—Properties and Selection: Irons and Steels (Vol. 1, 9th ed.), Metals Park, Ohio, U.S.

Azar, W.A. (1989). "Analytical and experimental evaluation of fiber reinforced plastic bridge decks under fatigue loads." M.S. Thesis, California State University, Long Beach, U.S.

Bakeri, P.A. and Sunder, S.S. (1990). "Concepts for hybrid FRP bridge deck systems." Serviceability and Durability of Construction Materials, Proceedings of the 1st Materials Engineering Congress, Denver, Colorado, U.S., pp. 1006-1015.

Brown, R.T. and Zureick, A. (1999). "Lightweigh composite truss section decking." 3rd International Workshop on Very Large Floating Structures, Honolulu, Hawaii, U.S., paper 7-1-3.

CALTRANS (1997). "Experimental fiber-reinforced plastic deck panels for the Schuyler Heim Bridge." CALTRANS RFQ/RFP 59A0028, California Department of Transportation, Sacramento, California, U.S.

Cassity, P., Richards, D. and Gillespie, J. (2000). "A 'compositely acting' FRP deck and girder system." Bridges to the Future, Proceedings of the 17th Annual International Bridge Conference, "In press", Pittsburgh, Pennsylvania, U.S.

GangaRao, H.V.S., Thippeswamy, H.K., Shekar, V. and Craigo, C. (1999). "Development of glass fiber reinforced polmer composite bridge deck." SAMPE Journal, Vol. 35, No. 4, pp. 12-24.

Harik, I., Alagusundaramoorthy, P., Siddiqui, R., Lopez-Anido, R., Morton, S. Dutta, P. and Shahrooz, B. (1999). "Static testing on FRP bridge deck panels." Proceedings of the 44th International Sampe Symposium and Exhibition, Long Beach, California, U.S., pp. 1643-1654.

Hayes, M.D., Ohanehi, D., Lesko, J.J., Cousins, T.E., and Witcher, D. (2000). “Performance of tube and plate fiberglass composite bridge deck.” Journal of Composites for Construction, Vol. 4, No. 2, pp. 48-55.

Henry, J.A. (1985). “Deck-girder systems for highway bridges using fiber reinforced plastics.” M.S. Thesis, North Carolina State University, Raleigh, U.S.

McCormick, F.C. (1978). “Laboratory and field studies of a pedestrian bridge composed of glass reinforced plastic.” Bridge Engineering—proceedings of a conference conducted by the Transportation Research Board, No. 665, pp. 99-107.

McGhee, K.K., Barton, F.W. and McKeel, W.T. (1991). “Optimum design of composite bridge deck panels.” Advanced Composite Materials in Civil Engineering Structures, Proceedings of the Specialty Conference, ASCE, Las Vegas, Nevada, U.S., pp. 360-370.

Morrison Molded Fiber Glass Company (1989). EXTREN Fiberglass Structural Shapes—Design Manual. Bristol, Virginia, U.S.

ODOT (2000). Evaluation of Salem Avenue Bridge Deck Replacement, Final Report, Dec. 1, 2000, Ohio Department of Transportation, Edited by Mark P. Henderson, P.E.

Plecnik, J.M. and Azar, W.A. (1991). “Structural components, highway bridge deck applications.” International Encyclopedia of Composites, Vol. 6, pp. 430-445.

Taly (1998). Design of Modern Highway Bridges, New York, New York: McGraw-Hill.

Transportation Research Board (1998). “TR News, Special Issue on Highway Bridges: Progress and Prospects.” Jan-Feb, No. 194.

Strongwell, Inc. (1998). EXTREN—Design Manual. Bristol, Virgina, U.S.

USDOT (2000). “The U.S. Department of Transportation’s Comprehensive Truck Size and Weight Study”. (Publication No. FHWA-PL-00-029). August, 2000.

VDOT (1996). Virginia Hauling Permit Manual, Commonwealth of Virginia, Department of Transportation, January 24, 1996.

Zureick, A. (1997). “Fiber-reinforced polymeric bridge decks.” Proceedings of the National Seminar on Advanced Composite Material Bridges, FHWA.

Vita

Anthony B. Temeles was born in Livingston, NJ on January 15, 1975, to David and Maureen Temeles. For the majority of his youth, he grew up in Scotch Plains, NJ, and graduated from Scotch Plains Fanwood High School in June, 1993. He attended Lehigh University (Bethlehem, PA) from 1993 to 1997, where he received a Bachelor of Science in Civil Engineering (June 1997) with an emphasis on Structural Engineering. He attended Virginia Tech (Blacksburg, VA) from 1998 to 2000, where he received a Master of Science in Civil Engineering (May 2001) with an emphasis on Structural Engineering. Anthony took his first job with Modjeski and Masters in October 2000, and is currently working in their Moorestown, NJ office practicing Bridge and Roadway Design.